MOISTURE-TEMPERATURE REALTIONSHIPS IN A SAND DUE TO OUTWARD, RADIAL FREEZING

Final Report

Erling A. Juel, B.S.

May 1989

Prepared for

Publication Cost: $18.00

ABSTRACT

A "clean" sand is commonly specifed as backfill around the evaporator section of thermosyphons designed to maintain the thermal regime of pernnially, frozen, thaw-unstable soils. A series of laboratory tests were performed to determine the magnitude of moisture migration. The test results indicate the moisture migration can result due to outward radial freezing in a nonfrost susceptible sand possessing a low to moderate degree of saturation. Moisture did not migrate when the sand was saturated prior to freezing. The redistribution of moisture changes the thermal properties of the soil system which effects the maximum radius of freezing by desiccating soil at the outermost radius of influence and increasing the degree of saturation around the evaporator. The desiccated soil region will experience an accelerated rate of thaw due to a lower volumetric latent heat of fusion. In addition, the radius of freezing is reduced as moisture migrates towards the evaporator section. These effects warrant additional considerations that must be addressed when designing refrigerated foundations with thermosyphons.

TABLE OF CONTENTS

LIST OF FIGURES

LIST OF TABLES

ACKNOWLEDGEMENTS

CHAPTER 1

INTRODUCTION

The desire to use slab-on-grade designs for heated buildings and other structures overlying thaw-unstable permafrost has prompted the use of refrigerated foundations to maintain the existing thermal regime. A passive refrigeration system consisting of thermosyphons is often employed to remove heat from the underlying soils.

A thermosyphon is generally a long, slender pressure vessel with one end, the evaporator section, placed in the foundation soils and the other end, the condenser section, exposed to the atmosphere. The thermosyphon contains a pressurized fluid which evaporates at a temperature lower than the freezing temperature of the surrounding soil. When the temperature of the soil equals the boiling temperature of the working fluid, the fluid evaporates from the evaporator section and rises upward toward the condenser section. If the temperature of the condenser section is lower than the temperature of the soil, the vapor recondenses releasing energy in the form of vaporization latent heat. A change of phase from a gas to a liquid causes a reduction in pressure in the condenser section setting up a pressure differential. The cycle continues as the

fluid returns by gravity, back to the evaporator section.

When a refrigerated foundation for a proposed structure is designed, a clean sand or sand and gravel is often specified as backfill around the evaporator sections. Under varying soil properties and thermal influences, moisture may be redistributed due to freezing caused by the evaporator section. If moisture migrates toward the cold evaporator section, it may cause a desiccating effect in the soil outside the zone of freezing.

The removal of moisture from the soil will lower the volumetric latent heat and the volumetric specific heat in both the frozen and unfrozen states. This will cause an accelerated rate of thaw in localized areas when passive thermosyphons become inactive. This is an important parameter when designing refrigerated foundations. The initial number and spacing of the evaporator sections may become inadequate to maintain the thermal regime. A better understanding is needed of the moisture-temperature redistribution relationships in the backfill soils in which the evaporator sections are placed to ensure that an adequate foundation is designed.

Radial conduction is the principle mode of heat transfer through the soil towards the evaporator section. With heat extraction, a cylindrical zone of frozen soil forms parallel to the longitudinal axis of the evaporator section. Besides climatic constraints and external sources

of heat, the maximum radius of freezing is a function of the physical and thermal properties of the backfill soil. Physical properties include dry density, grain-size distribution, pore fluid, degree of saturation, and soil-moisture characteristics. Thermal properties include thermal conductivity, volumetric heat capacity, and the volumetric latent heat. Since many of these physical and thermal properties are a function of the soil moisture content, they may be changed significantly if moisture is redistributed in the soil surrounding the evaporator section.

Currently, a lack of knowledge exists as to whether or not moisture redistribution occurs in a "clean" sand used as backfill around the evaporator section of a thermosyphon. It is widely accepted that moisture migration and ice segregation can occur while freezing fine-grained (frost susceptible) soils. The goal of this study was to construct a freezing tank apparatus in which a "clean" sand could be frozen radially outward from a center heat sink resembling an evaporator section. The soil mass in this study was frozen at different freezing rates and at three initial moisture contents. The soil mass was instrumented with fifteen thermistors and nine tensiometers by which moisture-temperature relationships could be observed.

Chapter 2 concentrates on heat transfer in soils. This includes modes of heat transfer and thermal properties of

soils. The last section of this chapter reviews techniques available for analyzing outward, radial heat transfer in soils for both phase change and nonphase change considerations.

Moisture migration mechanisms in freezing soils are addressed in Chapter 3. This chapter includes the effects of soil-water properties and environmental factors on migration potentials. Although the majority of the literature reviewed concentrated on moisture migration (frost heave) in fine-grained soils, an insight was gained on the factors and mechanisms of moisture migration in all soils.

The experimental set-up and test procedure are discussed in Chapter 4. Dimensions and major components of the freeze tank are given as well as properties of the soil medium used in this study. Specific details of the thermistors used to measure temperatures and tensiometers used to measure negative pore pressures are presented. In addition, the experimental procedure followed is outlined so that further experiments may be performed.

Chapter 5 is reserved for discussions on experimental observations and the data collected during each of the freezing tests. Moisture-temperature relationships and changes in moisture distribution are given for each test.

Chapter 6 summarizes the results of this study and gives recommendations for future studies.

CHAPTER 2

HEAT TRANSFER IN SOILS

With increased construction activity in cold regions, there has been an increased need to understand the physical and thermal geotechnical environment. The impact of a building or structure on the existing environment often dictates the performance and the life of that facility.

The melting of perennially frozen, thaw unstable ground under a structure can lead to several undesirable results. One effect is differential settlements due to nonuniform melting and thaw consolidation. Also, the melting of thaw unstable soils can cause a reduction in the bearing capacity which can cause foundation failure. In other words, the degradation of the existing thermal regime in thaw unstable soils promotes the degradation of the physical regime.

There currently exists five design-construction approaches with regard to thaw unstable soils. The first is avoidance by choosing an alternative location. The second is to remove the unsuitable soils and replaced them with more desirable material. The third is to design the structure to withstand the consequences of thawing by making

5

allowances for building maintenance and rehabilation. The fourth is to prethaw and allow the thaw unstable permafrost to settle prior to construction. The last is to preserve the thermal regime by negating the thermal effects produced by the proposed facility.

The thermal influences of the facility could be removed or intercepted by a refrigerated foundation before degradation of the permafrost could occur. This system could either be active (mechanical) or passive (nonmechanical). A complete understanding of heat transfer through soils is needed to adequately design the system to maintain thermal equilibrium between the facility and the temperature-sensitive environment. This understanding includes knowledge about the modes of heat transfer, rates of freezing and thawing, thermal characteristics of the ground, mechanics of the refrigeration system, and physical properties of the soils. Also, a thorough knowledge is warranted about the relationships between moisture and temperature in the foundation backfill.

2.1 Modes of Heat Transfer

The three modes of heat energy transfer are conduction, convection, and radiation. Of these, conduction is the principle mode in frozen and thawed soils. Heat transfer by convection may be significant in a soil if the pore fluids

are in motion. Thermal energy transfer by radiation is insignificant in the interior of a buried soil mass, but may become significant for a soil surface exposed to the atmosphere. Therefore, in this study, heat transfer by conduction will be emphasized, convective heat transfer will be discussed, and heat energy by radiation will not be discussed.

2.1.1 CONDUCTION

Conduction is a form of heat energy transfer which is transmitted through points of contact between two bodies at different temperatures or through the body itself. Molecular vibrations and collisions are the vehicles of conductive heat transfer (Lunardini, 1981). These microscopic, molecular interactions result in a transfer of kinetic energy, or thermal energy, from molecules of a relatively warm region to a relatively colder region. This reflects one of the basic governing laws of thermal energy transfer; heat energy flows from a high energy potential (high temperature) to a lower energy potential (low temperature).

The fundamental, analytical expression for one-dimensional, steady-state heat transfer by conduction is given by Fourier's law which is:

$$Q_{cond} = - k A \frac{dT}{dx} \qquad (2.1)$$

where Q_{cond} = heat flow per unit time,

   k = thermal conductivity of material
   transmitting the heat energy,

   A = cross-sectional area perpendicular to
   the direction of heat flow, and

   dT/dx = thermal gradient between two points of
   interest.

Fourier's law states that the transfer of thermal energy between two points is proportional to the thermal gradient between the two points, the surface area of conduction perpendicular to flow, and the ability of the material to conduct heat energy. The negative sign indicates that heat flow occurs from high temperatures to low temperatures correlating to a descending or negative thermal gradient. Fouriers's law is analogous to Darcy's law in soil mechanics which describes fluid flow through a porous medium.

2.1.2 CONVECTION

Convection in soils is a heat and mass transfer phenomenon in which the heat energy is directly related to the rate of mass movement of the fluid. The conveying fluid

can be either a gas or a liquid. Heat energy is transferred into and out of the moving fluid through conduction along the boundary surfaces where the fluid is in contact with the solid soil particles.

Convective heat transfer can be significant in soils if the pore fluids are in motion. The one-dimensional convective heat flux rate due to pore fluid movements under steady-state conditions is given by; Andersland and Anderson (1978)

$$Q_{conv} = C \rho A v \frac{dT}{dx} \qquad (2.2)$$

where Q_{conv} = convective heat transfer per time per unit length,

     C = heat capacity of pore fluid,

     ρ = density of pore fluid,

     A = area perpendicular to flow,

     v = fluid velocity in x direction,

    dT = temperature change, and

    dx = distance.

The convective heat transfer of pore water can significantly influence both freezing and thawing rates in soils. Cold water released from downward melting during thaw settlement can be displaced upward and can lower the

thermal gradient (Andersland and Anderson, 1978). Also, moving ground water, acting like a heat sink, has "thermal inertia" and can erode frozen soils or halt the advancement of a freezing front. Another example of convective heat transfer occurs during frost heave where the migration of moisture towards a zone of freezing retards the moving freeze front by releasing latent heat energy due to fusion.

2.2 Thermal Properties of Soils

Soils may be composed of mineral grains, organics, ice, water, air, and other substances. Therefore, the thermal properties of soils are a composite of the thermal properties of the constituents. Thermal conductivity and thermal diffusivity are thermal properties that describe the rate of heat transfer through a material. Latent heat and heat capacity are properties that measure a soils ability to store thermal energy. Thermal properties affect temperature distribution as well as the extent and rate of freezing and thawing in a soil mass.

2.2.1 Thermal Conductivity

The thermal conductivity (k) of a soil is defined as the measured amount of heat transmitted through a unit cross-sectional area of soil having a unit thickness under a

unit thermal gradient during one unit of time. Thermal conductivity is commonly expressed in units of W/m-K (BTU/Hr-ft-F). A partial list of material thermal conductivities of several materials is presented in Table 2.1 (Johnston, 1981).

Table 2.1

Thermal Conductivities of Several Materials

Material	W/m-K	Btu/hr-ft-F
Air	0.024	0.014
Water	0.605	0.35
Ice	2.230	1.29
Quartz	5.8	3.35
Argillite	3.3	1.9
Aluminum	173	100
Steel	43.5	25
Extruded Polystyrene	0.036	0.02

The thermal conductivities of many soils have been explored by Kersten (1949) and Penner (1970). The thermal conductivity of soils has been found to be primarily a function of the soil dry density, the moisture content, mineral constituents, and whether the pore water is frozen or thawed. In general, the thermal conductivity of soils increases with increasing dry density and moisture content. Quartz which dominates the minerlogical assemblage of coarse-grain soils has a higher thermal conductivity than thin, platy minerals which make-up fine-grain soils. Table

2.1 shows that the thermal conductivity of ice is more than 3.5 times that of water. Hence, the thermal conductivity of a soil is usually greater in a frozen state than in a thawed state.

Kersten (1949) formulated four equations for determining soil thermal conductivity. These equations define the thermal conductivity based upon soil texture, unit weight, moisture content, and the thermal state of the pore water. Fine-grained soils contain 50 per cent or more, by weight, silt and clay sized particles. Coarse-grained soils contain more than 50 percent sand and gravel. The following equations give thermal conductivities for soils based upon Kersten's work.

a) Thawed, fine-grained soils;

$$k = 0.1442 [0.9(\log w) - 0.2] 10^{(0.6243\rho)} \qquad (2.3a)$$

b) Frozen, fine-grained soils;

$$k = 0.00144 \; 10^{(1.373\rho)} + (w)(0.01226) \; 10^{(0.4994\rho)} \qquad (2.3b)$$

c) Thawed, coarse-grained soils;

$$k = 0.1442 [0.7(\log w) + 0.4] 10^{(0.6243\rho)} \qquad (2.3c)$$

d) Frozen, coarse-grained soils;

$$k = 0.01096 \; 10^{(0.8116\rho)} + (w)(0.0046) \; 10^{(0.9115\rho)} \qquad (2.3d)$$

where ρ = soil dry density, gm/cm^3 and,

w = soil moisture content (%).

Penner (1970) measured thermal conductivities of clayey soils between $0°C$ and $-22°C$. Penner observed that the thermal conductivity changed significantly between $0°C$ and $-2°C$. At temperatures below $-2°C$, the change in thermal conductivity was small. The temperature change between $0°C$ and $-2°C$ corresponds to the finite, fusion temperature range of the pore fluid. This leads to the conclusion that thermal conductivity between $0°C$ and $-2°C$ is related to the amount of unfrozen water in the soil. In Penner's soils (Leda clay and Sudbury silty clay), the majority of the pore fluid had changed phase at $-2°C$, and therefore the change in thermal conductivity below $-2°C$ is small. Penner comments that this unfrozen water-temperature relationship for thermal conductivity is an essential consideration while studying the mechanics of frost heave which occurs in this narrow temperature range.

Nixon and McRoberts (1973) also showed that the thermal conductivity of a soil is a function of the unfrozen water content, which in turn is a function of the temperature. However, Nixon and McRoberts have concluded that the magnitude and the temperature dependence is insignificant for most geotechnical applications.

2.2.2   Volumetric Latent Heat of Fusion

The volumetric latent heat of fusion (Lv) represents the amount of heat that must be supplied to, or removed from, a unit volume of soil in order to melt the ice or freeze the water contained within the soil matrix. The volumetric latent heat of a soil is a function of the amount of water contained in a given volume of soil. This relationship is given by

$$Lv = \rho_{dry} \, (w/100) \, L_f \qquad\qquad (2.4)$$

where ρdry = soil dry density and

L_f = latent heat of fusion of pore fluid.

The units of volumetric latent heat are kJ/m^3 (BTU/ft^3) and represent the energy required to change the phase of the pore fluid. The latent heat of fusion for water is given as 334 kJ/kg at 0°C (143.4 BTU's per pound at 32°F). Figure 2.1 depicts the relationship given in Equation 2.4 between volumetric latent heat, moisture content, and soil dry density over a range of common soil values.

Under certain conditions, the phase change of the soil moisture may occur over a temperature range rather than at a specific fusion temperature. This freezing point depression may be due to the presence of solutes in the pore water or films of adsorbed water on the soil particle surface of
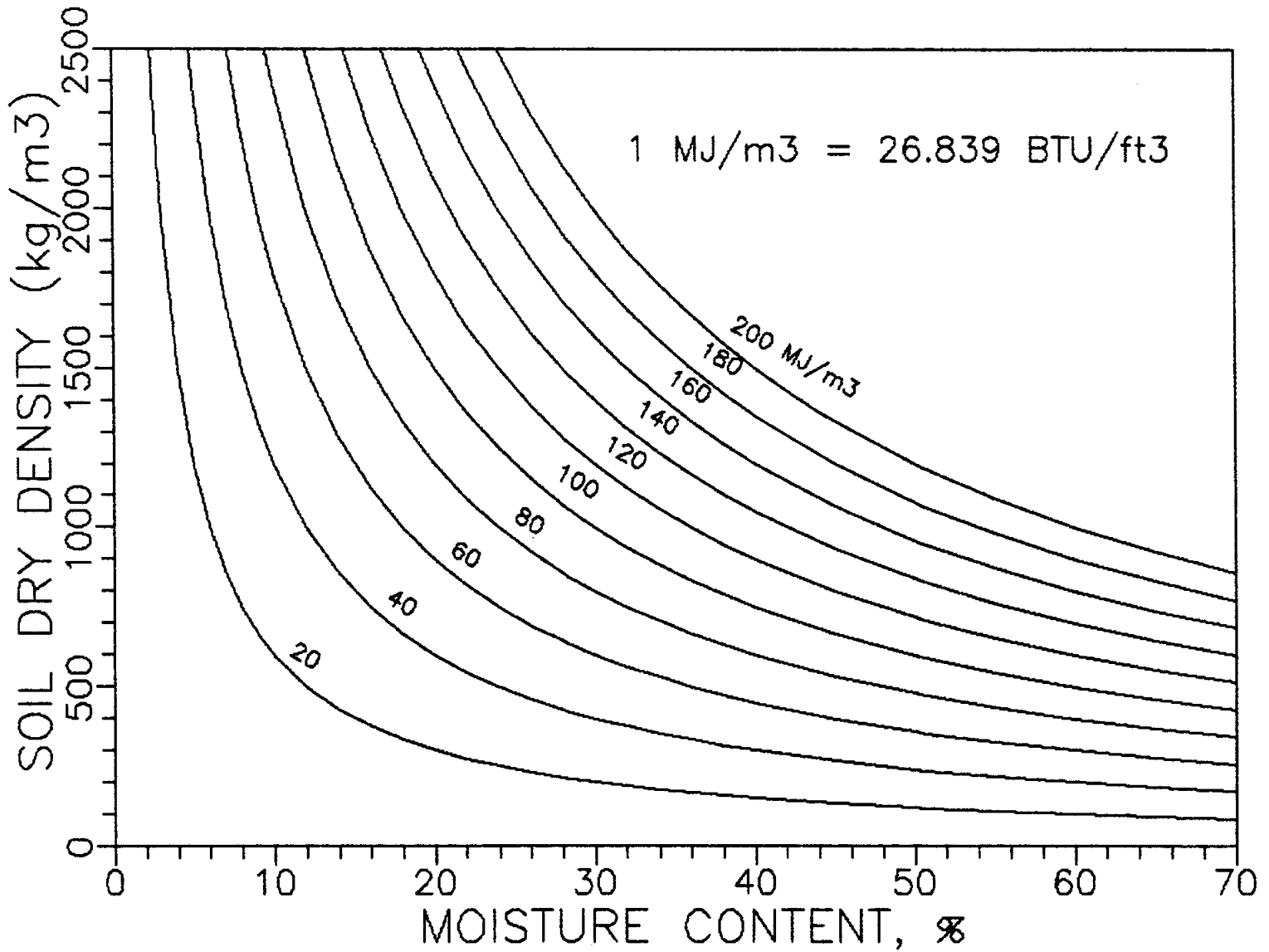
Figure 2.1 Volumetric latent heat of fusion of soil.

fine-grained soils. In this case, Phukan (1985) indicates that the volumetric latent heat of fusion should be expressed as

$$Lv = \rho_{dry} \; (w/100) \; (1-w_u/100) \; L_f \qquad (2.5)$$

where w_u = unfrozen moisture content (%).

2.2.3 Specific Heat

The specific heat (c) of a substance is defined as the unitless ratio of the heat energy required to cause a unit change in temperature of a unit mass of substance to the heat energy required to change the same unit mass of water the same unit change in temperature. Table 2.2 gives values of specific heat for various common materials (Johnston, 1981).

Table 2.2

Specific Heat Values for Some Common Materials

Material	Specific Heat
Water	1.00
Ice	0.50
Soil Minerals	0.17
Air	0.24
Concrete	0.21
Asphalt	0.40
Extruded Polystyrene	0.24
Organic Soil	0.40

2.2.4 Heat Capacity

The heat capacity (C) of a material is the amount of heat energy required to raise the temperature of a unit mass by one degree. The most common units of heat capacity are kJ/kg-K (Btu/lb.-F). The heat capacity of a substance is equal to the specific heat of that substance multiplied by the heat capacity of water which is 4.187 kJ/kg-K (1 Btu/lb.-F). The heat capacities of selected substances (Johnston, 1981) are presented in Table 2.3.

Table 2.3

Heat Capacities of Various Substances

Material	kJ/kg-K	Btu/lb.-F
Water	4.187	1.00
Ice	2.094	0.50
Soil Minerals	0.710	0.17
Air	1.0	0.24
Concrete	0.895	0.21
Asphalt	1.674	0.40
Extruded Polystyrene	1.0	0.24
Organic Soil Solids	1.674	0.40

The ability of a material to store thermal energy can also be represented volumetrically. This is done by multiplying the heat capacity (kJ/kg-K) by the density of

the material (kg/m^3) resulting in units of kJ/m^3-K $(Btu/ft^3$-F).

A soil is a composition of several materials. Thus the equation for volumetric heat capacity of a soil must account for the contribution of each substance. It was stated above that the heat capacity of water is twice that of ice. Therefore, the phase state of the pore water is important in calculating the volumetric heat capacity. The following equations illustrate how the volumetric heat capacity of a soil is calculated for a soil with a discrete fusion temperature.

For frozen soil:

$$C_{v,f} = \rho_{dry} [C_s + \frac{(Ci)(w)}{100}] \qquad (2.6a)$$

and for a thawed soil:

$$C_{v,t} = \rho_{dry} [C_s + \frac{(Cw)(w)}{100}] \qquad (2.6b)$$

where: ρ_{dry} = soil dry density,

$C_{v,f}$ = volumetric heat capacity of frozen soil,

$C_{v,t}$ = volumetric heat capacity of thawed soil,

w = percent moisture by dry weight,

C_s = heat capacity of mineral grains,

C_i = heat capacity of ice, and

C_w = heat capacity of water.

Although air may be a large portion of the soil volumetrically, its mass fraction and volumetric heat capacity contribution to the soil is small relative to the water and the soil grains. Therefore, the effects of air are excluded from the above calculations.

2.2.5 Thermal Diffusivity

The ease with which a soil will undergo a change in temperature is called thermal diffusivity. Thermal diffusivity is proportional to the thermal conductivity and inversely proportional to the volumetric heat capacity and is given by the following equation:

$$\alpha = \frac{k}{C_v} \qquad (2.7)$$

where α = thermal diffusivity,

k = thermal conductivity, and

C_v = volumetric heat capacity of the soil.

The most common units of thermal diffusivity are m^2/hr (ft^2/hr).

The thermal diffusivity will be different for a fine-grain soil and a coarse-grain soil because the thermal conductivity is related to the soil's texture (Kersten, 1947).

A soil will exhibit a different thermal conductivity and volumetric heat capacity depending on whether the pore fluid is frozen or thawed. Likewise, the thermal diffusivity of a soil will also be different in the frozen and unfrozen states.

The diffusivity of water is only one-eighth that of ice (Johnston, 1981). Therefore, the thermal diffusivity of thawed ground is considerably lower than that of frozen ground. In other words, given the same quantity of heat energy applied to the same volume of soil, a frozen soil will experience a faster rate of temperature change than a thawed soil. Also, coarse-grain soils have slightly higher diffusivity values than fine-grain soils at the same dry density and moisture content.

2.2.6 Enthalpy

All materials above absolute zero contain some thermal energy. The temperature of a substance indicates the relative magnitude of its thermal energy. A change in internal energy (enthalpy), H, of a substance at a constant pressure will cause a similar change in the temperature at a rate proportional to the specific heat. Conversely, a change in temperature will cause a proportionate change in enthalpy. This relationship is shown by the following

equation:

$$C_{v_p} = (dH/dT)_p \qquad\qquad (2.8)$$

where: C_{v_p} = volumetric specific heat at constant pressure,

dH = change in enthalpy per unit volume, and

dT = change in temperature.

Enthalpy has units of kJ/m^3 (Btu/ft^3). Van Wylen (1985) states that the specific heat with constant pressure and constant volume of solids and liquids are nearly equal. Therefore, the constant pressure subscript (p) can be dropped.

In this study, the specific heat was determined on a volumetric basis and the enthalpy at the cold side of the fusion temperature (0°C) is zero. The volumetric enthalpy increases above 0°C at a rate of $C_{v,t}$ times the unit change in temperature where $C_{v,t}$ is the volumetric specific heat of the thawed soil. Below 0°C, enthalpy increases negatively at a rate of $(C_{v,f})$ (dt) where $C_{v,f}$ is the volumetric specific heat of the frozen soil. A break in continuity in the enthalpy-temperature relationship occurs at temperatures representing phase change. Using the relationships given in Equation 2.8, Figure 2.2 illustrates volumetric enthalpy as
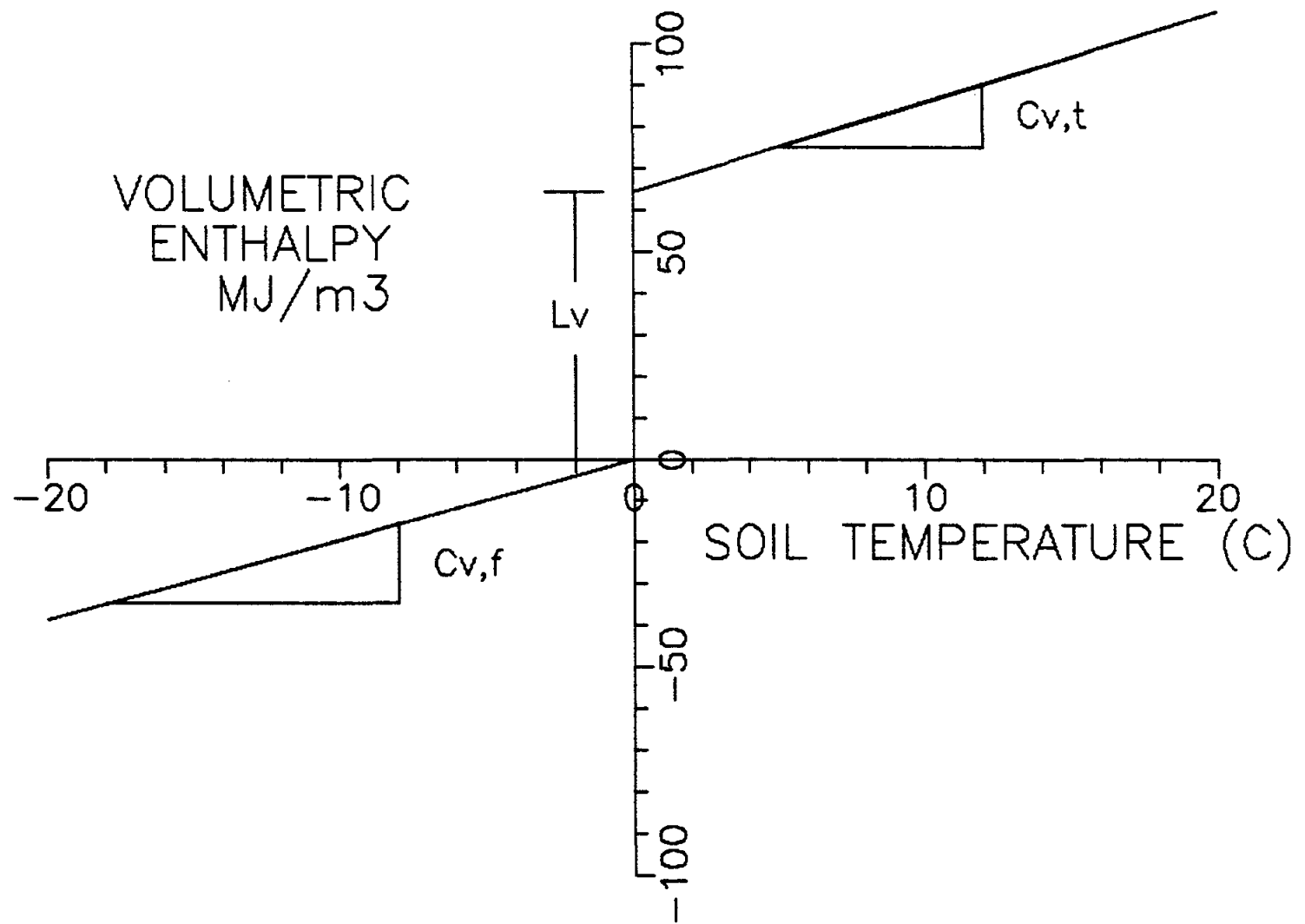
Figure 2.2 Enthalpy-temperature relationships for a soil system.

a function of temperature for a soil. This figure assumes that all the pore fluid changes phase at a discrete fusion temperature (0°C). A soil with a freezing point depression or a pore fluid which changes phase over a temperature range can also be represented by a figure similar to Figure 2.2 as long as the enthalpy-temperature relationships are known.

2.3 Conductive Heat Transfer in Cylindrical Coordinates

Conductive heat transfer in a soil system can be analyzed under two different flow conditions; steady-state and nonsteady-state. Steady-state analyses can be used to describe heat flow and the temperature distribution when the imposed thermal gradient or individual soil temperatures do not vary with time. The steady-state condition represents the situation when the quantity of energy entering a soil element is equal to the energy leaving the element. Analysis with steady-state conditions is relatively simple but is limited to applications that do not address moving phase change boundaries.

Nonsteady-state analyses involve a time-varying thermal gradient, changes in heat storage, and can also be used to locate the phase change boundary with respect to time and space. Nonsteady-state heat transfer with phase change considerations can be further subdivided into two groups; exact solutions and approximate solutions. Exact solutions

for heat transfer analysis with moving phase change boundaries in a cylindrical symmetry exist only for the case where the heat sink or source is considered to be a line. Approximate solutions must be used when the heat source or sink has a radius greater than zero.

2.3.1 Steady-state Heat Flow

Steady-state heat flow in a soil mass occurs when the imposed thermal gradient becomes stationary. The quantity of heat entering a unit volume of soil is equal to the quantity of heat leaving the same unit volume. Therefore, the net change in heat storage of the unit volume is zero with respect to time. At this point, thermal equilibrium has been achieved. Fourier's law can be applied to the radial geometry shown in Figure 2.3. This geometry represents a cylinder surrounded by an infinite, homogeneous soil mass. In this figure, outward cooling is considered and the temperature increases with increasing radial distance from the center. The radius r_p represents the exterior surface of the heat sink, r is the radius of interest, and r_2 is the outer radius where the temperature is known or assumed constant. T_p, T_r, and T_2 are the temperatures at the radii, r_p, r, and r_2 respectively. As stated in section 2.1.1, Fourier's law of conduction is
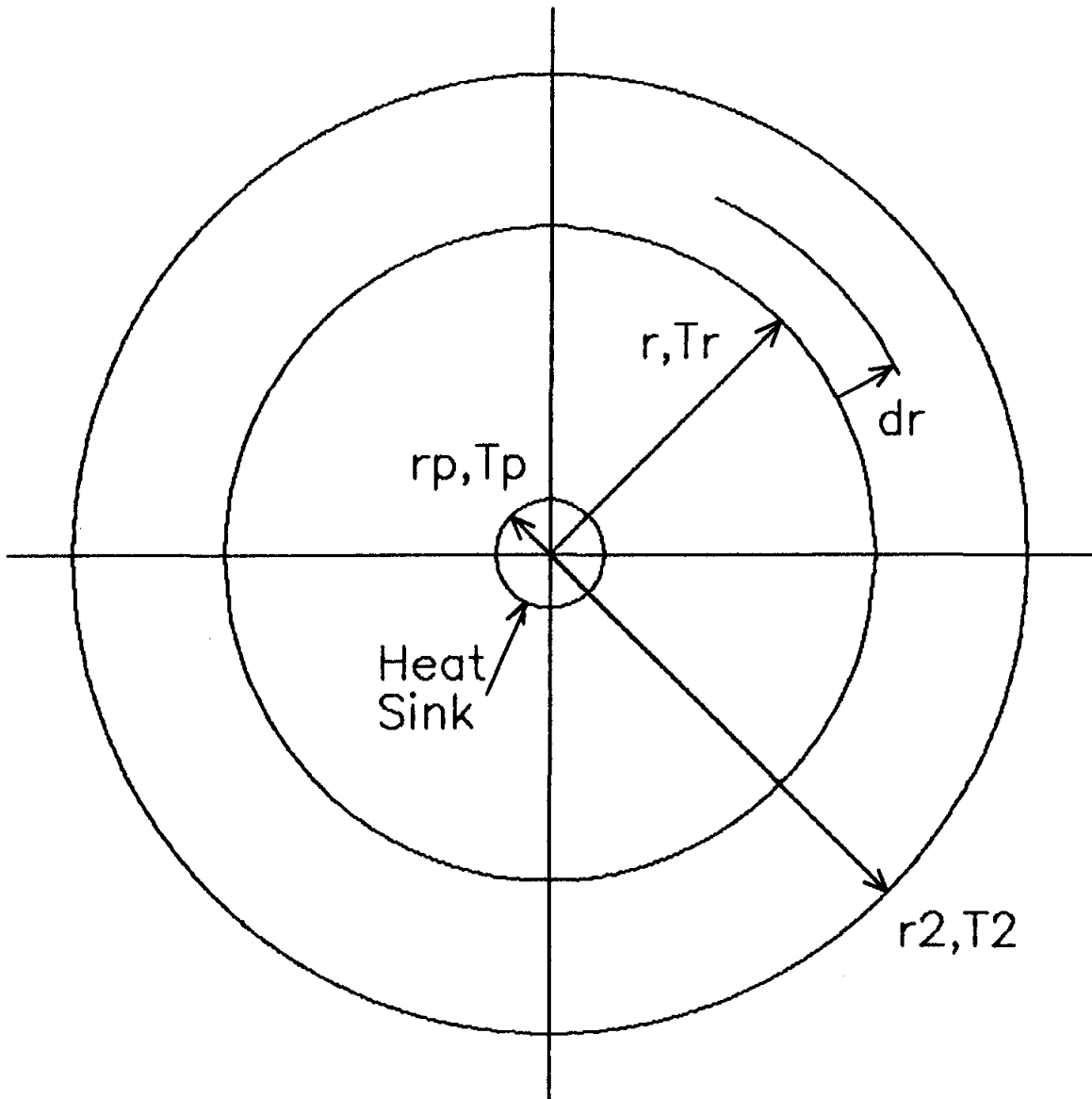
Figure 2.3 Radial geometry for outward freezing in
an infinite, homogeneous soil mass.

given as

$$Q = -k \ A \ dT/dx \qquad (2.9)$$

With radial flow, the cross-sectional area perpendicular to the direction of heat is a function of the radius (r). In cylindrical coordinates, the steady-state heat transfer relationship is given by

$$Q = -k \ 2\pi r \ \ell \ dT/dr \qquad (2.10)$$

where   r = radial distance from center, and

ℓ = length of system orthogonal to heat flow.

Integrating Equation 2.10 between r_p and r yields

$$\frac{\ln \ (r/r_p)}{2 \pi k \ell} = \frac{T_r - T_p}{Q} \qquad (2.11)$$

Letting,

$$R = \frac{\ln \ (r/r_p)}{2 \pi k \ell} \qquad (2.12)$$

and solving for Q results in the heat conduction equation in cylindrical coordinates (Equation 2.13).

$$Q = \frac{T_r - T_p}{R} \qquad (2.13)$$

where R = thermal resistance of the soil mass in cylindrical coordinates.

Under steady-state conditions, the thermal gradient is stationary and can be described with the aid of Figure 2.4. This figure considers a volume of soil having a unit thickness perpendicular to the figure, bounded by radii r and r_2, and two arbitrary rays. By definition, the heat energy crossing radius r_2 (Q_{in}) is equal to the heat energy crossing radius r (Q_{out}). Equating the two heat flows gives

$$\frac{T_r - T_p}{\frac{\ln (r/r_p)}{2\pi k \ell}} = Q_r = \frac{T_2 - T_p}{\frac{\ln (r_2/r_p)}{2\pi k \ell}} \qquad (2.14)$$

Solving for T_r in Equation 2.14 yields,

$$T_r = T_p + \left[(T_2 - T_p) \frac{\ln (r/r_p)}{\ln (r_2/r_p)} \right] \qquad (2.15)$$
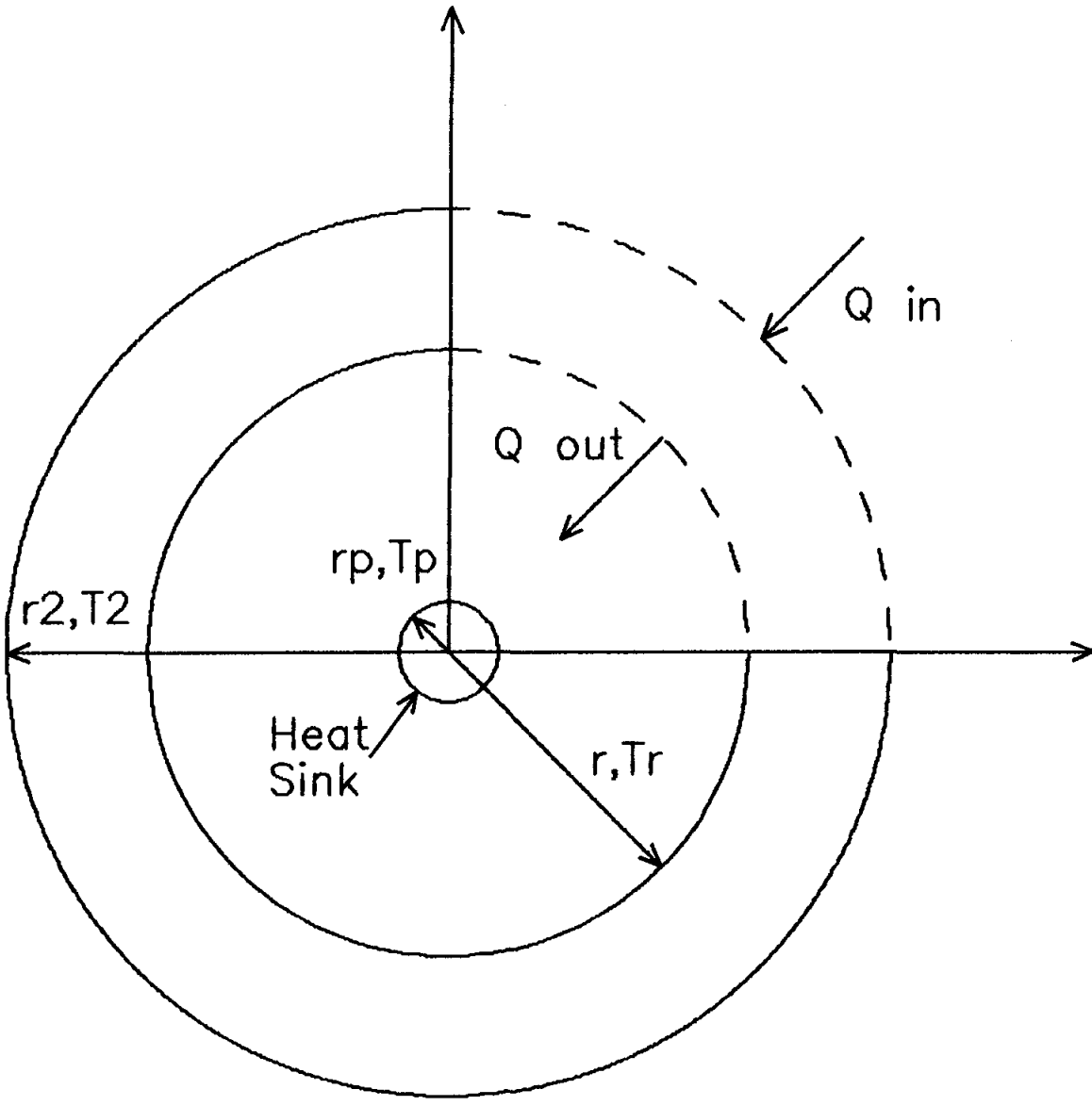
Figure 2.4   Nomenclature for steady-state heat transfer
with radial geometry.

This equation (2.15) is used to calculate the temperature (T_r) at any radius r only if two temperatures and corresponding radii are known and the thermal conductivity is uniform throughout the soil mass. Alternatively, solving for radius r in Equation 2.14 gives an equation which locates the radius for any temperature (T_r).

$$r = e^{\left[\dfrac{T_r-T_p}{T_2-T_p}\ \ln\ (r_2/r_p)\ +\ \ln\ r_p\right]}$$ (2.16)

The steady-state heat conduction equations are limited in their application because they do not consider moving phase change boundaries or changes in thermal storage. This is a major disadvantage for thermal analysis in cold regions where the rate of melting and freezing of pore fluids is an important consideration.

2.3.2 Heat Transfer With Phase Change

No general, exact analytical solution has been formulated that addresses phase change around a finite cylinder surrounded by an infinite, homogeneous soil mass (Lunardini, 1981). The boundary between different phases of

a substance is constantly shifting with the addition or removal of heat energy. Exact solutions expressing the relationships between temperature, location, and time are limited to a few simple geometric situations. These solutions tend to be nonlinear and transcendental.

In 1860, Franz Neumann provided a general solution for a semi-infinite body, initially at a nonfusion temperature, subjected to a step change in surface temperature such that a change in phase would occur (Zarling, 1987). In the early 1900's, J. Stefan also provided a solution for semi-infinite medium exposed to a step change in its surface temperatures. In contrast to Neumann, Stefan assumed that the initial temperature of the medium was at its fusion temperature. This assumption implies that all the energy conducted through the system is used in changing the phase of the substance.

Ozisik and Uzzel, Jr. (1979) provided an exact solution for solidification due to a line source ($r_p=0$, Figure 2.3) in cylindrically symmetric medium with phase change occurring over an extended, finite temperature range. Because of the mathematical complexities of an exact solution in cylindrical coordinates, researchers have typically used approximate solutions.

A Stefan-type solution (quasi-steady solution) is an example of an approximate solution which does not solve the

phase change parameters exactly. The Stefan-type solution
assumes that all the heat energy conducted through the
medium is liberated or stored during the phase change
process. This assumption over estimates the radius of
freezing or thawing since the sensible heat of the material
is neglected. However, the accuracy of the Stefan-type
solution improves as the ratio of sensible heat to latent
heat goes to zero. This ratio is known as the Stefan number
and is given as;

for the freezing case:

$$Ste\# = \frac{C_{v,f} (T_f - T_p)}{L_v} \qquad (2.17a)$$

and for the thawing case:

$$Ste\# = \frac{C_{v,t} (T_p - T_f)}{L_v} \qquad (2.17b)$$

where T_p = pipe temperature and

T_f = fusion temperature.

A Stefan-type solution can be derived for an infinite,
homogeneous material in cylindrical coordinates with outward
freezing from a finite cylinder (Figure 2.5).
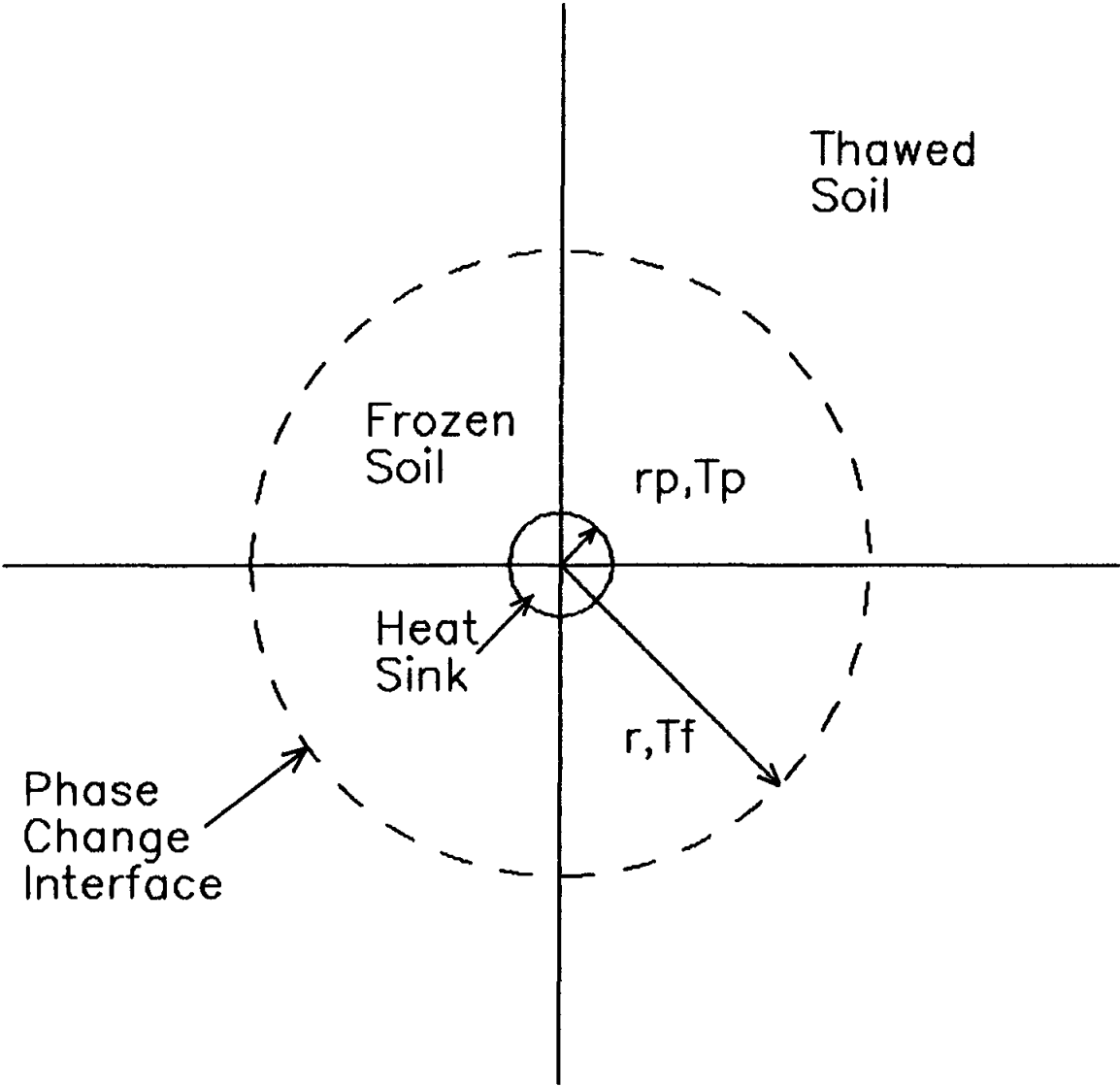
Figure 2.5 Outward, radial freezing with phase change
in an infinite, homogeneous soil mass.

Setting

$$Q_{cond} = Q_{fusion} \qquad (2.18)$$

or

$$\frac{T_f - T_p}{\dfrac{\ln(r/r_p)}{2\pi k_f \ell}} = 2\pi L_v \ell r \frac{dr}{dt} \qquad (2.19)$$

where Q_{cond} = conductive heat energy,

Q_{fusion} = heat energy required for phase change,

T_f = fusion temperature,

T_p = pipe temperature ($T_p < T_f$),

r = radius of freeze front,

r_p = outside radius of pipe,

k_f = thermal conductivity of frozen soil,

ℓ = length of pipe,

L_v = volumetric latent heat of fusion, and

t = time.

Equating both sides of Equation 2.19 and rearranging terms results in

$$(T_f - T_p)dt = \frac{L_v}{k_f} [r \ln(r) - r \ln(r_p)] dr \qquad (2.20)$$

Integrating Equation 2.20 between r_p and r yields the Stefan-type solution for outward radial freezing in an infinite, homogeneous medium from a finite cylinder.

$$(T_f-T_p) \ t \ = \ \frac{L_v}{k_f} \left[\frac{r^2}{2} \ \ln(r/r_p) \ - \ \frac{(r^2 - r_p^2)}{4} \right] \qquad (2.21)$$

In some applications, the outward radial extent of freezing, given by Equation 2.21, is limited by the left hand term, $(T_f-T_p)t$. This expression is sometimes given in freezing degree-days (FDD) which is the cumulative measure of the time and temperature difference that the temperature remains below freezing, $0°C$ ($32°F$).

The accuracy of the Stefan-type solution can be enhanced by accounting for the sensible heat effects in both the frozen and thawed regions. Thornton (1976) estimates these heat effects and adds them to the volumetric latent heat of fusion to produce an "effective" latent heat of fusion. This correction is used in place of L_v and is given by

$$L_v' \ = \ L_v \ + \ 0.5 \ C_{v,f}(T_f-T_p) \ + \ C_{v,t}(T_g-T_f) \qquad (2.22)$$

where T_g = original ground temperature outside radius of fusion.

The Stefan-type solution can also be used for outward radial freezing in a multilayered soil system such as in Figure 2.6. If region 1 is initially frozen, the Stefan solution is applied to region 2 from r_1 outward and region 1 exhibits only thermal resistance to the movement of heat energy. This is given by

$$\frac{T_f - T_p}{\dfrac{\ln(r_1/r_p)}{2 \pi k_1 \ell} + \dfrac{\ln(r/r_1)}{2 \pi k_2 \ell}} = 2 \pi L_{v2} \ell r \frac{dr}{dt} \qquad (2.23)$$

Rearranging the terms

$$(T_f - T_p)dt = (\frac{L_{v2}}{k_1})[\ln(r_1/r_p)] \, r + (\frac{L_{v2}}{k_2})[r\ln(r) - r\ln(r_1)] \, dr \qquad (2.24)$$

Integrating Equation 2.24 between r_1 and r results in following:

$$(T_f - T_p)t = \frac{(L_{v2})(r^2 - r_1^2)}{2 \, k_2} \ln(r_1/r_p) +$$

$$\frac{L_{v2}}{k_2} [\frac{r^2}{2} \ln(r/r_2) - (\frac{r^2 + r_2^2}{4})] \qquad (2.25)$$

where subscripts 1 = region 1 and

2 = region 2.
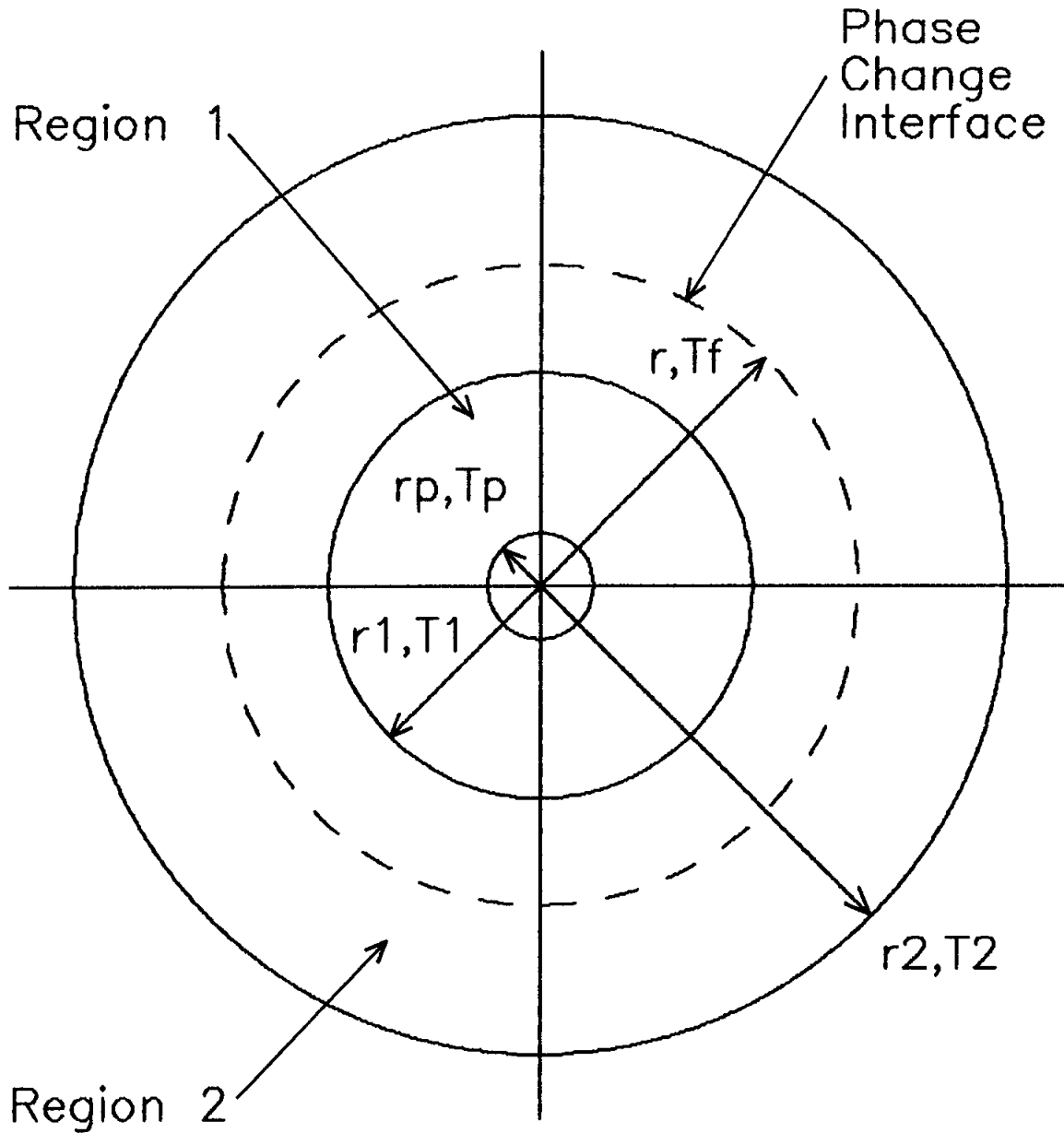
Figure 2.6   Nomenclature for outward freezing in a
              cylinderically layered soil.

If however, region 1 is initially thawed the problem must be solved by breaking it into two parts. First, region 1 is frozen from r_p to r_1 using Equation 2.21. Then, region 1 is treated as a thermal resistance layer and Equation 2.25 is used for freezing outward from r_1.

Heuer et al. (1985) use a correction for the freezing radius originally developed by Pekeris and Slichter (1939). This correction accounts for the sensible heat effects and is given by

$$r' = r \ (1-0.12 \ Ste\#)^{0.5} \qquad (2.26)$$

where r' = the corrected radius and

r = the radius calculated from Stefan-type solution.

Other approximate solutions exists for phase change in cylindrical coordinates. The reader is referred to Lunardini (1980) and Zarling (1987) for additional approaches.

2.3.3 Explicit Finite Difference Technique

Numerical analysis techniques can be used to model thermal systems with geometries that do not lend themselves to simple analytical solutions. Finite difference techniques using enthalpy have been written to model complex geometries and time-varying heat fluxes. Also, the enthalpy

approach can accurately monitor the moving phase change boundaries. The differential equation for the first law of thermodynamics written in cylindrical coordinates is given as (Callinan, 1983)

$$\frac{1}{r} \; \frac{(k \; r \; \partial T/\partial r)}{\partial r} + \frac{(k \; \partial T/\partial z)}{\partial z} = \frac{\partial H}{\partial t} \qquad (2.27)$$

where   H = volumetric enthalpy,

   k = thermal conductivity,

   T = temperature,

   t = time,

   r = radial distance, and

   z = axial distance.

Writing Equation 2.27 in an explicit finite difference form gives

$$H_{i,j}^{m+1} = H_{i,j}^{m} + \frac{k \, \Delta t}{\Delta r^2} \left[T_{i,j-1}^{m} + (1 - \frac{\Delta r}{2r_i}) \; T_{i-1,j}^{m} - 4T_{i,j}^{m} \right.$$

$$\left. + (1 + \frac{\Delta r}{2r_i}) \; T_{i+1,j}^{m} + T_{i,j+1}^{m} \right] \qquad (2.28)$$

where   i = radial position,

   j = axial position, and

   m = time position.

The temperatures are calculated using the enthalpy relationships given in Equation 2.8 (Section 2.2.6) and are summarized as follows:

if $0 \leq H \leq Lv$ then $T = 0°C$,

H > L_v then $T = (H-L_v)/C_{v,t}$

H < 0   then $T = H/C_{v,f}$

where C_v = volumetric heat capacity, and

subscribts   t = thawed and

             f = frozen.

Or these conditional statements could be written in terms of temperature:

if $T = 0°C$ then $0 \leq H \leq L_v$,

T > $0°C$ then $H = (T)(C_{v,t}) + L_v$, and

T < $0°C$ then $H = (T)(C_{v,f})$.

Stability of the explicit finite difference (Voller and Cross, 1981) is assumed when the time step is limited to

$$\Delta t < \frac{\Delta r^2 \, C_v}{2 \, k} \quad . \tag{2.29}$$

Callinan (1983) uses this numerical approach to model the thermal regime of a prebored, vertical pipe pile in

permafrost with a sand-water slurry backfill. The analysis included determining freeze-back rates of the slurry, thawing and freezing depths and radii due to seasonal ground surface temperatures, and the effects of the piling system on the thermal regime of the surrounding ground.

When the heat sink cylinder is buried in an infinite medium or the axial heat flow component is insignificant, the differential equation (Equation 2.27) reduces to

$$\frac{1}{r} \ \frac{(k \ r \ \partial T/\partial r)}{\partial r} = \frac{\partial H}{\partial t} \qquad (2.30)$$

Likewise, the explicit finite difference equation becomes:

$$H_i^{m+1} = H_i^m + \frac{k \ \Delta t}{\Delta r^2} \left[(1 - \frac{\Delta r}{2r_i}) \ T_{i-1}^m - 2T_i^m \right.$$

$$\left. + (1 + \frac{\Delta r}{2r_i}) \ T_{i+1}^m \right] \qquad (2.31)$$

CHAPTER 3

MOISTURE MIGRATION IN FREEZING SOILS

It has been known for many years that there exists a
potential for moisture migration in some types of soils
under certain freezing and environmental conditions. This
was first postulated because the amount of heave observed in
a freezing soil was more than could be explained due to the
volume change associated with the phase change of the pore
water (Taber, 1929; Watkins, 1931; and Casagrande, 1931).
The earliest scientists and engineers, in an attempt to
discover the mechanics of frost heave, were able to observe
moisture movements and the subsequent development of
segregated ice lenses in the vicinity of the zero degree
Celsius isotherm (freeze front). Frost heave is defined as
the volumetric change and resulting soil mass movements in
excess of that which can be attributed to the phase change
of the initial, insitu pore water (Miller, 1972). A theory
explaining frost heave must include a mechanism and a
vehicle for moisture migration towards the freezing front in
the soil mass. However, moisture migration towards the
freezing front may occur without resulting in frost heave or
segregated ice lenses.

Taber (1929) observed moisture migration while freezing

41

fine-grained soils. Taber concluded that the driving mechanism for moisture migration towards the freezing front was capillary action. Benkelman and Olmstead (1931) proposed that alternate freezing and thawing in any type of saturated soil will produce excessive frost heave. Benkelman and Olmstead also stated that heaving was independent of grain size and moisture-soil characteristics. This theory was not readily accepted (Taber, 1931; Casagrande, 1931; and Watkins, 1931) and was later disproved by Beskow (1938).

Based upon his experiments, Casagrande (1931) stated that:

> "Under natural freezing conditions and with sufficient water supply one should expect considerable ice segregation in non-uniform soil containing more than 3 percent of grains smaller than 0.02 mm, and in very uniform soils containing more than 10 percent smaller than 0.02 mm. No ice segregation was observed in soils containing less than 1 percent of grains smaller than 0.02 mm, even if the ground water level was as high as the frost line."

Three major factors are essential for frost heave and the formation of segregated ice lens features (Penner, 1959). They are

    1) a water supply,

    2) a frost-susceptible soil, and

    3) below-freezing temperatures.

Many factors influence the magnitude and rate of

moisture migration and frost heave. These factors can be divided into those which are inherent to the soil-water system (intrinsic factors) and those which are related to the environment under which the soil-water system is exposed (extrinsic factors). Intrinsic factors include such parameters as soil mineralogy, grain size, grain size distribution, soil density, hydraulic conductivity, freezing point depression, pore fluid composition, and soil-moisture characteristics. Extrinsic factors include such variables as heat extraction rates, temperature gradients, surcharge pressures, and the accessibility of moisture.

Much research has occurred on moisture-temperature relationships since Taber's first paper. Because frost heave and moisture migration are a function of many variables, many of which depend on each other, researchers have attempted to isolate a single factor and study the parametric effect on the entire process. As a result, an understanding of the influences of many of these variables exists today. However, a complete, working model of frost heave which can accurately predict heave rates and magnitudes in a natural soil does not currently exist due in part to the mathematical complexities of coupled heat and mass flow in a soil which is inherently heterogeneous and anisotropic. The reader is referred to Nixon (1987) for an up to date review of the status regarding ground freezing and frost heaving studies.

This chapter is divided into three sections. Section 1 describes some of the intrinsic factors of the soil-water system which effect moisture migration and frost heave. Section 2 discloses the influencing effects of the extrinsic variables. The last section discusses several mechanisms which attempt to explain moisture migration in a freezing soil.

3.1 Soil-Water Properties Effecting Moisture Migration

In explaining the mechanisms for moisture migration and frost heave, all the varying properties of the soil-water system must be accounted for. The rate and magnitude of frost heave and moisture migration is a function of these variables. Some of the more pertinent parameters include: size of soil grains, grain size distribution, soil density, water content, degree of saturation, saturated and unsaturated hydraulic conductivities, soil mineralogy, and pore fluid composition.

Altering one of the soil-water parameters will change the thermal and physical properties of the entire system and hence may change the outcome of the entire freezing process. For example, increasing the dry density of an unsaturated soil without a change in the given amount of water per volume will lower the gravimetric moisture

content, increase the thermal conductivity, increase the degree of saturation, increase specific surface area, alter the soil-moisture characteristics, and change the unsaturated permeability coefficient.

Researchers studying frost heave and moisture migration have attempted to simplify the problem by studying the effects of a single variable on the other variables and on the entire process. In this way, engineers obtain an understanding of a small piece of the frost heave-moisture migration puzzle. When all the "pieces" are understood, they can be assembled together to get a view of the entire "picture".

3.1.1 Grain Size and Grain Size Distribution

Grain size and grain size distribution characteristics have been the most extensively studied properties of the soil-water system with regard to frost heave and moisture migration.

Taber (1929), working with many blends of fine-grained and coarse-grained soils, demonstrated that the fine-grained soils exhibited a greater potential to develop ice segregation due to freezing than the relatively coarser grained soils under similar freezing conditions.

The frost heave susceptibility criteria given by Casagrande (1931), mentioned earlier, was also based on

grain size. Casagrande reported no ice segregation occurred in soils containing less than one percent of grains smaller than 0.02 mm. He also showed that a well-graded sand was more frost susceptible than a similar sized sand with a uniform grain size distribution. Casagrande further concluded that a well graded soil has more grain to grain contact than a poorly graded or gap-graded soil, and therefore, provides a better defined and more continuous liquid phase necessary for capillary water transportation.

Ice segregation and frost heave became increasingly evident in soils containing higher percentages of grain sizes between 0.05 and 0.1 mm (Beskow, 1938). Beskow's experiments showed that heaving became greater as the average grain size diameter decreased with maximum heaving occurring in soils with an average particle diameter between 0.005 and to 0.002 mm. The magnitude of frost heave decreased with an increase in the percentage of particles having an average diameter smaller than this range. Beskow postulated that the decrease in frost heave with grain size diameters smaller than 0.005 to 0.002 mm was a combination of decreasing hydraulic conductivities and immobile water films adsorbed on the finer-grained soils. Beskow's results are shown in Figure 3.1.

Linell and Kaplar (1959) reported that the conclusions of their experiments agreed with earlier workers. Namely,
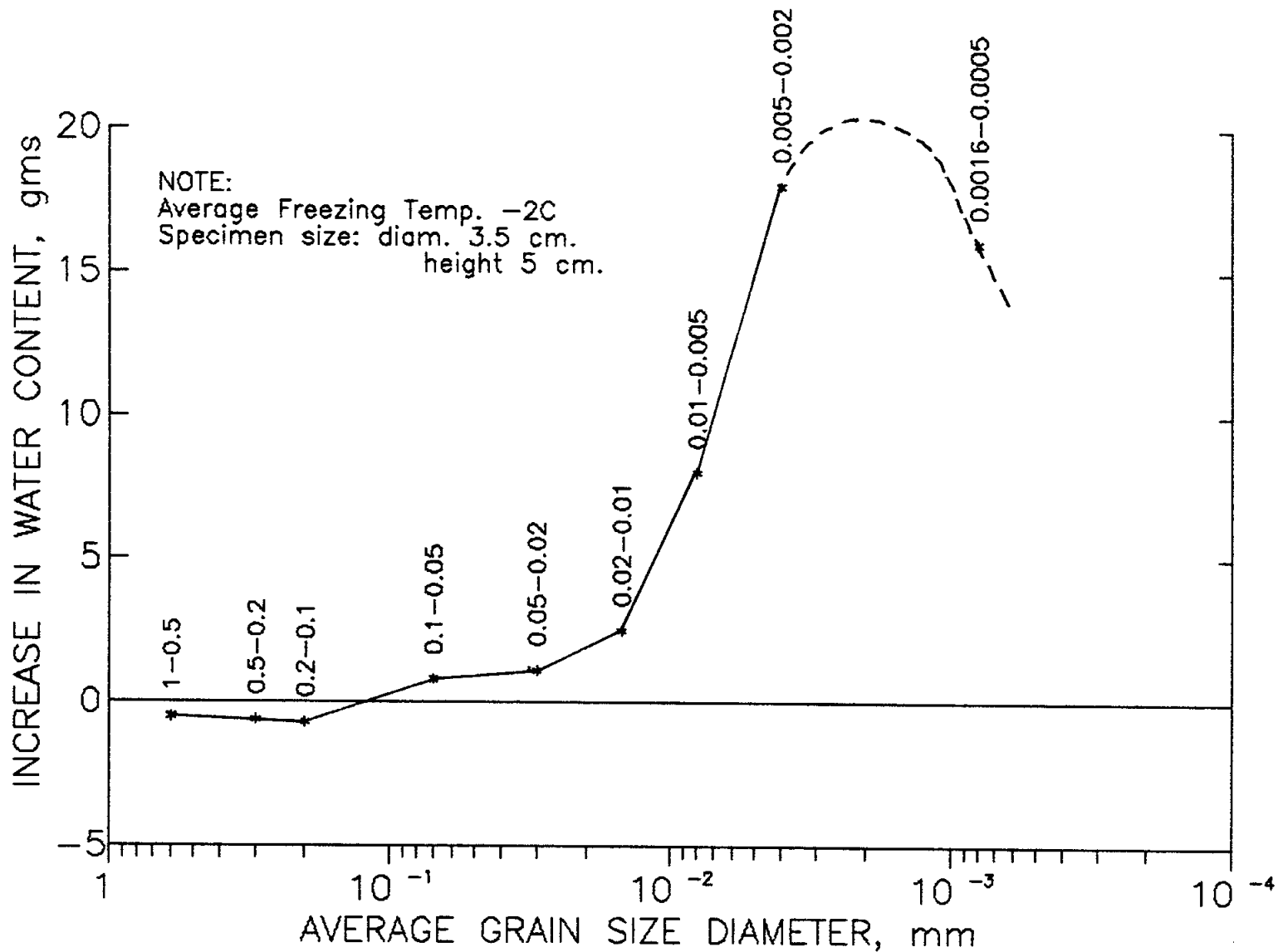
Figure 3.1 Moisture flux-average grain size diameter relationships
for pure soil fractions after Beskow (1938).

that ice segregation intensity is dependent upon both the percent of particles smaller than 0.02 mm and the grain size distribution within the soil. In addition, it was shown that silts and low plasticity (lean) clays had the highest heave rates. While high plasticity (fat) clays showed lower heave rates than silts and lean clays. As with Beskow (1938), Linell and Kaplar believed this was due to a decrease in hydraulic conductivity and an increase in surface tensions.

Grain size and grain size distribution are the most popular soil index properties on which to establish a frost susceptibility criteria (Chamberlain, 1981). Grain size analysis is easily determined in the laboratory and is a common index property used in engineering design and construction. Because frost heave is a function of many soil-water system and environmental variables, the grain size based frost susceptibility criteria should be used only as a guideline and not as a theoretically determined value.

Some soil-water system parameters such as; specific surface area, capillarity characteristics, and soil fabric; are a function of grain sizes and grain size distributions.

3.1.1.1 Specific Surface Area

The specific surface area is defined as the magnitude of soil surface area per unit mass. The most common units

of specific surface area are m^2/gm. The equations for specific surface area are:

for spheres;
$$A_s = \frac{4 \pi r^2}{4/3 \pi r^3 \rho_s} = \frac{3}{r \rho_s}$$
(3.1)

for plates;
$$A_s = \frac{2(1/\ell + 1/w + 1/h)}{\rho_s}$$
(3.2)

where A_s = specific surface area,

r = sphere radius,

ρ_s = mass density of soil particles,

ℓ = particle length,

w = particle width, and

h = particle height.

As can be seen, the specific surface area is a function of grain size and grain shape. Clay minerals are flat or platy particles and exhibit greater surface area per mass than spherical or cubic particles. The greatest attribute of specific surface area is water holding capacity. As the soil grain size decreases, the specific surface area increases and the water retention capability increases. Table 3.1 (Lambe and Whitman, 1969) shows typical specific surface areas of several size particles and associated moisture contents for a 5 Angstrom (1 Angstrom = 10^{-10}m) thick layer of water (about two water molecules thick).

Table 3.1

Specific Surface Areas and Water Contents
of Typical Soil Particle Sizes

Particle	Specific Surface Area m^2/gm	Water Content (%)
0.1 mm sand	0.01	5.7×10^{-4}
0.005 mm silt	0.23	0.01
kaolinite	15	0.75
illite	80	4.0
montmorillonite	800	40

Specific surface area is an important index property of soil and will be discussed later with reference to unfrozen water contents and adsorbed moisture films. Rieke et al. (1983) performed freezing experiments on various mixtures of the fine and coarse grained material and correlated specific surface area to frost susceptibility. The results demonstrated that an increase in specific surface area enhanced frost heave rates. The significance of specific surface area is similar to that of average grain size diameter since specific surface is directly related to grain size and shape.

3.1.1.2 Soil Fabric

Soil fabric is the arrangement of particles in a given soil mass and is related to void continuity, grain contact

frequency, and permeability. Lovell (1983) showed that a given soil could exhibit different frost susceptibility characteristics by altering the soil fabric. Figure 3.2 (after Lovell, 1983) illustrates two vastly different soil fabrics of a given soil in which the porosity, density, grain size and shape, and particle distribution are the same. Lovell commented that varying soil fabrics could be obtained by remolding a natural soil or by applying different compaction techniques. This may prove significant when correlating laboratory results to field conditions.

3.1.1.3 Capillarity

The ability of a continuous water column to exist above a free water surface gives rise to the principle of capillarity. Water particles will "wet" the surface of a solid when the adhesion between the water particle and the solid is greater than the cohesion between the water particle and other water particles. This enables water to rise in a tube with radius r to a height h until equilibrium is reached. Above the phreatic surface, the water column is in tension and the water pressure is negative. The height to which water will rise in a capillary tube is given as:

$$h_c = \frac{2\ S_t\ \cos \Theta}{r\ \rho_s\ g} \qquad (3.3)$$
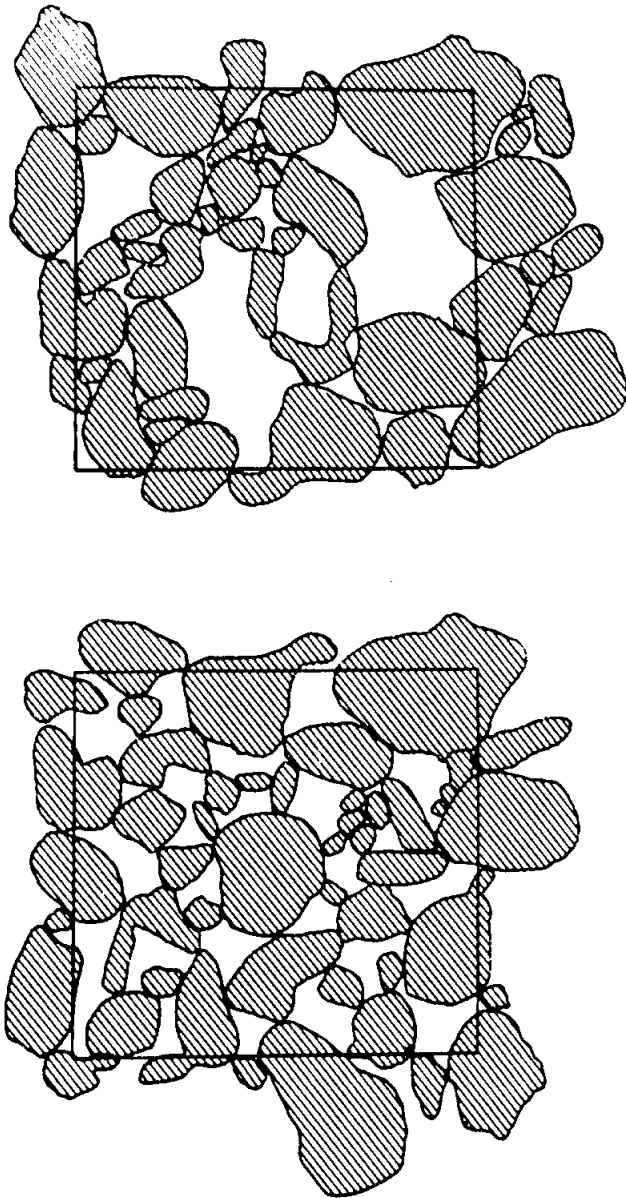
Figure 3.2   Two soils with equivalent index properties
             but with differing soil fabrics after
             Lovell (1983).

where h_c = capillary rise or head,

S_t = surface tension of liquid,

Θ = contact angle between liquid and tube,

r = radius of capillary tube,

ρ_s = mass density of soil particle, and

g = acceleration due to gravity.

In soils, the pores and interconnected voids act as capillary tubes. These voids vary in an almost infinite array of sizes and shapes for a given soil. Therefore a nearly infinite number of capillary heads are possible. Graphs which show moisture content or degree of saturation as a function of capillary heads or negative pore pressures are called soil-moisture characteristic curves. Figure 3.3a (after Lambe and Whitman 1969) illustrates a soil-moisture characteristic curve for two different conditions. The wetting curve represents moisture equilibrium at various points in a column of dry soil after it is placed in contact with a phreatic surface. The drying curve shows moisture equilibrium of an initially saturated soil column allowed to drain also in contact with a free water surface.

The difference in the two types of curves can be explained with the aid of Figure 3.3b. Diagram (i) in Figure 3.3b shows the capillary potential of water in a tube with radius r. Diagram (ii) shows the same tube with a section having a relatively larger pore radius. Initially,
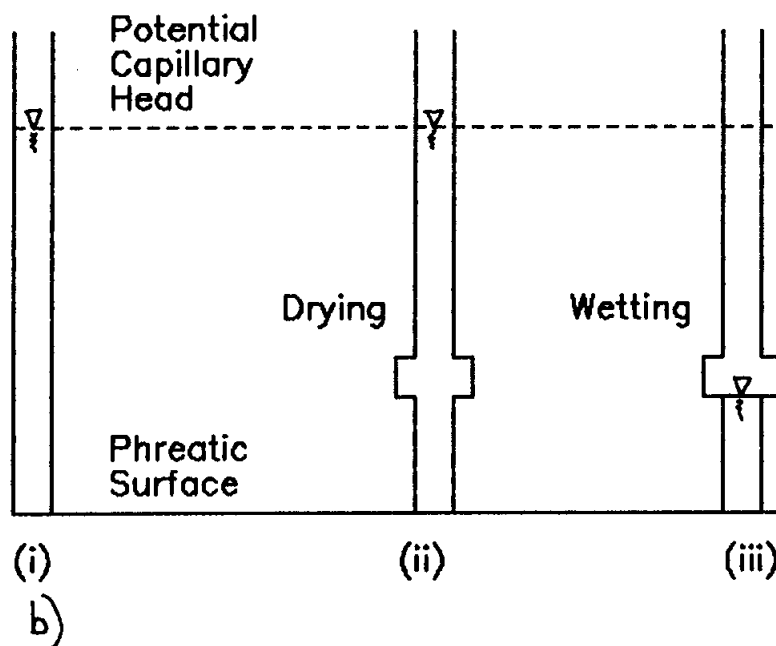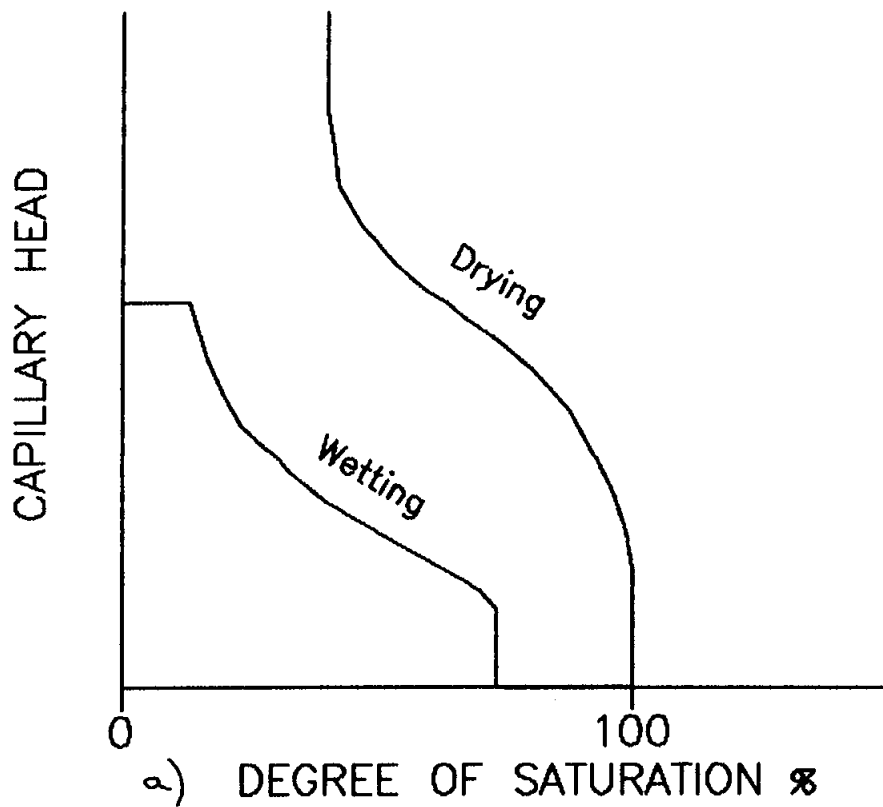
Figure 3.3 Soil-moisture characteristic curve; a) two
types of capillary head and b) the effect of
varying pore sizes on capillarity.

the tube is filled with water and then allowed to drain. As the water level drops, the equilibrium capillary head will equal the potential head. However, during the wetting cycle (diagram iii), the water will only rise up to the larger radius portion and will not have the same equilibrium capillary head as in the drying case.

Capillary water can exist in soil in three modes. When the voids are completely filled with water (saturation=100%) the soil is at capillary saturation. Partial saturation exists when saturation is less than 100% but continuous water films are present. The mode when the water films are discontinuous and air exceeds water in the voids is called water retention.

All frost heave theories include soil capillarity as a liquid moisture transport vehicle for transmitting water to the freezing front. The water supply may be a free water surface existing in the unfrozen soil at some distance below the freeze front (open system), or the water supply could be moisture contained in the surrounding unfrozen soil (closed system). The open system provides an unlimited water supply. The closed system contains a finite amount of water which may be redistributed upon freezing.

Taber (1930) showed the relevance of the capillary vehicle. Taber was able to stop frost heave and moisture migration in a frost susceptible soil by placing a strata of coarse-grained, nonfrost susceptible quartzose sand between

the constant water supply and the freeze front.

Other researchers, Miller (1972), Williams (1972), Penner, (1959), and Gold (1957), have demonstrated the importance of capillarity as a vehicle of moisture transportation. The capillary head is enhanced by an additional negative pore pressures which may develop on the cold side (behind) the freeze front. This negative pressure is the result of thermodynamic equilibrium conditions at the ice-water interface (Nixon, 1987) which will be discussed later.

3.1.2 Soil Dry Density

The dry density of a soil has an indirect effect on the magnitude and rate of frost heave (Linell and Kaplar, 1959). It was mentioned earlier that an increase in dry density reduces the hydraulic conductivity and the porosity, increases the capillary effect, the grain contact points, and specific surface as well as altering the thermal properties of the soil. The effect of density varies with the type of soil. In a summary on the effects of soil density in frost heave tests, Linell and Kaplar (1959) generalize their findings as follows:

1) clayey soils show a decrease in heave rates with an increase in dry density,

2) silts and silty soils exhibit an increase in heave rates with increasing dry density, and

3) in sandy soils, heaving rates increased with dry density up to a maximum value and then decreased with increasing dry density.

The varying effects of dry density on different soil types illustrates the "domino effect" on soil-water variables caused by altering only one variable. The various soils respond differently to decreases in porosity and hydraulic conductivity. Figure 3.4 (after Linell and Kaplar, 1959) shows the results upon which the conclusions were based.

Penner (1959) demonstrated a relationship between dry density and soil moisture suction in a soil comprised of 6 percent clay-size and 94 percent silt-size particles. Penner's results, Figure 3.5, show an increase in suction pressures with increases in dry density which compares with Linell and Kaplar's conclusions for silty soils.

3.1.3 Freezing Point Depression and Unfrozen Water

Free water under standard conditions will freeze at 0°C (32°F). The presence of solutes and interfacial surface energies such as capillary and adsorption forces will cause a decrease in temperature at which fusion begins (Johnston, 1981). This temperature difference is called the freezing-point depression. In general, the freezing-point depression
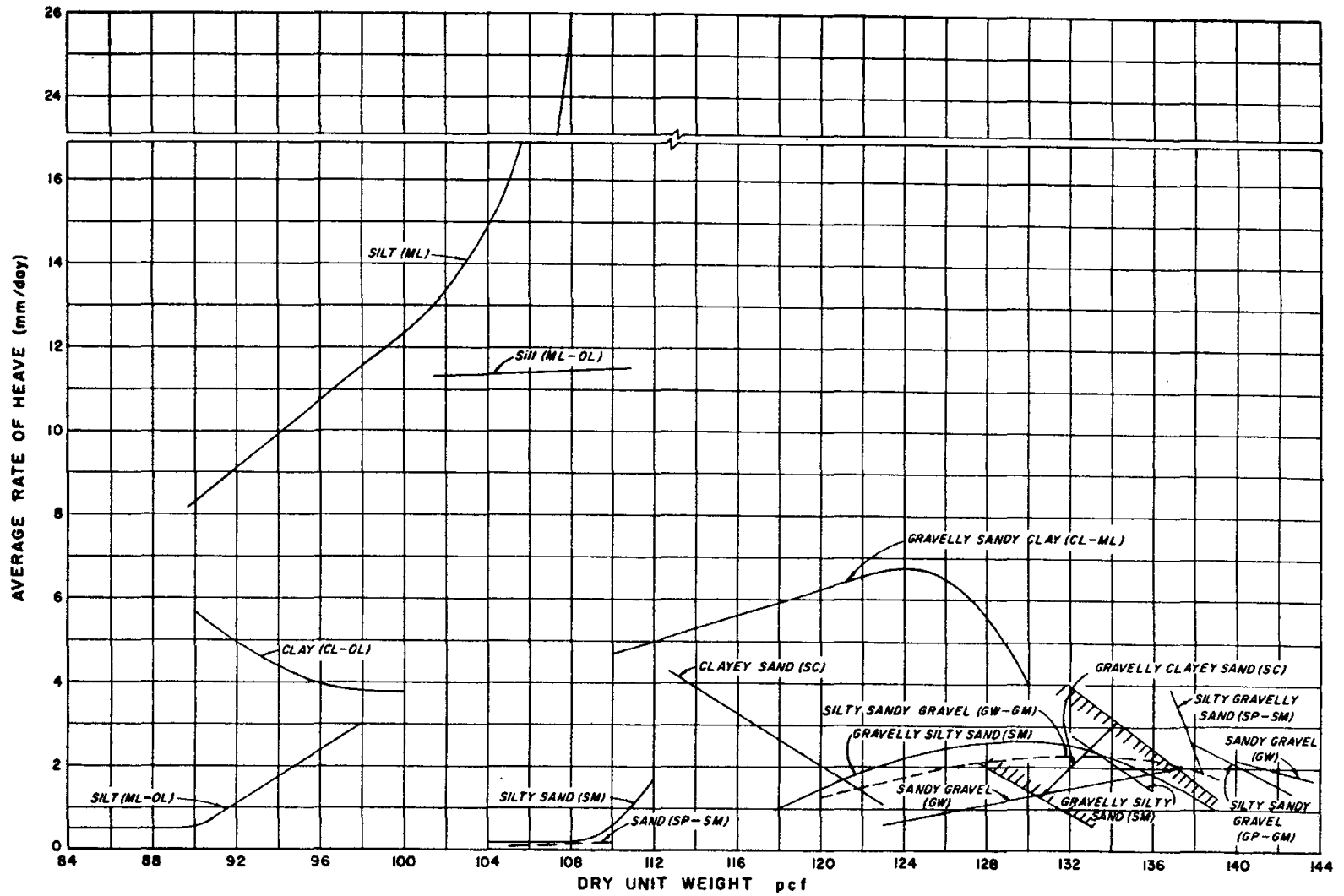
Figure 3.4 Average heave rates for many different soil types at varying dry densities after Linell and Kaplar (1959).
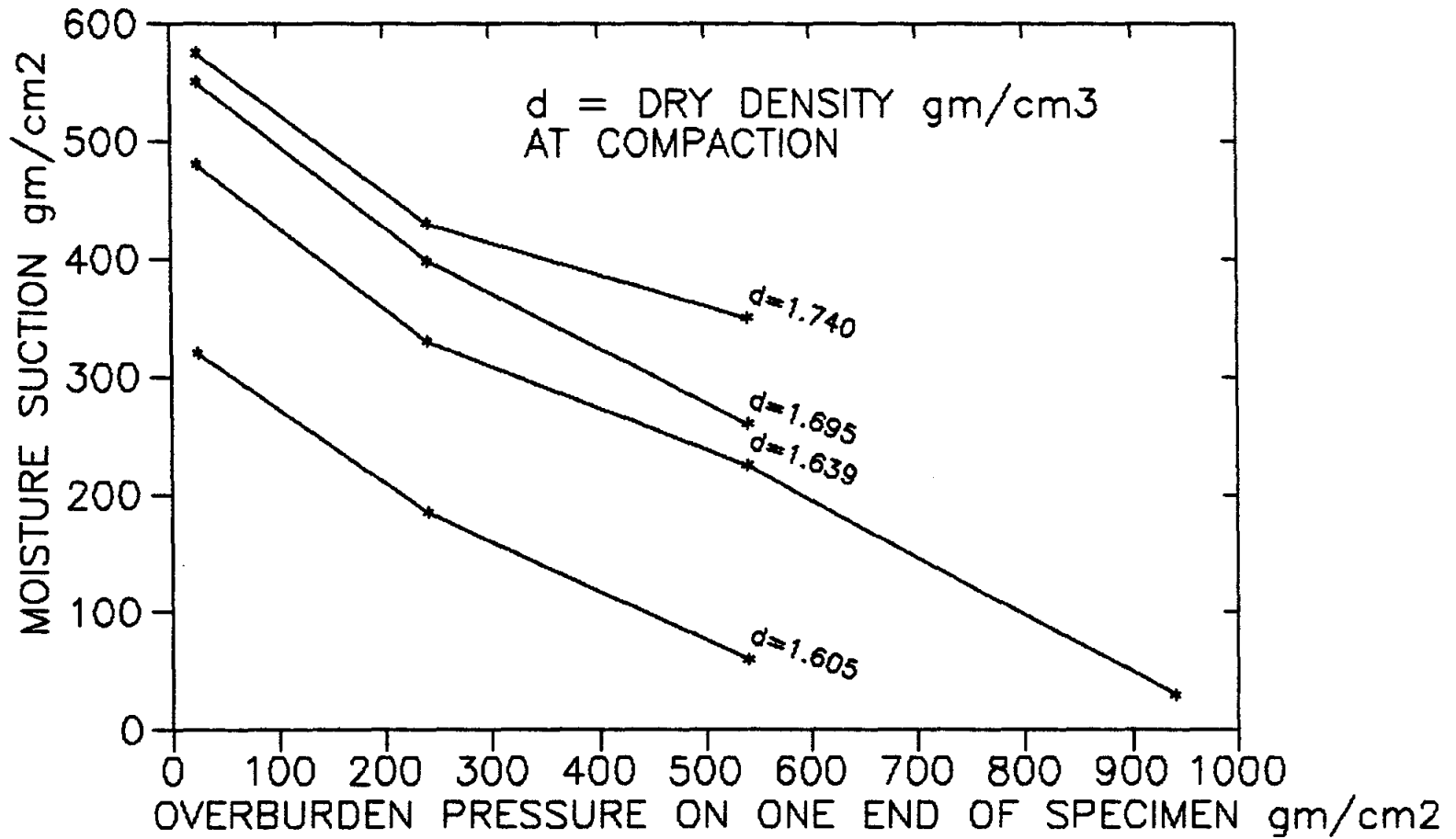
Figure 3.5 Pore water suctions as a function of dry density and over-
burden pressures after Penner (1959).

is a function of the pore water composition and the curvature radius of the water interface in the soil pores. A finite temperature range of fusion is associated with soils exhibiting a freezing-point depression (Lunardini, 1981).

Freezing point depressions are evident in soils with dissolved solids in the pore water. As the fusion begins, the dissolved particles are excluded from the forming ice crystal. Freezing of water causes a higher concentration of dissolved solids in the remaining unfrozen water, thus requiring lower temperatures for continued phase change. Similarly, as the water in the center of a void freezes, the radius of curvature of the unfrozen water surface in contact with soil grain decreases, increasing the capillary suction. The freezing of a soil is synonymous to that of drying the soil. Different of soils will experience different freezing-point depressions and extended fusion temperature ranges due to varying grain sizes, void sizes, and specific surface areas.

The Kelvin equation is generally used to describe the relationship between pore fluid fusion temperature and the radius of curvature of the ice-water interface (Andersland and Anderson, 1978).

$$\Delta T = T_m - T = \frac{2\ T_m\ \sigma_{iw}}{L_f\ \rho_i\ r_i} \qquad (3.4)$$

where ΔT = the depression of fusion temperature
below T_m,

T_m = fusion temperature of free pore
fluid,

T = temperature of ice-water interface,

σ_{iw} = ice-water interfacial energy,

L_f = latent heat of fusion,

ρ_i = mass density of ice, and

r_i = radius of curvature of ice-water
interface and pore radius.

Figure 3.6 illustrates the application of the Kelvin equation to an advancing ice front in a soil with varying pore radii. This relationship shows that the depression in the fusion temperature (T) below T_m is inversely proportional to the radius of the pore openings or "pore throats". Also, the movement of the ice-water interface through the pore opening will occur at a lower temperature in fine-grained soils than in coarse-grained soils.

The extended fusion temperature range results in a condition where the pore fluid can exist in two states; ice and water. The total moisture content (w) in this range is expressed as:

$$w = w_i + w_u \qquad (3.5)$$

where w_i = water content of ice and

w_u = water content of unfrozen water.
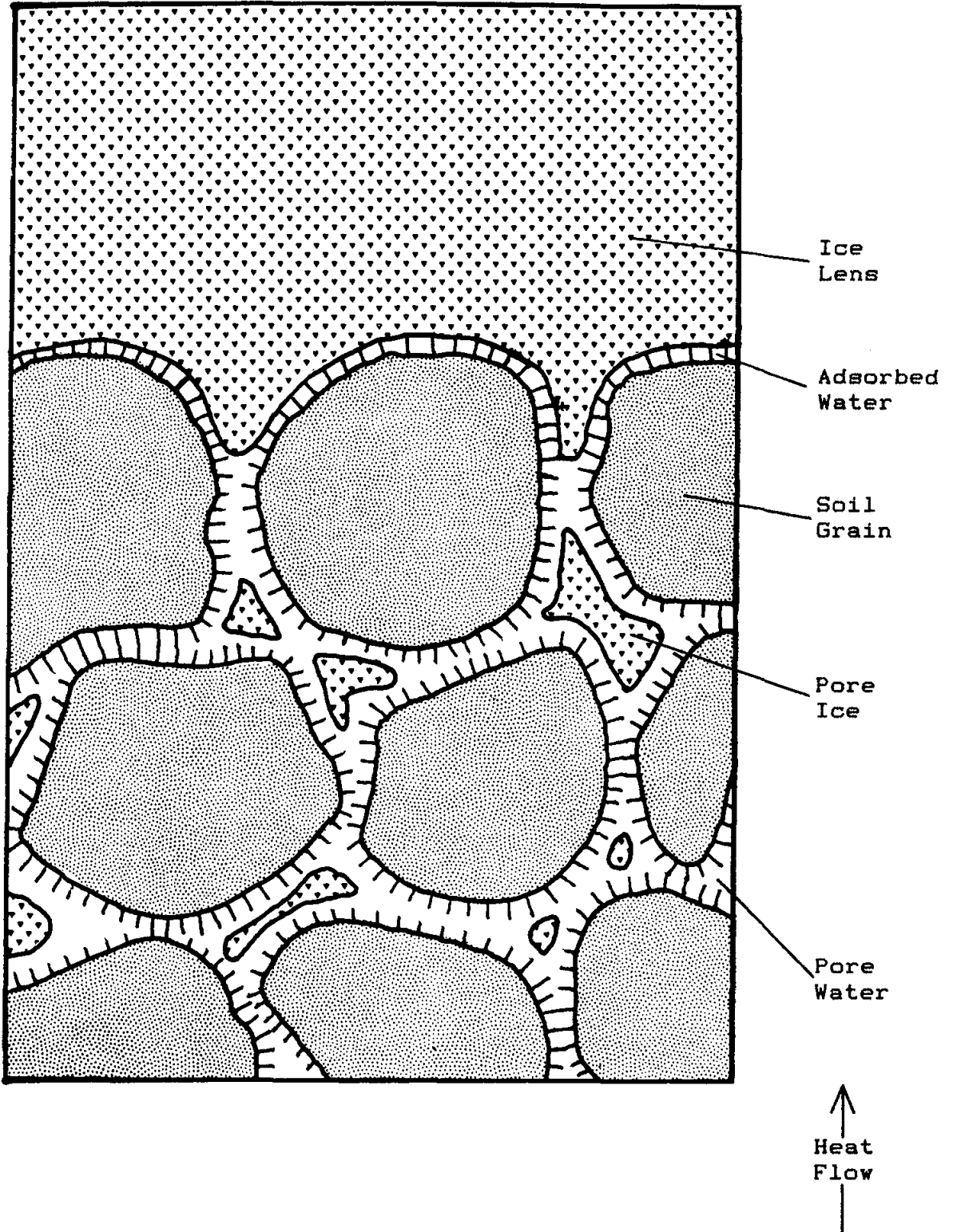
Figure 3.6   Enlarged cross-section of granular soil showing
              the advancing ice front, pore ice, and adsorbed
              water films.

The frozen water appears first in the center of voids while the unfrozen water remains as a film on the soil grain surface. The films of unfrozen water provide a path for moisture migration to occur even through the majority of the pore fluid may be frozen. The greater the unfrozen moisture content of a soil below 0°C, the more potential there exists for continuous surface films by which moisture can migrate.

Williams (1964) showed that a relationship existed between the temperature below the initial freezing point of the pore water at which a given unfrozen water content occurred and the negative pore pressures corresponding to the same water content at room temperature. As the soil suction is increased for a given moisture content so does the unfrozen water content for at given temperature below freezing. Dillon and Andersland (1966) showed that a relationship existed between the specific surface area and the unfrozen moisture content at various temperatures. As the specific surface area of a soil increases so does the unfrozen moisture content for a given temperature below freezing. The soil-moisture characteristic (soil suction) and the specific surface area are both a function of soil grain radii. Finer-grained soils exhibit a larger capillary pressure and a greater specific surface area which leads to a higher unfrozen water content at a given temperature as shown in Figure 3.7 (after Anderson and Morgenstern, 1973).
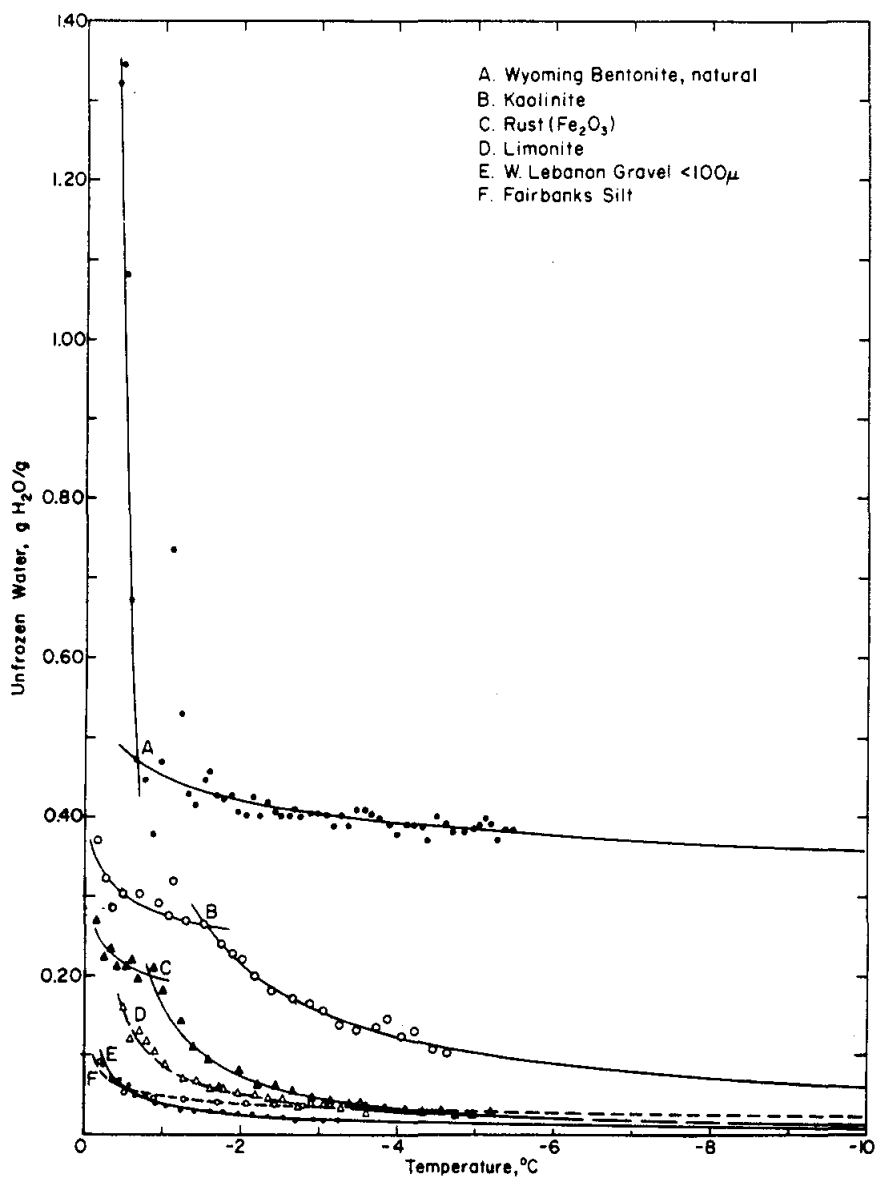
Figure 3.7   Unfrozen moisture contents at various
temperatures for several soils after
Anderson and Morgenstern (1973).

3.1.4 Hydraulic Conductivity

Moisture migration to the zone of freezing is directly related to the hydraulic conductivity of the soil. The driving mechanism for moisture migration is the increasing surface tension created in the pore fluid as the soil freezes (dries) and/or the negative pressures developed when energy imbalances occur as the pore fluid changes phase. Moisture migration occurs mainly along the films of unfrozen water held to the grain surface in an unsaturated or frozen soil. Hydraulic conductivity is related to the degree of saturation and soil-water temperature. When saturation occurs, the hydraulic conductivity reaches a maximum value; saturated hydraulic conductivity. As the degree of saturation decreases so does the continuity of water films and hence the unsaturated hydraulic conductivity. Also, the unfrozen moisture content decreases as the temperature of a soil system is lowered below the freezing point depression. In addition, the viscosity of the unfrozen water films increases with decreasing temperatures. Freezing the soil has the same effect as decreasing the degree of saturation; the continuity of unfrozen moisture films is reduced thereby reducing the effectiveness of the moisture transport mechanism. Figure 3.8a illustrates the relationship between negative pore pressures and hydraulic conductivity for
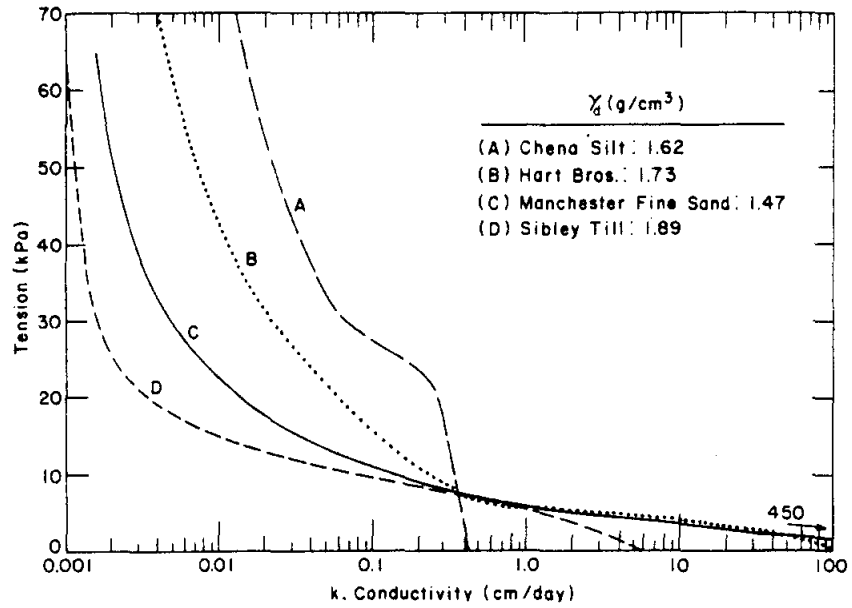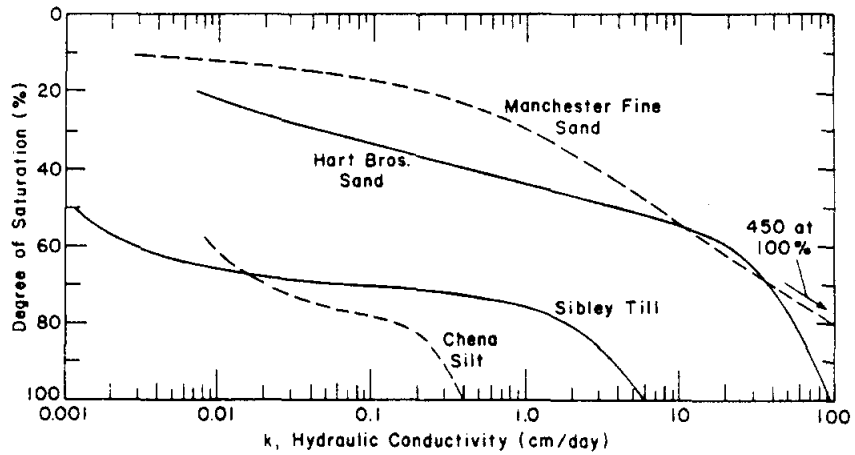
Figure 3.8   Hydraulic conductivity relationships as a
function of a) soil suction and b) degree
of saturation after Ingersoll (1981).

several representative soils (after Ingersoll, 1981). Figure 3.8b shows the dependence of hydraulic conductivity on the degree of saturation for the same soils (after Ingersoll, 1981).

The movement of water through a frozen zone of soil has been observed in experiments performed by Mageau and Morgenstern (1980), Horiguchi and Miller (1983), Oliphant, Tice, and Nakano (1983), Nakano, Tice, Oliphant, and Jenkins (1983), and Rieke, Vinson, and Mageau (1983). Movement is along the continuous, unfrozen films of adsorbed water held to grain surface.

3.2 Environmental Factors Effecting Moisture Migration

Environmental factors are independent of the soil-water systems but still influence the rate and magnitude of moisture migration. Environmental factors include temperatures, temperature gradient, heat extraction rates, and surcharge pressures.

Heat extraction rates during soil freezing have been studied extensively with varying conclusions. Beskow (1938) indicated that the heave rate was independent of the heat extraction rate. Penner (1959) concluded that the heat extraction rate had a significant influence on the rates of frost heave and moisture migration. Penner (1972) duplicated his earlier results and further supported the

dependence of heat extraction rate on the rate of heave. Loch (1979) reported conclusions similar to Penner's work; however, his earlier work (1977) indicated that the heat extraction rate had no influence upon frost heave rate.

The contradictory conclusions stem from the range of heat extraction rates studied (Chamberlain, 1981). Beskow (1938) and Loch's earlier work (1977) concentrated on a narrow range of heat extraction rates and therefore found no influencing effect on the rate of frost heave. Penner (1959 and 1972) and Loch (1979) conducted experiments over a wide range of heat extraction rates and showed the significance of this parameter on heave rate. Penner's (1972) conclusions are summarized as follows:

1) The heat-removal rate influences the heaving rate.

2) With an increasing heat-removal rate, the heaving rate increases and appears to rise to a maximum; it then decreases and intersects the theoretical void (insitu) water curve and becomes coincidental with it (Figure 3.10).

3) The rate of frost penetration is not the same for different soils at the same rate of heat extraction.

4) The heave-rate response to increasing heat-removal rates is not the same for all frost susceptible soils.

Figure 3.9 (after Andersland and Anderson, 1978) shows the relationship between the heat removal rate and the rate of frost heave for several soils. Figure 3.10 (after Penner, 1972) shows the varying effect of frost penetration
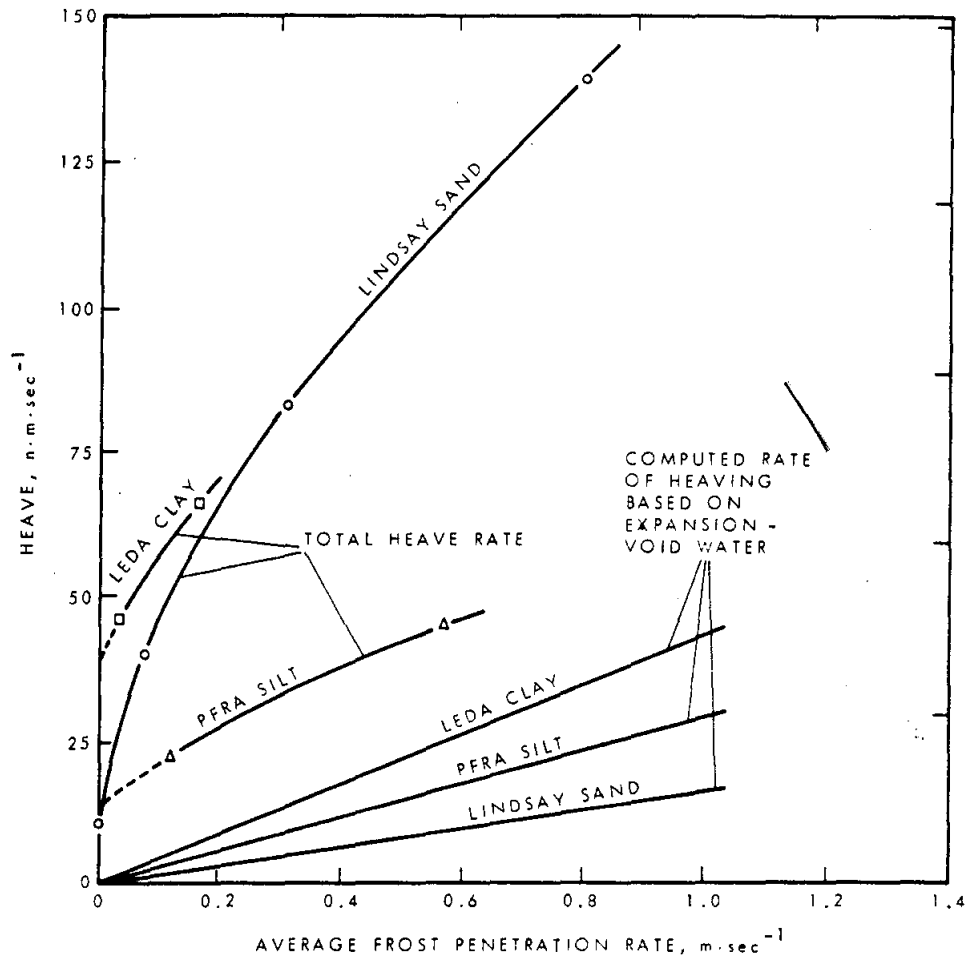
Figure 3.9   The relationship between heat extraction
rates and frost heave rates after
Andersland and Anderson (1978).
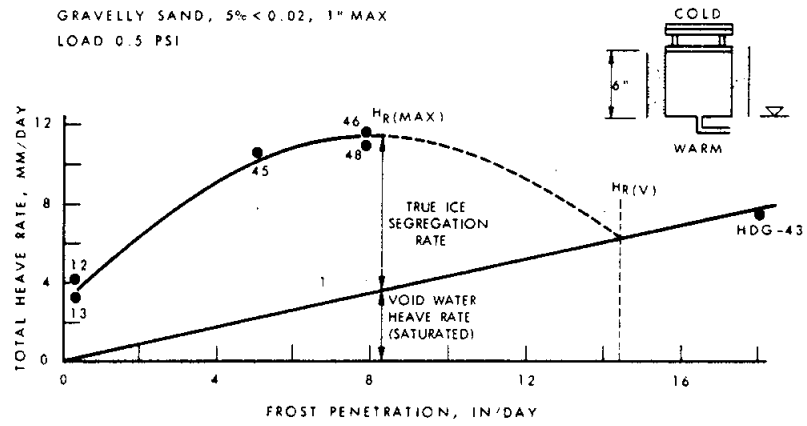
Figure 3.10 The varying effect of heat extraction
rates on the frost heave of a gravelly
sand after Penner (1972).

on frost heave for a gravely sand.

The effects of temperature and temperature gradient on frost heave have been studied by Penner and Walton (1979), Holden, Jones, and Dudek (1981), and Loch (1979). It is generally accepted that the temperature gradient effects the hydraulic conductivity, frost penetration rate, and the thickness of the frozen fringe. The heave rate increases as the thermal gradient is increased in the unfrozen soil below the frozen fringe (Chamberlain, 1981).

The first frost heave experiments by Taber (1929) proved that heaving could be reduced by increasing the applied vertical stress on the heaving soil. When heave displacements are prevented in a frost susceptible soil a positive pressure is developed at the ice-water interface (Penner, 1959). Penner (1959) theorized that there exists a critical shut-off pressure for a given pore size at the ice-water interface such that heaving is terminated. Gold (1957) commented that the effects of surcharge pressure on heaving decrease with decreasing pore size. The shut-off pressures are largest for clays and dense silts.

The fusion temperature of the pore fluid depends upon the pressure imposed on the soil-water system. Penner (1959) gives this relationship in a form of the Clausius-Clapeyron equation shown below.

$$\frac{dP_t}{dT} = \frac{L_f}{T_m \, (V_i - V_w)} \qquad\qquad (3.6)$$

where dP_t = total change in pressure,

dT = the depression in fusion temperature below T_m,

L_f = latent heat of fusion,

T_m = fusion temperature of free water,

V_i = specific volume of ice, and

V_w = specific volume of water.

In a saturated soil-water system, the total change in pressure of the water is always equal to the total change in pressure on the ice (Penner, 1959). Substituting the known values in the equation indicates that the freezing point depression is increased by 0.00748°C per atmosphere of pressure applied to the system. In an unsaturated soil the pore fluid pressure remains constant as the ice pressure is increased. This situation results in a 0.0899 °C increase in the freezing point depression per atmosphere of pressure applied.

3.3 Moisture Migration Mechanisms

Moisture migration towards the freezing front is essential for frost heave and ice segregation. Although

moisture redistribution may occur without resulting in any frost heave or the formation of segregated ice features. Most moisture is transported along continuous films of moisture in contact with the soil particles. Vapor transported moisture may be a contributing factor in an unsaturated soil, with continuous air passages and discontinuous liquid moisture films.

3.3.1 Transport Along Continuous Films

It has been shown that moisture migration occurs through a frozen soil along continuous moisture films to the growing ice lens behind (cold side) the initial freezing temperature isotherm. Several frost heave theories have attempted to explain the driving mechanism for the moisture movements. The first attempt, capillary theory, explained the mechanism as being the result of increased surface tensions near the freezing front. With increasing negative temperatures, the pore fluid freezes and the remaining unfrozen water occupies regions of higher surface energies (smaller radii). Also, the thicknesses of the adsorbed water films decrease with lowering temperatures. The net effect is similar to that of the drying process in a soil. A gradient of negative pore fluid pressures is established by which water at atmospheric pressure or low negative pressures flows to a region of higher negative pressures in

an attempt to establish energy equilibrium.

The Kelvin equation predicts capillary suctions as well as depressed freezing temperature as the advancing ice front penetrates small pore openings and the curvature of the ice-water interface increases. Nixon (1987) states that the capillary model is incapable of predicting the magnitude or rate of frost heave. Konrad and Morgenstern (1980) report that the suction generated in the frozen fringe is in excess of that which can be attributed strictly to capillary pressures. Penner (1979) showed that the pressure required to retard growing ice lenses (shutoff pressure) was larger than could be predicted by the capillary theory alone.

Winterkorn (1955) applied Gibbs free energy and the second law of thermodynamics to the freezing soil system. The relationship is given by the following equation:

$$dG = V \, dP - S \, dT \qquad (3.7)$$

where G = Gibbs free energy,

V = specific volume,

P = pressure,

S = enthropy, and

T = absolute temperature.

If the net energy change of the system is zero, then any change in energy of one component must be balanced by a

equal change in the other component.

Rewriting Equation 3.7, assuming equilibrium (dG=0) at the ice lens-water interface, results in the following general equation:

$$(V_i \ dP_i) - (S_i \ dT) = (V_w \ dP_w) - (S_w \ dT) \qquad (3.8)$$

where   i = ice component, and

w = water component.

Rearranging the terms in Equation 3.8 yields

$$(V_i \ dP_i - V_w \ dP_w) = (S_i - S_w) \ dT \qquad (3.9)$$

Letting

$$L_f = (S_w - S_i) \ T_f \qquad (3.10a)$$

or

$$(S_i - S_w) = \frac{-L_f}{T_f} \qquad (3.10b)$$

where L_f = latent heat of fusion, and

T_f = fusion temperature (absolute) of bulk pore water

and substituting into Equation 3.9 yields

$$(V_i \ dP_i) - (V_w \ dP_w) = -L_f \ \frac{dT}{T_f} \qquad (3.11)$$

The specific volume is defined as the volume occupied per unit mass of substance or

$$V = \frac{1}{\rho} \qquad (3.12)$$

where ρ = mass density.

Substituting this relationship into Equation 3.11 yields

$$\frac{dP_i}{\rho_i} + \frac{dP_w}{\rho_w} = -L_f \frac{dT}{T_f} \qquad (3.13)$$

Making the assumption that there is no change in pore water pressure $(dP_w=0)$ and the ice pressure is due to ice thickness and applied stresses such that

$$dP_i = dq + \rho_i \, dh_i \qquad (3.14)$$

where q = applied stress or surcharge on ice and

h = height of ice lens

and also assuming that

$$dT = T_s - T_f \qquad (3.15)$$

where T_s = segregation freezing temperature (absolute) or temperature at base of growing ice lens.

yields

$$\frac{q + \rho_i \, h_i}{\rho_i} = -L_f \frac{T_s - T_f}{T_f} \qquad (3.16)$$

Solving for T_s in Equation 3.16 gives

$$T_s = T_f \left[1 - \left(\frac{q + \rho_i \, h_i}{\rho_i \, L_f} \right) \right] \qquad (3.17)$$

The above equation shows that the segregation freezing temperature is less than the fusion temperature of bulk pore water and the difference is determined by the frost heave pressures (Takagi, 1978).

Going back to the general equation representing equilibrium at the ice lens-water interface (Equation 3.8) and rearranging terms differently yields,

$$dP_w = \frac{L_f \, dT}{V_w \, T} + \frac{V_i}{V_w} \, dP_i \qquad (3.18)$$

Integrating

$$\int_0^{P_w} dP_w = \int_{T_f}^{T_s} \frac{L_f}{V_w} \frac{dT}{T} + \frac{V_i}{V_w} \int_0^{P_i} dP_i \qquad (3.19)$$

gives

$$P_w = \frac{L_f}{V_w} \ln \frac{T_s}{T_f} + \frac{V_i}{V_w} P_i \qquad (3.20)$$

Using series expansion,

$$\ln \frac{T_s}{T_f} = (x-1) - \frac{(x-1)^2}{2} + \frac{(x-1)^3}{3} - \ldots = \frac{T_s - T_f}{T_f} \qquad (3.21)$$

and assuming that the ice pressure is equal to atmospheric pressure (0 gauge pressure), Equation 3.20 reduces to

$$P_w = \frac{L_f}{V_w} \left(\frac{T_s}{T_f} - 1 \right)$$ (3.22)

Earlier it was shown that $T_s \leq T_f$ (Equation 3.17) and therefore

$$\left(\frac{T_s}{T_f} - 1 \right) \leq 0$$ (3.23)

This implies (Konrad and Morgenstern, 1982) that

$$P_w = \frac{L_f}{V_w} \left(\frac{T_s}{T_f} - 1 \right) \leq 0$$ (3.24)

which means that the pore water pressure at the base of the growing ice lens is negative and increases negatively with increasing dT ($T_s - T_f$).

The potential for moisture migration along continuous unfrozen water films in freezing, frost susceptible soil is generally considered to be the combined effect of the following:

1) negative pressures generated due to thermodynamic imbalances,

2) capillary suctions generated by decreasing radii of unfrozen pore water,

3) increased surface tensions due to thinning adsorbed water films, and

4) mass transfer associated with temperature gradients.

3.3.2 Vapor Transport

In most freezing soil studies, the effects of moisture transfer in the vapor phase are assumed negligible. Under some conditions vapor transported moisture may provide a measurable contribution to the overall moisture redistribution (Farouki, 1981). Moisture vapor movement is prohibited form occurring in a saturated soil. The effect of vapor transport may be considered small in a fine-grained, frost susceptible soil with a moderate to high degree of saturation. The availability of interconnected voids is a prerequisite for this mode of moisture transportation. Therefore, vapor movement considerations may be pertinent in coarse-grained soils with a low to moderate degree of saturation. The potential for soil moisture diffusion in the vapor phase is a function of the vapor pressure gradient. The vapor pressure gradient is a function of the temperature gradient and soil moisture tension (Jumikis, 1957).

Vapor pressure gradients are created when a saturated vapor is exposed to a temperature gradient because the pressure of the saturated vapor is determined only by its temperature according to the general gas law. By

definition, the saturation vapor pressure is the pressure of the vapor when completely saturated for a given temperature. Table 3.2 gives saturated vapor pressures and vapor densities of water vapor at temperatures near 0˚C.

Table 3.2

Saturated Vapor Pressure and
Vapor Densities Near 0˚C

Vapor Temp. (C)	P_{sat} (mm Hg)	Vapor Densities (gm/m3)
-5	3.163	3.353
-4	3.410	3.615
-3	3.673	3.893
-2	3.956	4.193
-1	4.258	4.513
0	4.579	4.854
1	4.926	5.222
2	5.294	5.612

Vapor diffusion is governed by Fick's law which states that the rate of diffusion is proportional to the concentration gradient. The concentration gradient is defined as the difference in quantity of matter per volume per unit length along the path of diffusion. An equation for vapor diffusion utilizing Fick's law is given as follows:

$$W_v = \frac{D_a A}{R\ T}\ t\ \frac{dp}{dx} \qquad (3.25)$$

where W_v = mass of substance diffused (gm),

D_a = coefficient of diffusion of water vapor in air (cm^2/sec),

R = gas constant (cm/K),

A = area perpendicular to diffusion (cm^2),

T = absolute temperature (K),

t = time (sec),

dp = difference in pressure (gm/cm^2), and

dx = unit length of diffusion path (cm).

The diffusion coefficient (D_a) describes the ability of one gas to diffuse into another when a unit concentration gradient is imposed. Vapor phase transport is a very slow process which depends on the magnitude of the diffusion coefficient (Farouki, 1981). Lunardini (1981) gives an equation for calculating the diffusion coefficient of water vapor in air for varying temperatures and pressures.

$$D_a = \frac{23.95}{p} \left(\frac{T}{273}\right)^{2.3} \tag{3.26}$$

where D_a = diffusion coefficient (cm^2/sec),

p = total pressure (gm/cm^2), and

T = absolute temperature (K).

In soils, the coefficient of diffusion is restricted to interconnected, air-filled voids and is reduced due to the tortuosity of these voids. The coefficient of diffusion for vapor in air can be corrected for the degree of

saturation of the soil and the tortuosity. Farouki (1981) gives this correction originally reported by Penman (1940) as follows:

$$D_s = 0.66 \ D_a \ (1- \ S_r/100) \ n/100 \qquad (3.27)$$

where D_s = diffusion coefficients corrected for a given soil,

S_r = degree of saturation expressed as a percent (volume of water per volume of voids), and

n = porosity expressed as percent (volume of voids per total soil volume).

It is impossible to separate the effects of moisture migrated by continuous moisture films and that transported in the vapor phase (Nakano et al., 1983). With vapor phase transport, all the pore vapor in the unfrozen soil portion is a potential source for transport to and condensation at the freezing front. This is further complicated by a constantly changing and moving freezing isotherm.

Moisture migration in freezing soils is a very complex problem due to the inter-dependent coupled heat and mass transfer processes. Although many pieces of an all encompassing theory are known, a complete and thorough understanding of the mechanics and processes of soil freezing is not available. Therefore, only a qualitative understanding exists to date (Nixon, 1987).

CHAPTER 4

EXPERIMENTAL SETUP

The objective of this study was to prepare a laboratory model of an evaporator section of a vertical thermosyphon and to determine if a redistribution of pore water occurs in a clean sand due to radial freezing. This was accomplished by circulating a refrigerated glycol solution through a centered heat exchanger to radially freeze a moist sand.

The sand medium was instrumented with fifteen thermistors and nine tensiometers to measure temperature and negative pore pressures respectively. The temperature drop across the heat exchanger and the mass discharge of the glycol solution were determined in order to calculate the heat removal rate from the soil.

Thermistor and tensiometer readings were taken periodically throughout the cooling and freezing stages of the test. The flow within the cooling pipe wae measured during freezing. At the conclusion of the experiment, the frozen sand was cross-sectioned and several samples were taken to determine the distribution of moisture contents.

Three different freezing tests were performed on the sand. Several environmental and physical parameters were varied with each test. Test variables included: temperature

of circulating glycol, mass discharge of the glycol, dry

density of the sand, and the initial moisture content.

The primary objectives of this study were to:

> 1) determine if moisture redistribution or
> migration occurred within the sand, and

> 2) observe freezing rates, thermal conductivities,
> and steady-state heat flow in the experimental
> test to correlate these with theoretical
> calculations.

This chapter is divided into five sections which

describe the experimental setup used to perform the

objective of this study. Section 1 gives dimensions of the

freezing tank and describes the equipment used for the

study. The index properties as well as other

characteristics of the soil are given in Section 2. Section

3 is used to describe the methods of temperature

measurement. A description of the procedure and equipment

used for pore pressure measurements is given in Section 4.

The procedure used for each test is detailed in Section 5.

4.1 Freezing Tank and Equipment

The freezing tank constructed for this study was

capable of freezing a soil mass having the shape of a right

circular cylinder with a diameter of 121.9 cm (48") and a

height of 61.0 cm (24"). Figure 4.1 shows a detailed plan
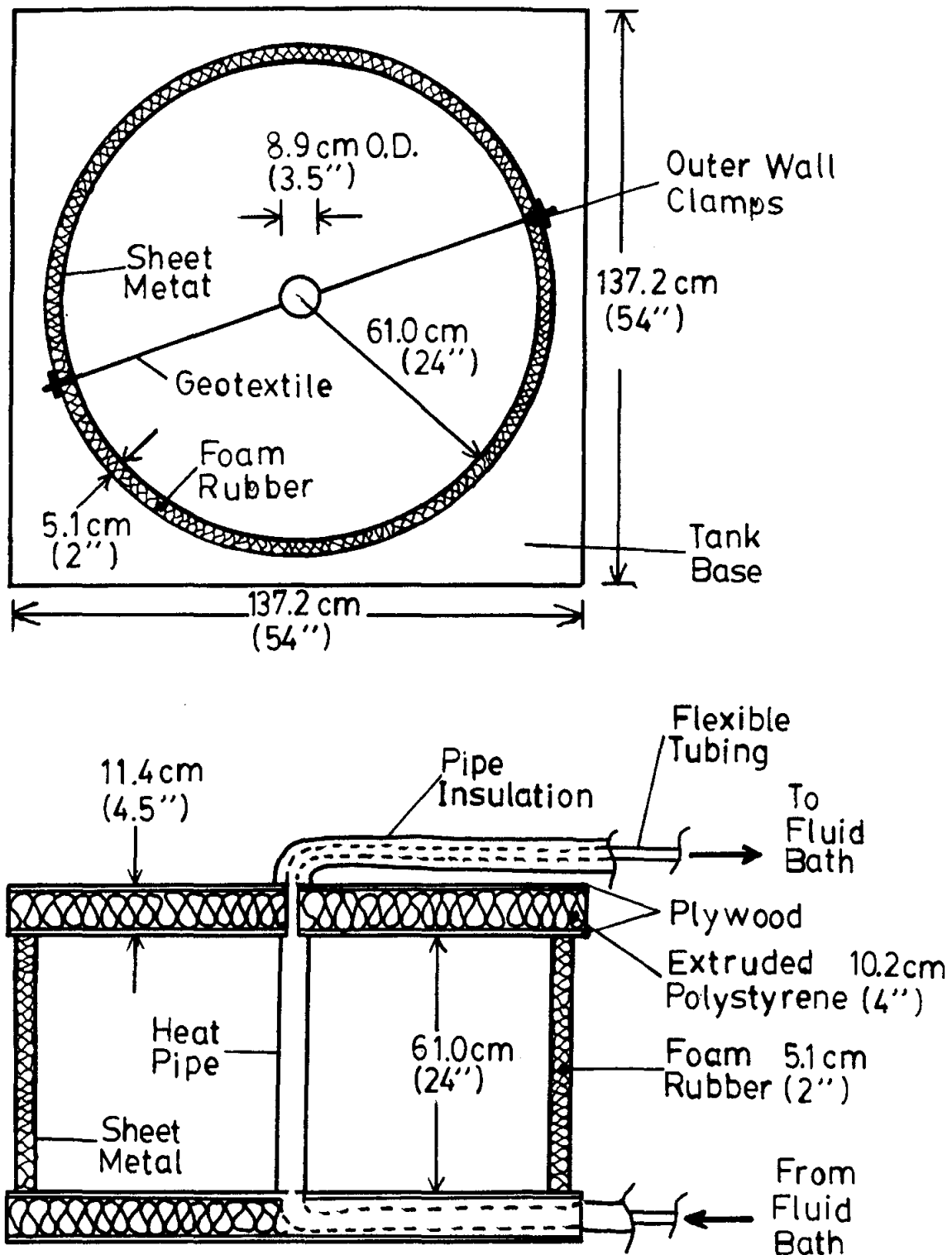
Figure 4.1 Plan view and cross-sectional view of the freezing tank used.

view and a cross-sectional view of the freezing tank. The outer radius of the soil mass was contained by wall of 14 gauge sheet metal. This outer wall was made from two halves which were joined together with bolts. This configuration facilitated disassembling the tank when the freezing process was terminated. A woven, split film geotextile was placed through the center of the tank where the two halves met to aid in the dissection of the frozen soil mass. The top and bottom of the tank consisted of plywood and 10.2 cm (4") of extruded polystyrene insulation board. The insulation was used to reduce the heat flow from occurring across the top and bottom boundaries. Thermistors and tensiometers were buried in the soil to measure temperature and negative pore pressures respectively.

The soil was frozen in an outward, radial direction away from a 7.6 cm (3") inside diameter, 8.9 cm (3.5") outside diameter, aluminum pipe. A refrigerated glycol solution was circulated through the pipe. The glycol solution constituted a 50-50 mixture of ethylene glycol and water. The cooling fluid (glycol solution) was cooled and circulated by a temperature controlled fluid bath which was connected to the center pipe by insulated, flexible tubing. The flexible tubing included quick disconnect fittings which eased freeze tank assembly. The temperature and the mass discharge of the circulating fluid were controlled with the refrigerated fluid bath unit. The temperature-controlled

bath was capable of a maintaining fluid temperature down to -20°C within ±0.1°C.

Both the freezing tank and the temperature-controlled fluid bath were situated in a thermostatically-controlled cold room located in the basement of the Duckering Building on the campus of the University of Alaska-Fairbanks. The cold room allowed the ambient air temperature to be maintained slightly above the soil freezing temperature (0°C). The inaccuracy of the cold room thermostat resulted in a 5°C temperature fluctuation (from 0°C to 5°C) during operation. This warranted the use of a foam rubber blanket which was wrapped around the outer tank wall to attenuate the ambient air temperature fluctuations.

4.2 Soil Properties

When thermosyphons are placed in insitu soils after the structure or facility to be protected has already been constructed, there is no control over the type of soil in which the evaporator section is placed. However, the characteristics of the backfill can be specified when the use of thermosyphons is incorporated into the original foundation design. Such backfill variables may include gradation, density control, and initial moisture contents. The gradation of the backfill would dictate the water

holding capacity and the frost susceptibility of the backfill soil. The dry density and moisture content affect many thermal properties of the backfill such as thermal conductivity, volumetric latent heat, and volumetric specific heat. For most geotechnical applications, a clean sand is usually specified for the evaporator section bedding. A "clean" sand would imply a sand with less than 4% by weight of minus #200 sieve size material (0.075mm) and therefore considered nonfrost susceptible. Sand sized material has a high water holding capacity and desirable physical properties. Once frozen, a high water holding capacity soil would require more heat energy to thaw than a soil with less water per volume. This characteristic can be thought of as "thermal inertia".

In this study, sand obtained from a local sand and gravel supplier was used. The sand was obtained from an alluvial sand and gravel pit adjacent to the Chena River in Fairbanks, Alaska owned and operated by H & H Contractors, Inc.

The grain size distribution was determined in accordance with American Society for Testing and Materials (ASTM) D-422-84. The particle size distribution curve is shown in Figure 4.2. The material consisted of 2.6% gravel (>4.75mm), 96.3% sand (<4.75mm and >0.075mm) and 1.1% silt and clay sized particles (<0.075mm) as defined by the
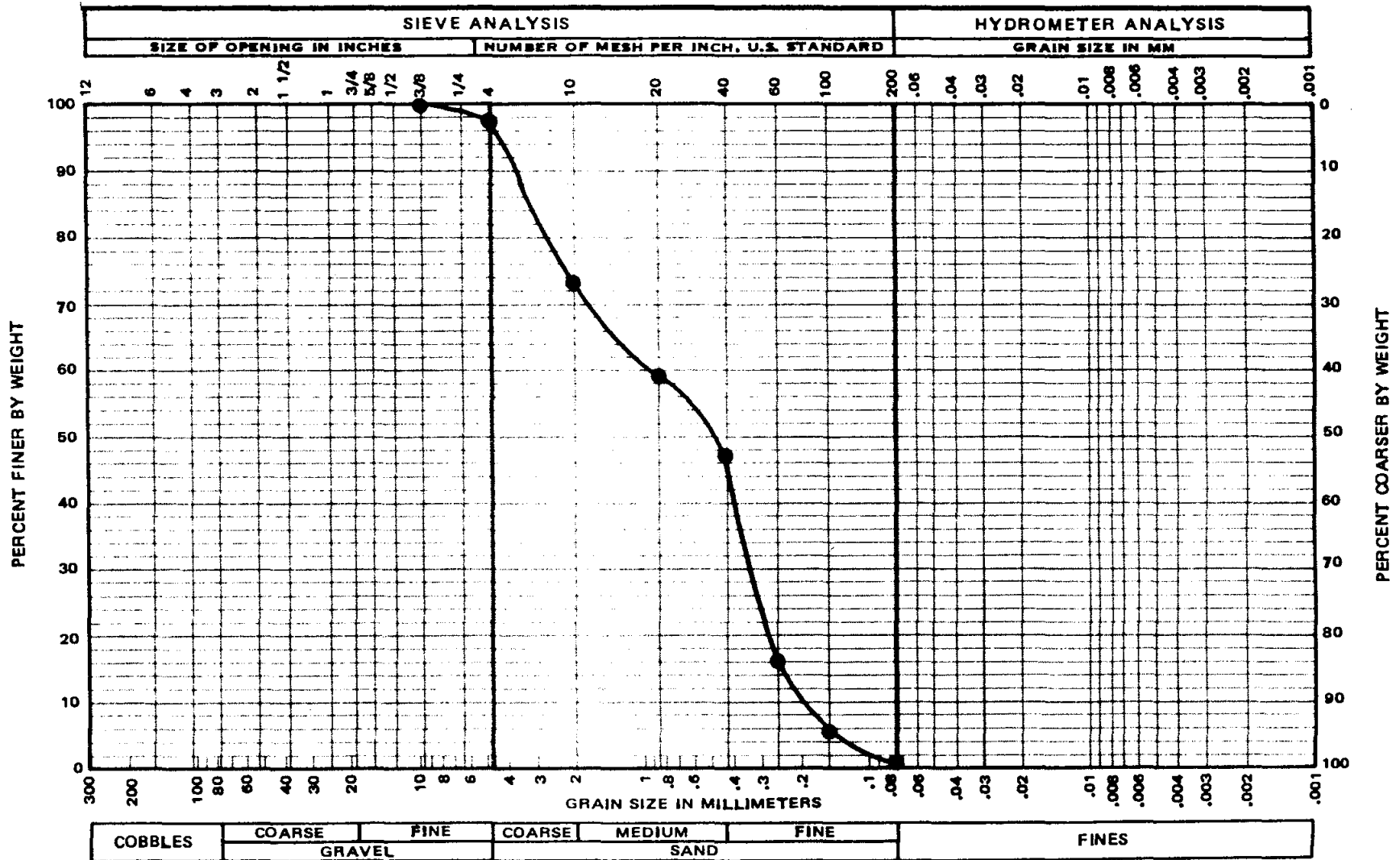
Figure 4.2   Particle size distribution of the experimental sand.

Unified Soil Classification (USC) system. The particle size distribution curve can be quantitatively described in terms of the degree of curvature and the uniformity of the grain size curve. The coefficient of curvature and the coefficient of uniformity are defined as follows:

$$C_c = \frac{D_{30}^2}{(D_{60})(D_{10})} \qquad (4.1)$$

$$C_u = \frac{D_{60}}{D_{10}} \qquad (4.2)$$

where C_u = coefficient of uniformity,

C_c = coefficient of curvature,

D_{10} = effective grain size, diameter corresponding to 10% finer on the particle-size distribution curve,

D_{30} = diameter corresponding to 30% finer,

and D_{60} = diameter corresponding to 60% finer.

A well graded soil has a coefficient of curvature between 1 and 3 and a uniformity coefficient greater than 4 for gravels and greater than 6 for sands. Noncompliance with either criteria results in poorly graded soil classification. The experimental sand has a C_u of 4.2 and a C_c of 0.61. According to the USC system, this soil is classified as SP, poorly graded sand.

The maximum dry densities, determined from both the standard and the modified Proctor tests were performed in accordance with ASTM D-698-84 and D-1557-84 respectively. The standard Proctor value for the sand is 18.04 kN/m^3 (114.8 pcf) at an optimum moisture content of 10.4 %. The modified Proctor value is 18.57 kN/m^3 (118.1 pcf) at an optimum moisture content of 9.3%. Figure 4.3 shows the relationship between moisture and dry density for both the standard and modified Proctor tests.

The average specific surface area of the test soil was determined using the following formula based upon the weighted average principle.

$$S_{ave} = \frac{\displaystyle\sum_{n=1}^{i} A_i \frac{P_i}{d_i}}{\displaystyle\sum_{n=1}^{i} \frac{P_i}{d_i}} \qquad (4.3)$$

where S_{ave} = average specific surface area of soil,

   A_i = surface area of ith sieve size fraction,

   P_i = percentage of ith sieve size fraction by weight of total sample, and

   d_i = average particle diameter of ith sieve size fraction.

The average specific surface area of the test sand is 130.1 cm^2/gm. Through back-calculations, it was determined
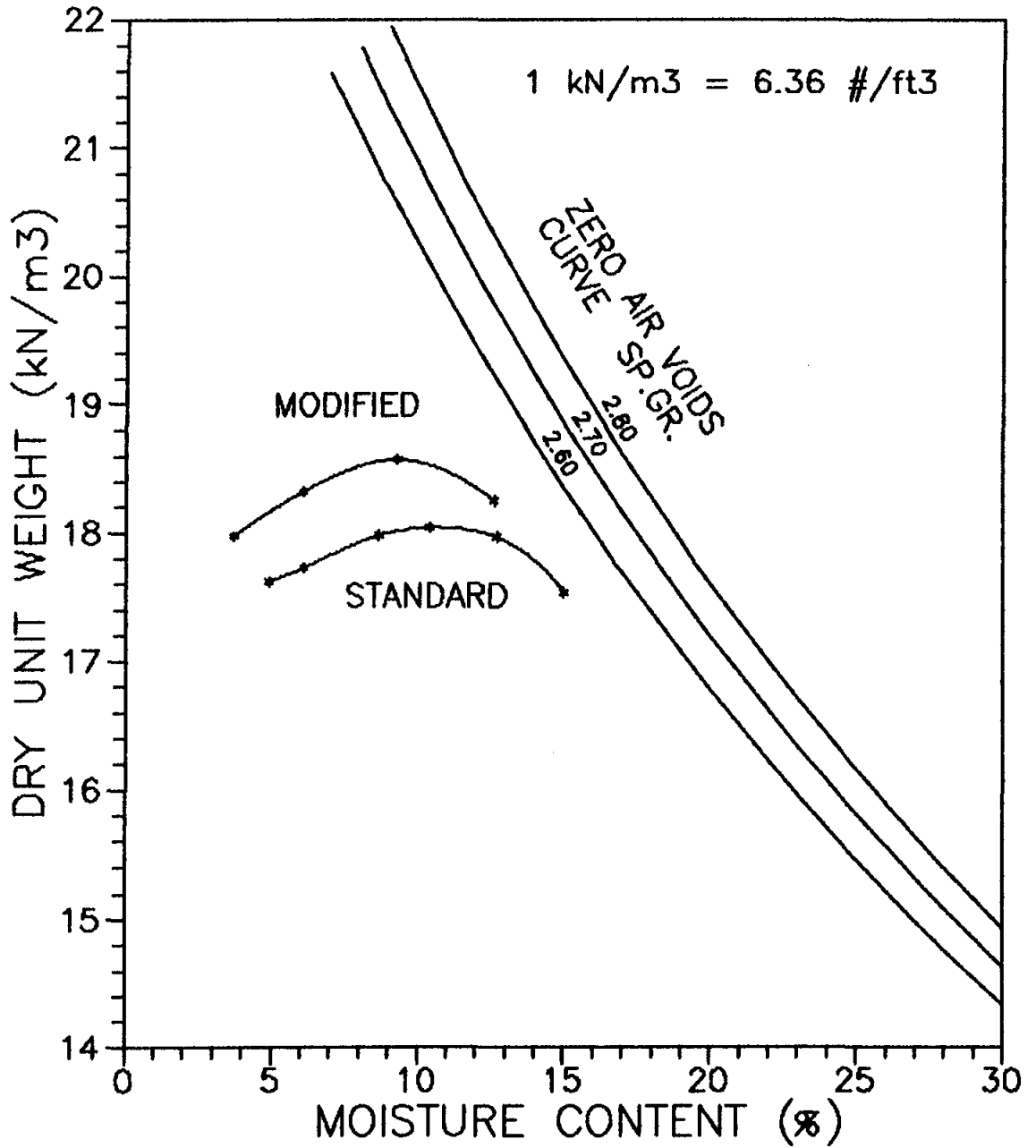
Figure 4.3 Moisture-density relationships of the experimental sand for the standard and modified Proctor compaction tests.

that the equivalent average grain size was 0.087 mm. This corresponds well to the specific surface area given for a 0.1 mm sand in Table 3.1 discussed earlier.

The soil-moisture characteristic curve for the sand was determined in order to calculate the moisture content of the sand at a any negative pore pressure. This was accomplished by using Tempe cells. A Tempe cell is a clear plastic cylindrical container with top and bottom porous ceramic stones. The ceramic stones are manufactored to have a specific air entry value (AEV). An air entry value is a measure of the air pressure required to force water from the porous ceramic when saturated which allows air to enter the stones (Ingersoll, 1981).

The sand was saturated and placed into the Tempe cell. The porous stones were saturated and de-aired. The cell was assembled with a water filled tube connected to the bottom ceramic stone. The other end of the water filled tube was submerged in a basin of water which represented a phreatic surface. As the Tempe cell was raised above the phreatic surface, the water in the attached tube was placed in tension which created negative pore water pressure (suction) in the sand. Moisture was evacuated from the sand until the suction forces equaled the matrix forces holding the water in the sand. The Tempe cell was then weighed and the change in moisture was determined. The process was continued until increasing suction forces caused negligible

changes in moisture contents. The procedure can not be reversed using the Tempe cells to produce a wetting curve and the hysteresis effect (Ingersoll, 1981). This is due to the limiting radii of the porous stones as discussed in Section 3.1.1.3. The soil-moisture characteristic curve for the sand used in the experiment is shown in Figure 4.4.

4.3 Temperature Measurements

Temperature measurements were obtained using seventeen thermistors, two thermometers, and a thermocouple. Fifteen thermistors were employed in the soil medium and two were placed in the stream of the cooling fluid just before and after the centered pipe (heat exchanger). A thermocouple was used to monitor the ambient room temperature during the first experimental test only. Thermometers yielded both ambient temperature and the temperature of the outside surface of the outer radius tank wall during the last two experiments.

A thermistor is a temperature sensitive resistor. The resistance of the thermistor changes as the temperature of the thermistor bead itself changes. The thermistors used in the this study were YSI 44033 (from the Yellow Springs Instrument, Co.). This model of thermistor has a negative temperature coefficient which means that the resistance
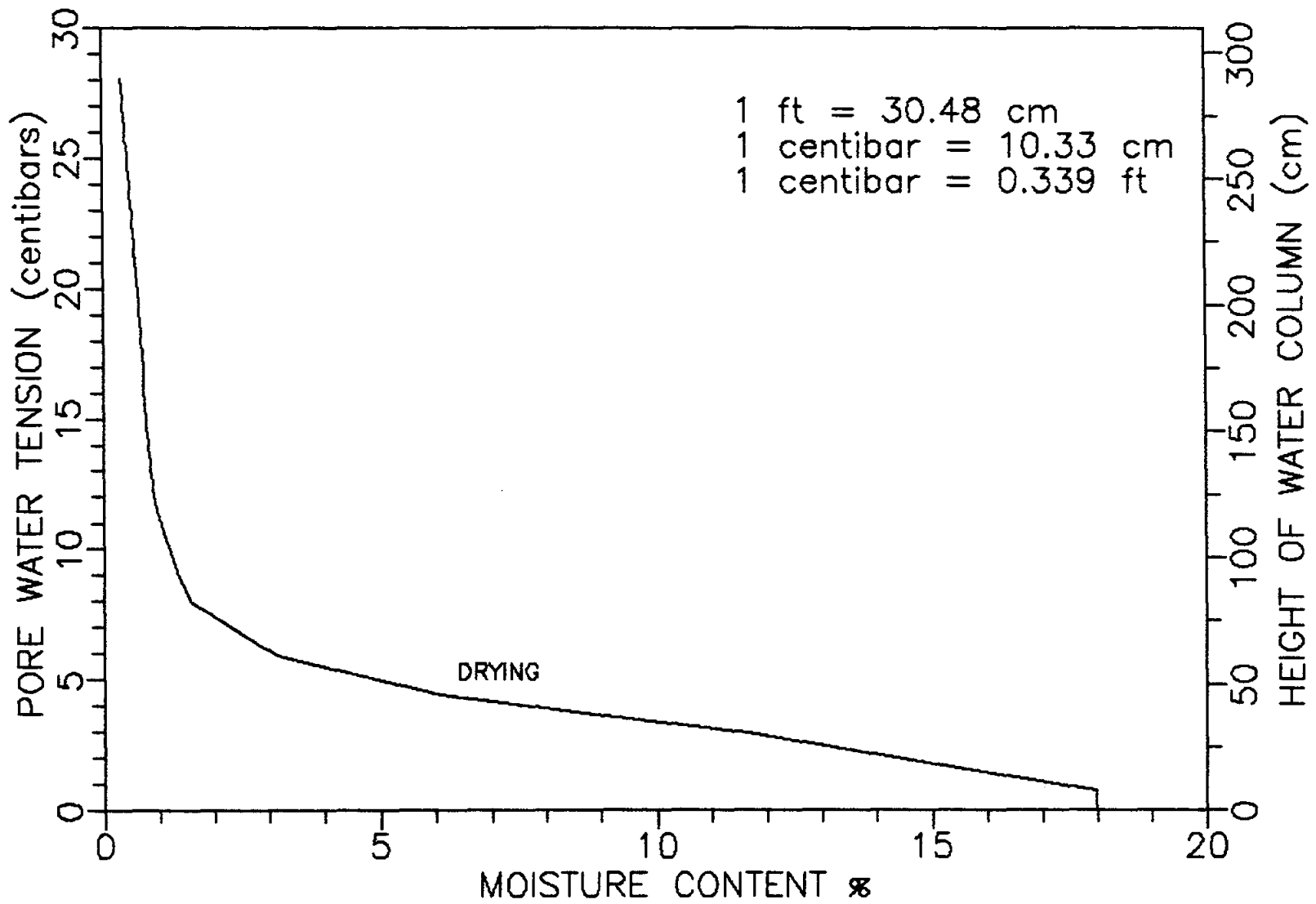
Figure 4.4 Soil-moisture characteristic curve for the test sand.

decreases with increasing temperatures. The temperature-resistance relationship is given by the following formula known as the Steinhart-Hart equation.

$$T = \{A + [B \ln(R)] + [C \ln(R)^3]\}^{-1} \qquad (4.4)$$

where T = degrees Kelvin,

R = resistance in Ohms, and

A, B, C = curve-fitting coefficients.

The manufactor-determined, standard coefficients for the YSI 44033 thermistor were used for the fifteen thermistors placed in the sand. The coefficients from the Yellow Springs Instrument Company (1977) are given in the following table.

Table 4.1

Steinhart-Hart Equation Coefficients
for the YSI 44033 Thermistor

Coefficient	Value
A	1.473264×10^{-3}
B	2.372096×10^{-4}
C	1.074362×10^{-7}

Figure 4.5 shows the temperature-resistance relationship for the YSI 44033 thermistor using the manufactor's
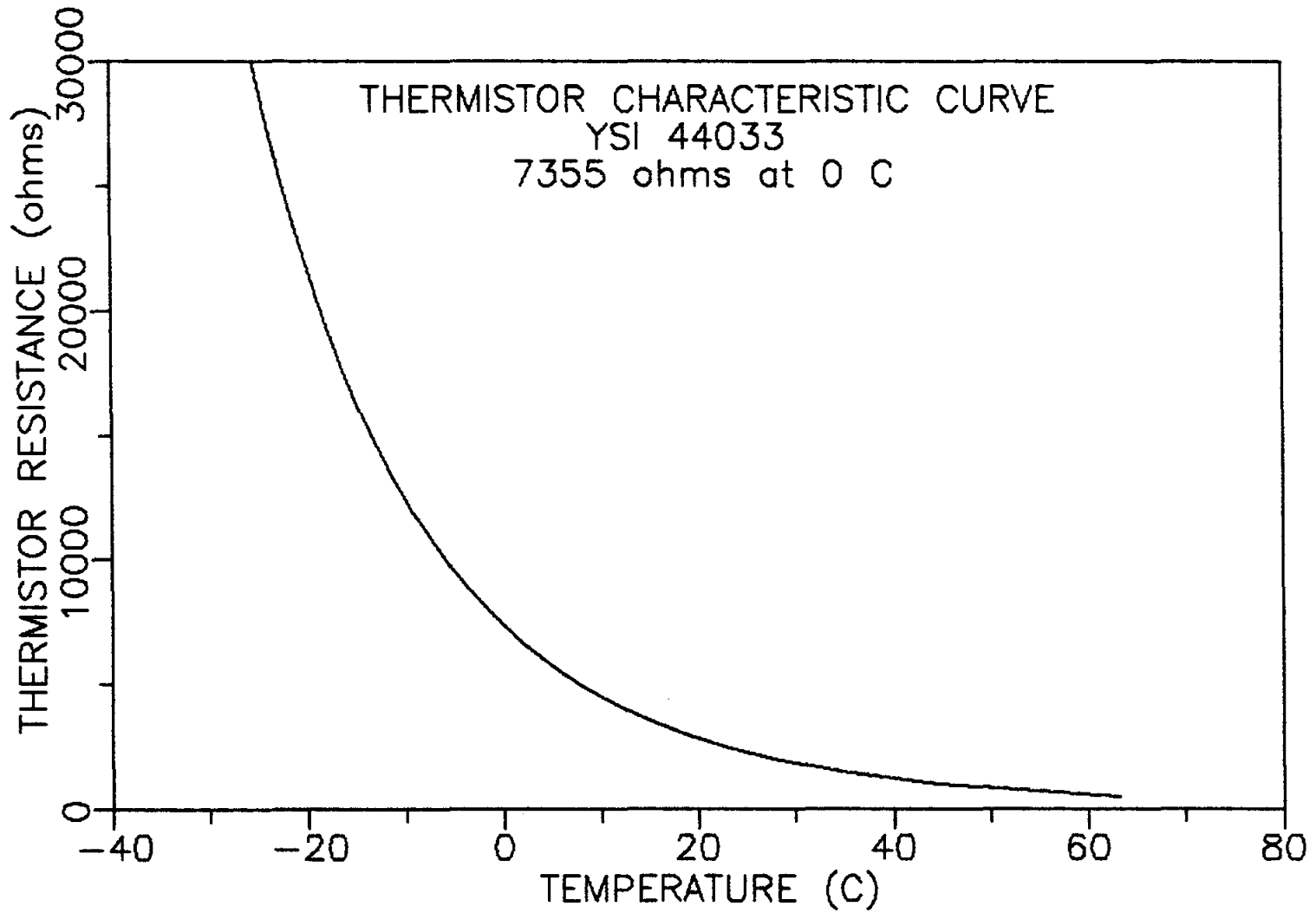
Figure 4.5   Temperature-resistance relationship of the YSI 44033 thermistor.

coefficients. The thermistors used for direct burial in the soil environment were fabricated by encapsulating the thermistor bead in a piece of copper tubing. This protected the thermistor bead from pressures generated during freezing in the soil-water medium. In addition, the thermistors were water-proofed using heat shrink tubing and a silicone rubber adhesive sealant. Following fabrication, the thermistors were placed in a water-ice bath having a temperature of 0°C and the resistances were determined and checked against the manufactor's specifications (7355 ohms at 0°C). The largest deviation was -27.3 ohms which equated to a temperature difference of -0.07°C. This was considered acceptable based on a desired accuracy of a 0.1°C for the thermistors to be buried in the soil.

The coefficients of the two thermistors placed in the stream of the circulated glycol solution were determined by the author. These two thermistors were attached to each other and placed into a fluid bath. The temperature of the fluid bath and the resistances of the two thermistors were recorded for three different temperatures spanning the range over which the thermistors were expected to operate. Using the results of the calibration exercise and the Steinhart-Hart equation, the three unknown coefficients were determined. The results of this calibration exercise are shown in Table 4.2.

Table 4.2

Calibration Data and Resulting Coefficients for the Thermistors in the Heat Exchanger

Fluid Bath Temperature	Thermistor Resistance #16	#17
-10.60°C	12,746.1 ohms	12,728.4 ohms
-22.40°C	24,944.1 ohms	24,928.8 ohms
-30.48°C	40,541.0 ohms	40,617.5 ohms

Thermistor	Curve - fitting coefficients A	B	C
16	1.631218 E-03	2.1386 E-04	1.846421 E-07
17	1.575068 E-03	2.22669 E-04	1.529687 E-07

During the experiment, thermistor #16 was placed in the flow of the cooling fluid just prior to entering the heat exchanger. Thermistor #17 was placed in the flow of the cooling fluid exiting the heat exchanger. Figure 4.6 shows the location of the thermistors used in the experiment.

The purpose of the two thermistors was to measure the temperature differential in the cooling fluid across the heat exchanger. The temperature drop and the mass discharge were used to calculate the rate of heat removal using the following equation:
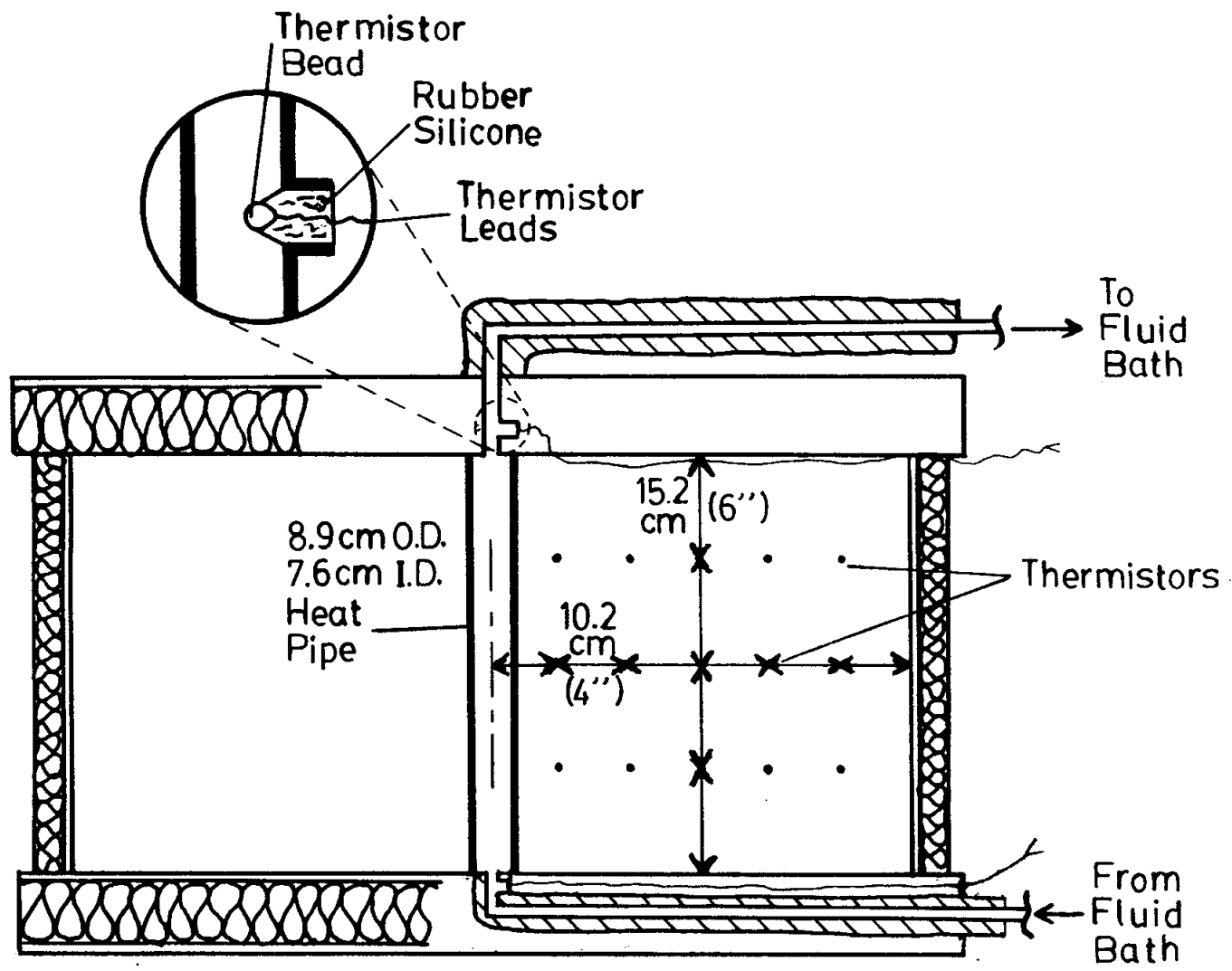
Figure 4.6   Thermistor locations in the soil medium and the freeze tank.

$$\dot{Q} = \dot{m} \, C \, dT \qquad\qquad (4.5)$$

where $\dot{Q}$ = heat energy removal rate,

$\dot{m}$ = mass discharge rate,

C = heat capacity of working fluid, and

dT = temperature drop across heat exchanger.

During the first test, the thermistors and the thermocouple were connected to a Hewlett Packard 3497 Data Acquisition Unit and a Hewlett Packard 85 micro-computer. A program was written to read the temperatures every 0.5 hour for the first eight hours and then hourly until completion.

Due to the unavailability of both the data acquisition unit and the micro-computer during the final two tests, temperature measurements were taken manually by reading the resistance of each thermistor. This was accomplished by using a Fluke 8081A Digital Multimeter. The ambient temperature and the temperature at the outer surface of the tank wall were obtained by using thermometers. The thermometers measured temperatures to the nearest whole degree Celsius.

4.4 Pore Pressure-Moisture Measurements

Soil tensiometers were used to measure negative soil water pressures in the sand during freezing. Moisture contents where indirectly determined by using the soil-moisture characteristic curve and the measured negative pore water pressures.

A diagram illustrating the tensiometer used in the experiment is given in Figure 4.7 (after Soilmoisture Equipment Corp., 1983). The primary components include a fluid reservoir, Bourdon-type vacuum gauge, flexible connecting tube, and a porous ceramic tip. The principle of the tensiometer is similar to the Tempe cell mentioned earlier. The deaired, saturated ceramic tip (AEV = 1 bar) is placed into a soil where it comes in contact with the soil water forming a continuous liquid. Any change in negative pore water pressure in the soil is transmitted through the ceramic tip and is registered on the Bourdon-type vacuum gauge.

For example, the soil pore pressures increase negatively as the soil surrounding the porous tip is desaturated, either by drying or freezing. In an attempt to establish pressure equilibrium, the pore water (lower potential) causes an attraction for the fluid contained in the tensiometer (higher potential). This attraction pulls fluid from the air-tight tensiometer causing an increased
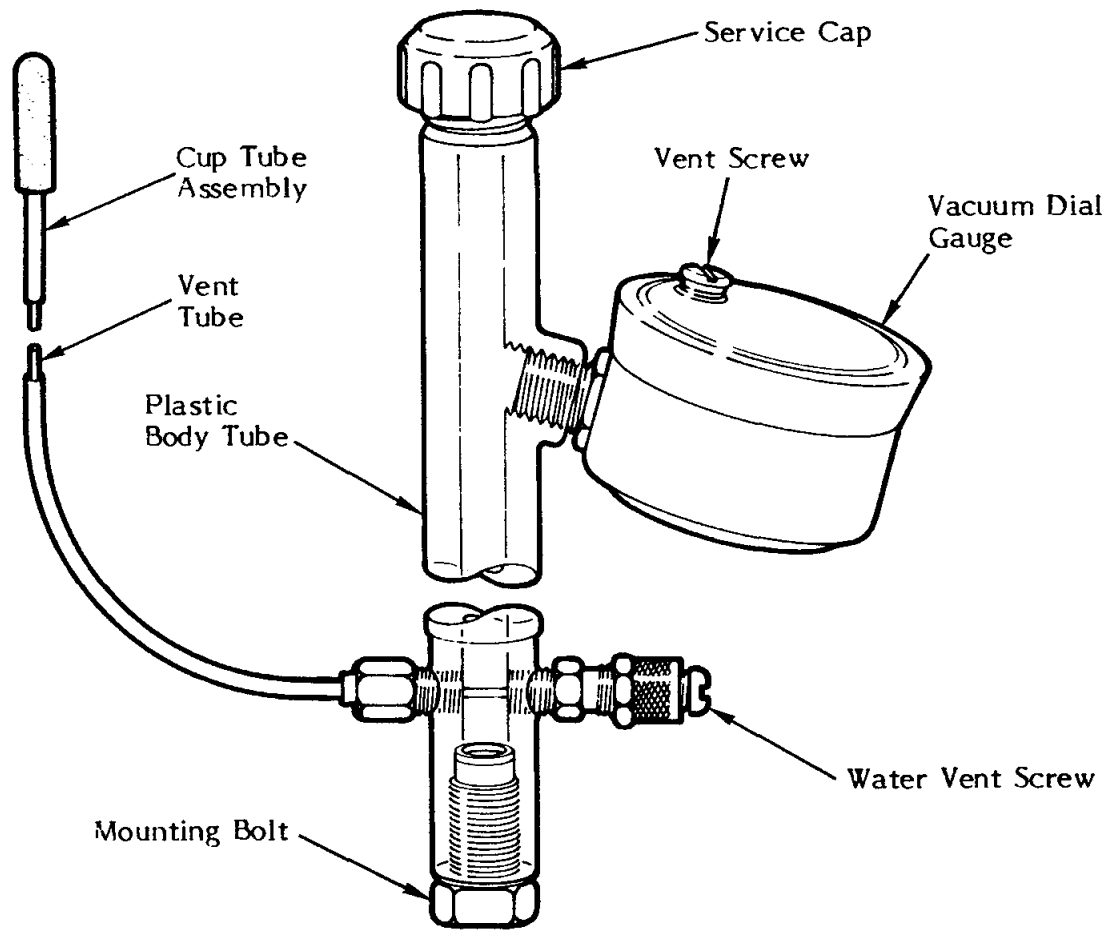
Figure 4.7   Diagram of 2100F tensiometer after Soilmoisture Equipment Corp. (1983).

Service Cap

Cup Tube
Assembly

Vent Screw

Vacuum Dial
Gauge

Vent
Tube

Plastic
Body Tube

Water Vent Screw

Mounting Bolt

negative pressure to be registered on the vacuum gauge. Equilibrium is established when the soil pore pressure is equal to the pressure in the tensiometer cavity. The process is also reversible until soil saturation occurs and the pore pressure becomes zero. The tensiometer can not measure positive pore pressure. The tensiometer vacuum gauge had a range of from 0 to 100 centibars (1 bar). However, at approximately 85 centibars dissolved air in the fluid expands and begins coming out of solution. This results in fluid loss through the ceramic tip and inaccurate gauge readings (Soilmoisture Equipment Corp., 1983).

Nine tensiometers were employed during each of the three freezing tests. In the first test, tensiometer tips were placed at three locations 15.2 cm (6"), 30.5 cm (12"), and 45.7 cm (18") above the base of the tank respectively. At each of the three elevations, three tensiometer tips were spaced at 15.2 cm (6"), 30.5 cm (12"), and 45.7 cm (18") radially outward from the center of the heat pipe. The radial distances were changed to 20.3 cm (8"), 30.5 cm (12"), and 40.6 cm (16") for the two remaining tests. This was done so that each of the tensiometer tip locations corresponded to the locations of the thermistors (see Figure 4.6 for thermistor locations).

The tensiometer bodies were situated on the top of the tank cover for easy access when taking gauge measurements. Placing the ceramic tip below the gauge causes an additional

tension to develop inside the tensiometer. This effect must be subtracted from the observed reading to get the actual soil water tension. This is done by using the following equation:

$$R_{cor} = R_{obs} - (h/10.33) \qquad (4.6)$$

where R_{cor} = corrected tensiometer reading (centibars),

R_{obs} = observed tensiometer reading (centibars), and

h = tip distance in centimeters below gauge.

The ceramic tip, flexible tubing, body cavity, and vacuum gauge may all be damaged if water is used as the working fluid and the tensiometer is exposed to temperatures below 0°C. Therefore a 50-50 solution of ethylene glycol and water was used in the tensiometers. Ingersoll (1981) recommends using as weak as ethylene glycol-water solution as possible to prevent freezing. This is due to the uncertainty that exists on the effects of the solution on the soil and on the tensiometer operation.

4.5 Test Procedure

The procedure required for each freezing test proved to be laborious and time consuming. The preparation prior to initial freezing of each test consisted of freeze tank

assemblage, soil preparation, placement of soil and instrumentation, connecting the temperature-controlled fluid bath to the freezing tank, and cooling the soil to prefreezing temperatures.

Soil preparation included adding sufficient water and thoroughly mixing the soil until the moisture content was both uniform and the desired value. The soil was placed in the freeze tank and compacted to a uniform density in 7.6 cm (3") lifts. The inplace density was determined twice for each test according to the procedure outlined in ASTM 2167-84. Also, inplace moisture contents were determined several times during soil placement. At the specified depths, thermistors and tensiometers were placed in the soil at their required radial distances. The tensiometers were recharged with a fresh ethylene glycol-water solution, deaired, and calibrated prior to placement.

Following soil and instrumentation placement, the insulated tank cover was situated into place. The temperature-controlled bath was then connected and circulation of the glycol solution was initiated to bring the soil mass to near-isothermal conditions, slightly above freezing temperatures (between 0°C and 1°C). Freezing of the soil began by setting the fluid bath to the desired temperature and discharge rate after near-isothermal conditions had been maintained for at least one day.

Periodic readings of the thermistors and tensiometers as well as mass discharge measurements were taken during the soil freezing stage. The experiment was terminated when temperatures approached those of steady-state conditions. The freeze tank was then disassembled and the frozen soil was dissected to determine the final distribution of moisture. Table 4.3 shows the major tasks performed and the range of task durations for one freezing test.

Table 4.3

Tasks and Task Durations
for One Typical Freezing Test

Task	Duration (days)
Freezing Tank Assemblage	1
Soil Preparation	1-3
Placement of Soil and Instrumentation	2
Connecting Fluid Bath	1
Precooling Soil Mass	7-14
Running Experiment	13-46
Dissection of Frozen Soil Mass	3-4
Total	28-71 days

CHAPTER 5

EXPERIMENTAL RESULTS

A   121.9 cm (48") diameter, 61.0 cm (24")   high

cylindrical   freeze   tank   with a   8.9   cm   (3.5")   diameter

vertical pipe down the center was fabricated.   The tank was

filled with soil and a cooled glycol solution was circulated

through   the   pipe to freeze the soil mass   in   an   outward,

radial direction.   The mass flow rate and the temperature of

the   cooling fluid controlled the heat removal   rate   during

freezing.   The soil consisted of a poorly   graded,   "clean"

sand.   A clean sand is generally considered to be   nonfrost-

susceptible and does not promote the formation of segregated

ice features.

A   clean sand is commonly specified as backfill   around

the   evaporator   section   of   thermosyphons.   The   thermal

properties of the backfill sand will be altered if   moisture

redistribution   occurs   during freezing.   The goal   of   this

study   is to examine the moisture-temperature   relationships

of a   sand due to outward radial freezing.

The   results of the three freezing tests performed   are

given   in this Chapter.   Section 5.1   gives the initial soil

properties, the environmental controls, the final conditions, and several average thermal properties for each test. The temperature measurements for each test and a comparsion of the results to available hand solutions are discussed in Section 5.2. Soil suctions due to freezing and tensiometer performance are addressed in Section 5.3. Finally, Section 5.4 is reserved for discussions on the observed initial and final moisture distributions.

5.1 Test Properties and Controls

Three separate tests were performed on the clean sand. The experimental procedure outlined in Section 4.5 was followed for each test. Several physical properties and environmental factors were altered for each test. The soil property variations included initial moisture content and soil dry density. The environmental variables consisted of the mass discharge and the temperature of the cooled, circulating fluid.

Altering the initial moisture content and the dry density resulted in different thermal properties of the sand for each test. These thermal properties include thermal conductivity, volumetric latent heat of fusion, and volumetric heat capacity. These physical and thermal properties determine the freezing rate of the soil as discussed earlier. Changing the mass discharge and the

temperature of the cooling fluid causes a change in the heat removal rate and in the final distribution of steady-state temperatures. Table 5.1 shows several of the pertinent experimental parameters and gives values for soil properties in each test.

The thermal properties given in Table 5.1 are an average value for the entire soil mass. When calculating the thermal properties, the mass density was assumed to be constant but the moisture content was assumed to be a function of capillary head according to the soil-moisture characteristic curve.

As previously mentioned, the average initial moisture content for each test was determined from the soil-moisture characteristic curve and from moisture content samples taken during soil placement prior to freezing. The average final moisture contents were calculated by averaging the moisture content samples taken during dissection of the frozen soil mass. The final average moisture content of test #1 was determined from 25 samples. The final average moisture content of tests #2 and #3 were determined from 30 samples each.

The average temperature of the cooling fluid and the average temperature drop across the heat pipe ($T_{out}-T_{in}$) were calculated by averaging the temperatures given by thermistor #16 and #17 (Section 4.3). The mass discharge

Table 5.1

Soil Properties and Environmental Factors
For Each Freezing Test

Test	Dry Density (kg/m3)	Average Initial Moisture Content (%)	Average Final Moisture Content (%)	Test Duration (hours)	Time to Freeze (hours)
1	1839.7	11.6	9.0	279	159.4
2	1754.8	7.1	6.9	654	373.5
3	1753.2	6.7	6.6	1075	360.0

Test	Final Outside Tank Temp. (C)	Average Cooling Fluid Temp. (C)	Average Mass Discharge (gm/sec)	Average Pipe Temp. Drop (C)
1	---	-18.37	22.77	0.32
2	-3.5	-8.52	10.30	0.14
3	-4.0	-8.86	10.73	0.26

Test	Average Frozen Thermal Conduct. (W/m K)	Average Thawed Thermal Conduct. (W/m K)	Average Frozen Heat Capacity (kJ/m3 K)	Average Thawed Heat Capacity (kJ/m3 K)	Average Volumetric Latent Heat (kJ/m3)
1	2.871	2.247	1754	2199	70895
2	1.613	1.685	1514	1779	42246
3	1.505	1.633	1492	1736	38919

rates listed in Table 5.1 are average values based upon measurements taken periodically throughout each test.

5.2 Soil Temperatures

The thermistors used during this study provided reliable temperature measurements. Figures 5.1 through 5.3 give average temperatures at radial distances corresponding to thermistor locations for test #1 through test #3 respectively.

In test #1, (Figure 5.1) the soil exhibited an apparent freezing point depression of 0.5°C based upon the measured temperatures. The freezing point depression was not considered to be inherent to the soil based upon the author's experience. Therefore another source causing this effect was sought and it was later determined that the water used during soil preparation and mixing contained high amounts of dissolved solids and salts. The source of this water was common tap water obtained in the Duckering building. Demineralized water was used in the remainder of the tests and subsequently, this freezing point depression is not observed in Figures 5.2 and 5.3 (tests #2 and #3).

Several temperature anomalies are observed in Figure 5.3. These are due to the inaccuracy and numerous breakdowns of the cold room refrigeration unit in which the freezing tank and temperature-controlled fluid bath were
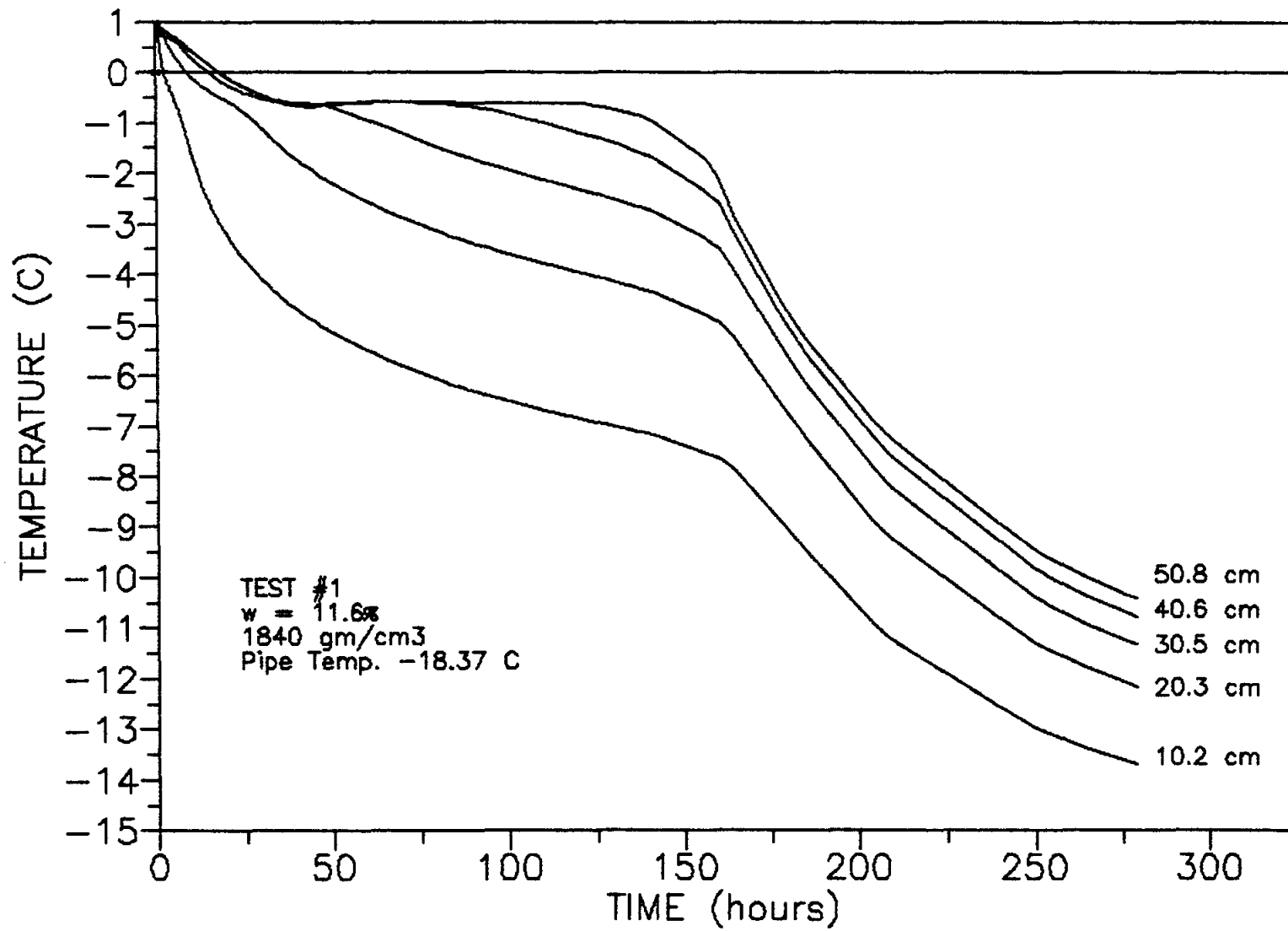
Figure 5.1   Average temperature profiles at various radial distances from center
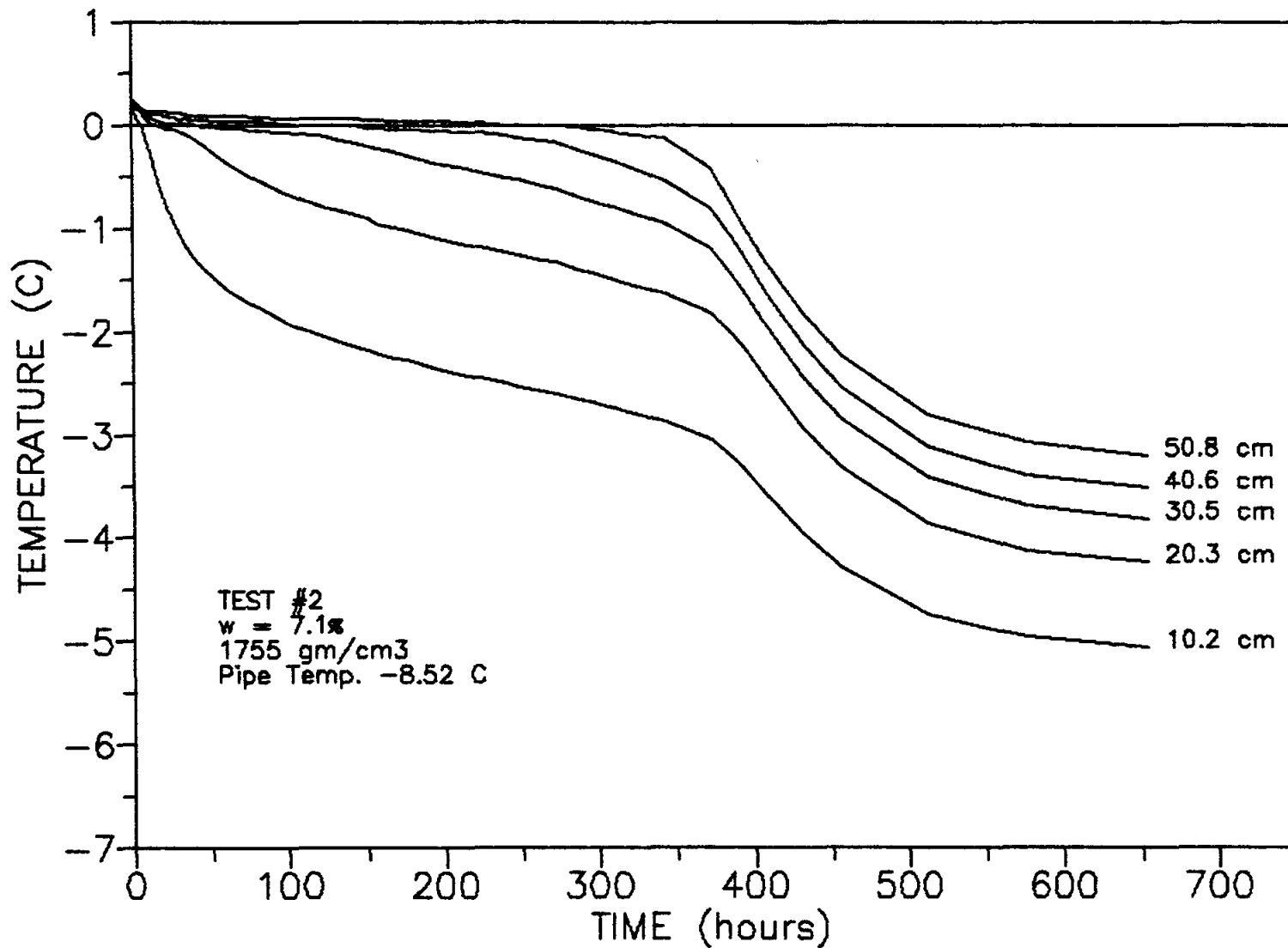of heat pipe for test #1.

Figure 5.2 Average temperature profiles at various radial distances from center
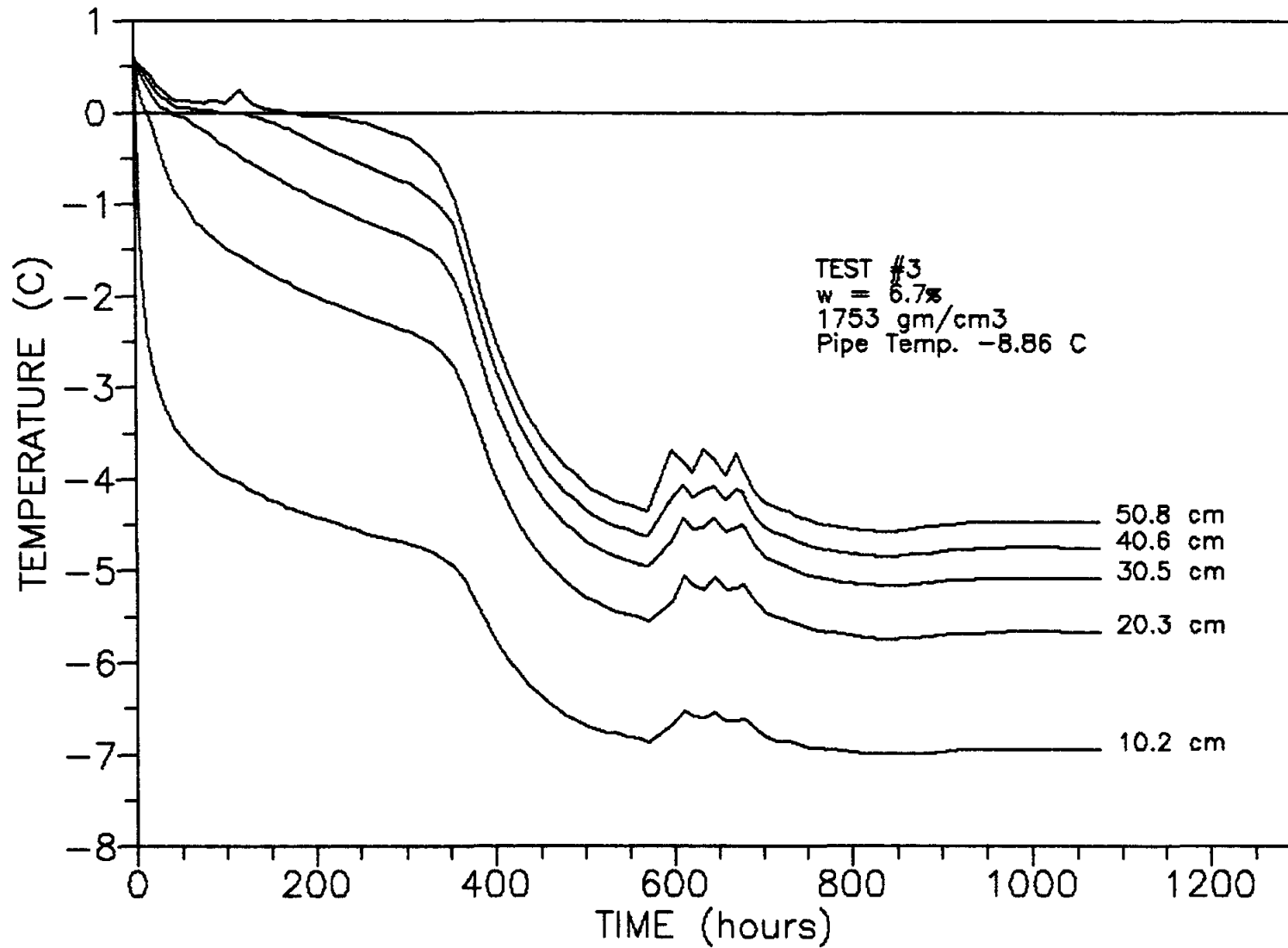of heat pipe for test #2.

Figure 5.3 Average temperature profiles at various radial distances from center of heat pipe for test #3.

situated. The heat generated by the circulation pump and the refrigeration unit of the fluid bath quickly increase the ambient temperature of the insulated cold room when the cold room refrigeration unit failed. This warranted constant monitoring of the cold room during the experiments.

Undesirable ambient temperature variations also occurred during the experiments due to the inability of the cold room refrigeration unit to maintain a constant ambient room temperature even when the unit was working. A layer of insulation was placed on the outer surface of the freeze tank to attenuate these effects. Figure 5.4 shows the ambient temperature inside the cold room and temperature of the tank wall-insulation interface. This graph also shows that the temperature variation of the cold room interior was about four degrees centigrade. The large temperature spikes in this figure are the result of cold room failures. The attenuation effect of the insulation is realized by comparing the temperatures.

Figures 5.1 to 5.3 illustrate three distinct stages of soil cooling observed during the experiments. First, the soil temperatures were lowered to the phase change temperature, $0°C$ ($-0.5°C$ in test #1), after the test was initiated. Next, the temperatures dropped following phase change. The rate of change decreased as the radius of phase change increased. The soil temperatures again suddenly dropped when the entire soil mass had been frozen. The
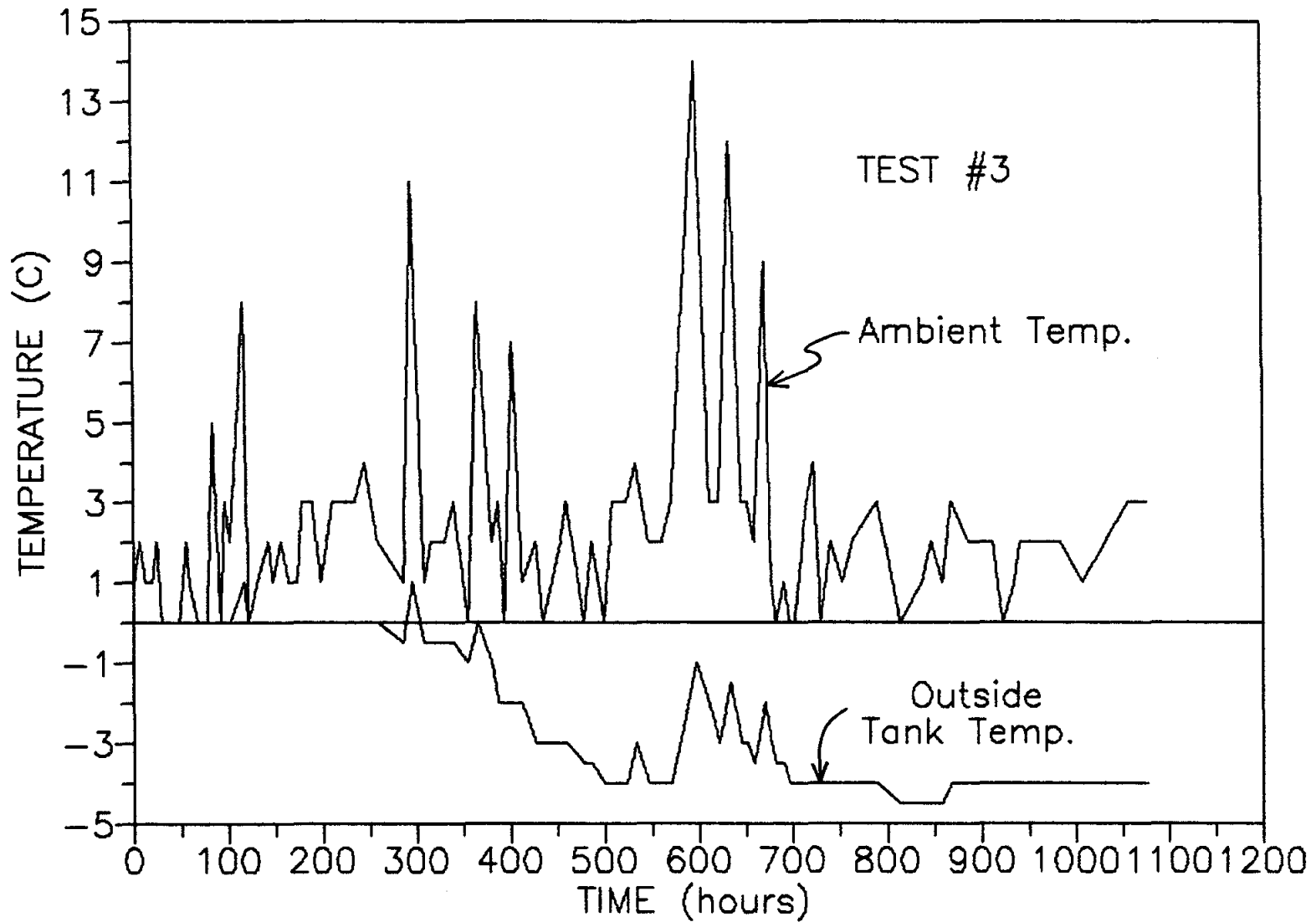
Figure 5.4   Temperature profiles for the cold room ambient temperature and outside tank wall temperature during test #3.

rate of temperature change decreased as the soil mass approached steady-state conditions. Test #1 was terminated due to a failure of the refrigeration unit. Test #2 was terminated at near steady-state temperatures while the final soil temperatures of test #3 reflect steady-state conditions.

5.2.1 Complete Phase Change

As was discussed earlier, no general exact analytical solution exists for phase change around a finite cylinder. However a Stefan-type solution is available by which actual conditions can be approximated. Stefan-type solutions assume that all the heat energy conducted through the soil system is equal to the heat energy required for phase change thereby neglecting sensible heat effects. This type of solution approaches the exact solution as the ratio of the sensible heat to latent heat (Ste #) goes to zero. Several corrections can be utilized to account for the neglected sensible heat which reduces the extent of freezing over-predicted by the Stefan-type solutions. Two of these corrections (discussed in Section 2.3.2) are the effective volumetric latent heat of fusion (L_v') and the reduced radius of freezing (r'). Explicit finite difference techniques employing the enthalpy method can also be used to monitor the moving phase change boundary.

The time required to freeze the entire soil mass for each test can be determined graphically from Figures 5.1 through 5.3. This occurs when the soil temperatures suddenly drop following phase change of the outermost soil. This observed time is compared to times predicted by the Stefan-type solution with and without the two corrections. A finite difference program was written and the time to complete phase change was determined. Table 5.2 gives the times to complete phase change for each test using the various techniques.

Table 5.2

Predicted Times In Hours For Complete Phase Change

Test	From Graphs	Stefan Solution	Lv' Corr.	r' Corr.	Finite Diff.
1	159.4	151.3	180.2	161.8	169.5
2	373.3	336.4	373.5	352.2	438.9
3	360.0	319.4	364.5	336.2	413.9

The Stefan-type solutions were calculated by using the average initial moisture content of the soil and the corresponding thermal properties. The finite difference program calculated the average thermal properties based upon the initial moisture content distribution given by the soil-moisture characteristic curve. In the calculations for test

#1, a fusion temperature of -0.5°C (31.1°F) was used based upon the temperature observations given in Figure 5.1.

The variation of the ambient room temperature does affect the freezing rate of the soil. The freezing process is accelerated as the room temperature is lowered and is retarded as the room temperature is raised. These transient effects were reduced somewhat by the outer wall insulation and were omitted from the finite difference program. The ambient room temperature was assumed to be 0.6°C (33°F).

As expected, the Stefan-type solution predicted the fastest times for complete phase change. The effective latent heat correction caused a greater time correction than the effective radius of freezing correction. The finite difference program calculated values closest to those determined by the effective latent of fusion.

The accuracy of all the Stefan-type solutions employed depend on the magnitude of the Stefan number (Ste #). The finite difference method accounts for the effects of sensible heat when using the enthalpy approach. The Stefan-type solutions approach the exact solution as the Stefan number approaches zero. Table 5.3 gives the Stefan number for each test calculated from the average thermal properties.

Table 5.3

Stefan Numbers For Each Freezing Test

Test	Ste #
1	0.4421
2	0.3053
3	0.3396

As the Stefan number increases, so does the amount of sensible heat neglected and therefore the Stefan solutions will predict faster freezing times than actual.

5.2.2 Steady-State Temperatures

Test #2 was terminated when the soil temperatures were near steady-state conditions. The final temperatures in test #3 were at steady-state conditions. Steady-state conditions for test #3 can be seen in Figure 5.3 where the change in temperature with respect to time is equal to zero. The theoretical steady-state temperature profile is easily calculated by knowing the final pipe temperature and the outside tank temperature. Also, the soil thermal conductivity was assumed to be uniform throughtout the soil mass. The thermal properties based on the initial average moisture content were used to calculate the theoretical, steady-state temperatures. These values are compared with the measured temperatures from test #2 and #3 in Figure 5.5.

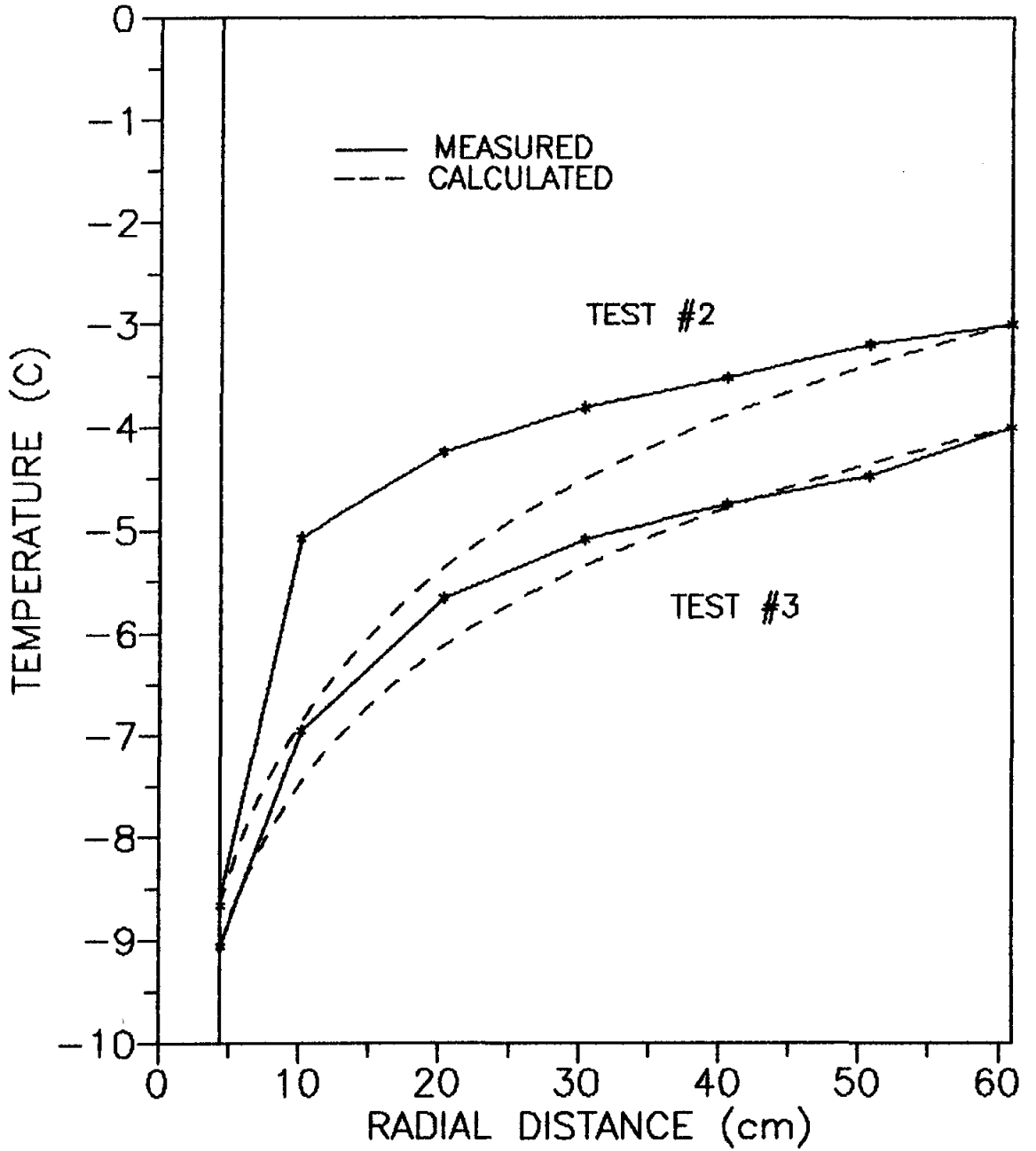The large deviation of the measured temperature profile

Figure 5.5   Final measured temperature profiles and
temperature profiles calculated by assuming
uniform soil thermal conductivity for test
#2 and test #3.

123

from that of the calculated profile for test #2 is due primarily to nonsteady-state conditions. Test #3 was terminated after steady-state conditions had been established. This deviance of the measured profile from the theoretical profile can be attributed to a change in thermal properties. The temperature profile for steady-state conditions is a function of the soil thermal resistance. The soil thermal resistance is a function of the soil thermal conductivity which in turn is a function of the soil dry density and the moisture content.

A soil thermal resistance profile for test #3 can be calculated by using the steady-state heat conduction equations and the measured temperature profile in Figure 5.5. A thermal conductivity profile can be calculated from the profile of thermal resistances. These two soil thermal property profiles are given in Figure 5.6. The moisture content profile can be established by using Kersten's (1949) equations (Section 2.2.1) and by making the assumption of uniform soil dry density. Kersten's relationship between thermal conductivity and moisture content for the sand is illustrated in Figure 5.7. The resulting radial distribution of moisture contents is given in Figure 5.8. The average moisture content calculated from the steady-state temperatures was 8.6%; slightly larger than the initial, average moisture content of (6.7%).
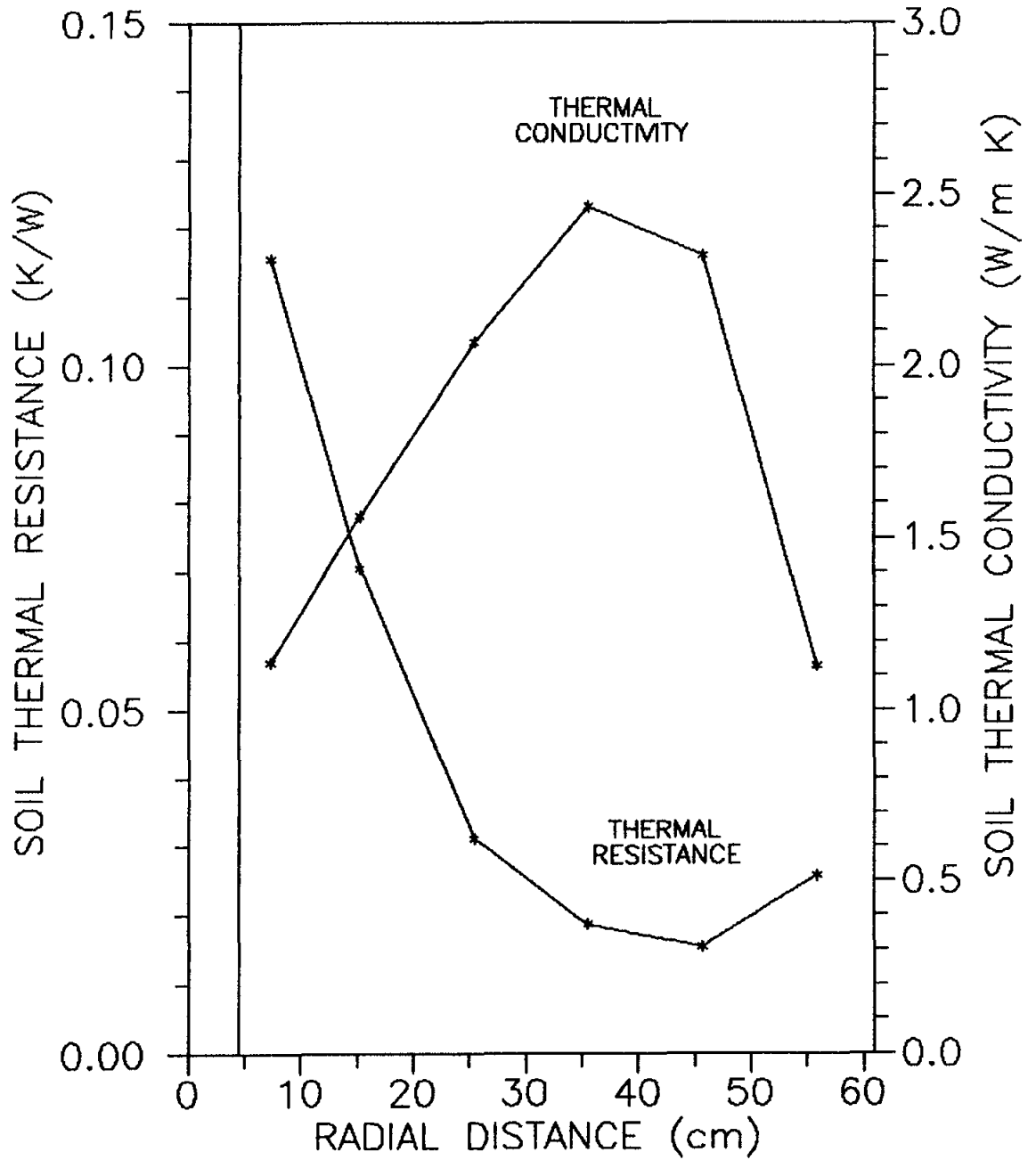
Figure 5.6   Thermal resistance and thermal conductivity
at various distances from the center for
test #3 based on measured steady-state
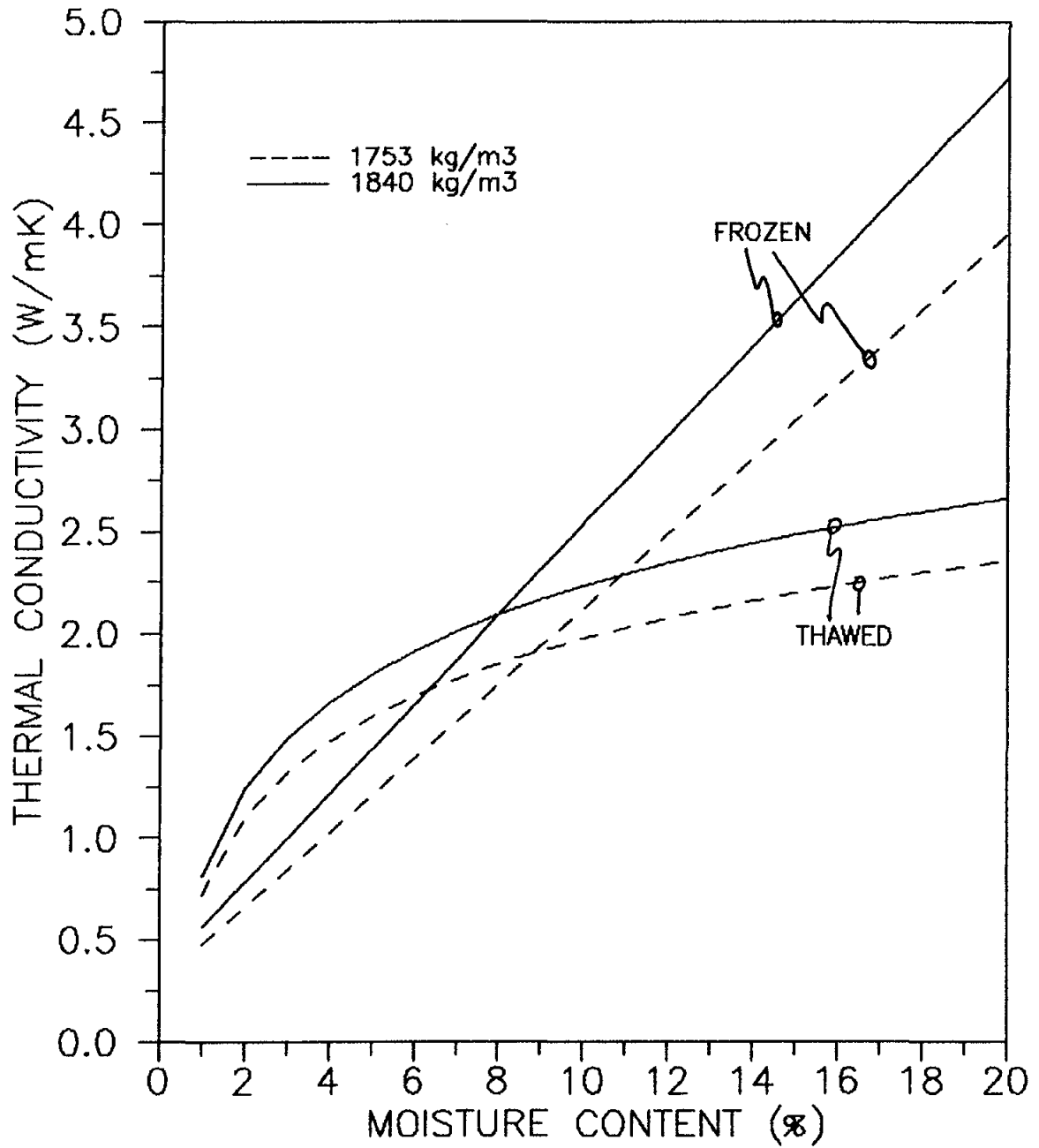temperatures.

Figure 5.7 Thermal conductivities of test sand
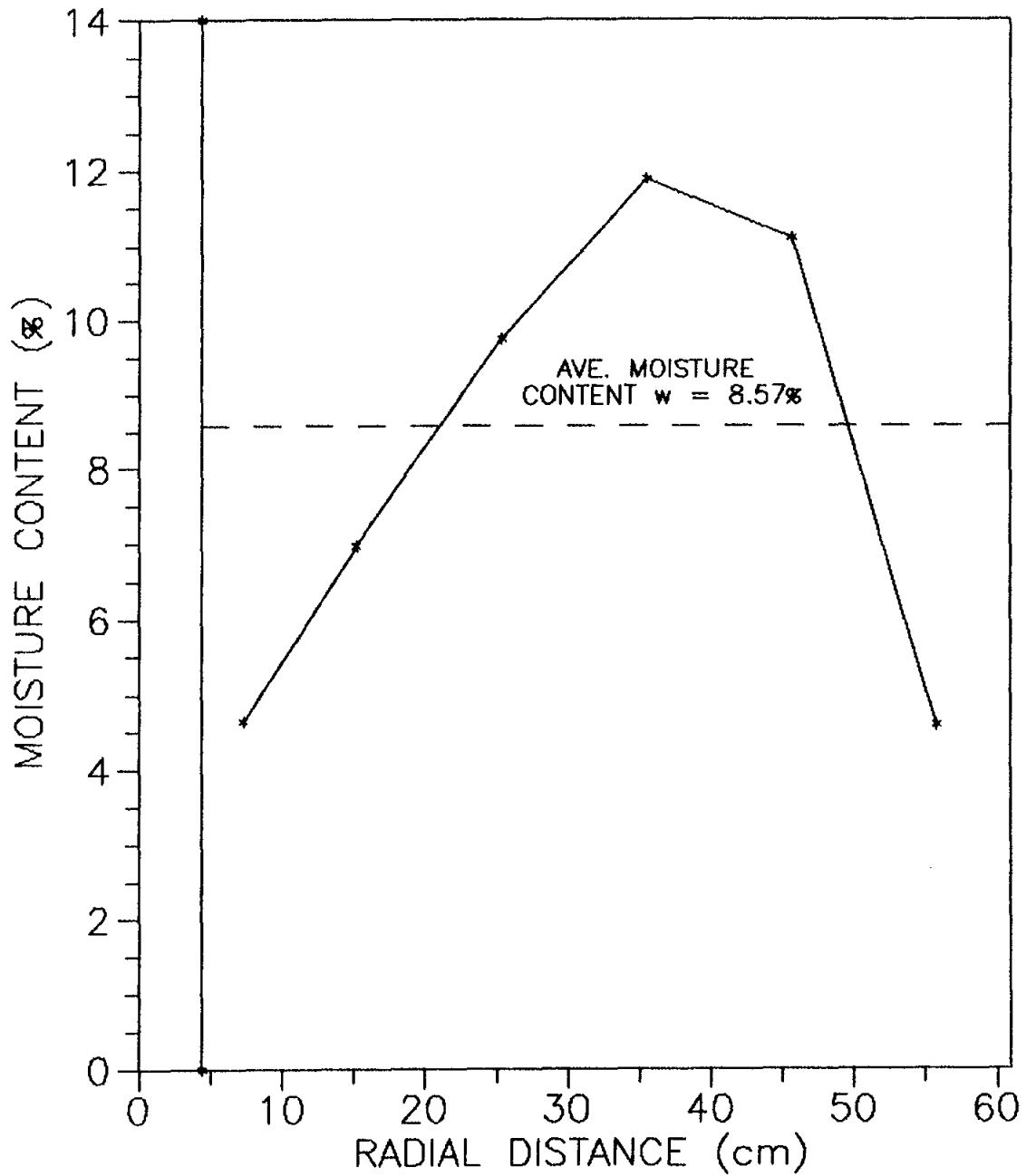   calculated from Kersten's equations.

Figure 5.8 Moisture content distribution based upon
measured steady-state temperatures for
test #3.

with increasing radii was calculated by assuming that the moisture content was uniform and equal to the average moisture content determined from the measured steady-state temperatures. In Figure 5.9, this theoretical distribution is compared to the cumulative distribution of water established from the steady-state analysis (Figure 5.8). Also, Figure 5.9 gives the theoretical, incremental increase in water based on the uniform, average moisture content for a 10.1 cm (4") radial interval and the calculated incremental increase in the water determined from Figure 5.8 for the same radial increment. Figures 5.8 and 5.9 show a definite redistribution of moisture towards the central region of the soil mass and a corresponding decrease or dessication of moisture at the outermost radius of the soil mass. Also, there is a slight dessication of moisture adjacent to the vertical pipe. Moisture redistribution will be addressed further in a later section.

5.2.3 Freezing Isotherm Velocities

The velocity of the zero degree (0°C) isotherm is a function of the imposed temperature gradient, the volumetric latent heat of fusion, and the radial distance from the center of the vertical pipe. The magnitude of the temperature gradient controls the heat removal rate. The volumetric latent heat of fusion determines the quantity of
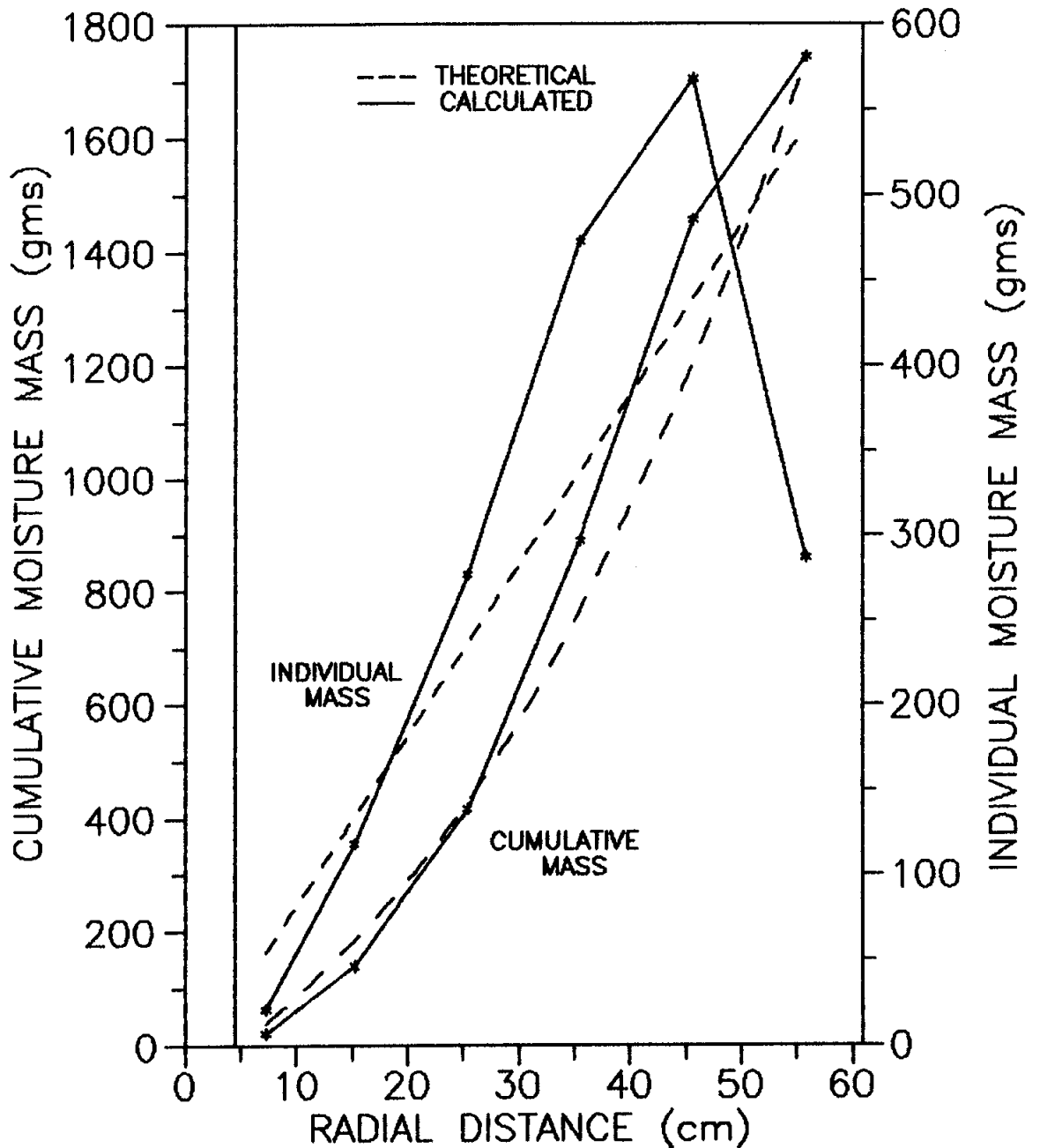
Figure 5.9 The theoretical (uniform moisture distribution) and the calculated relationships (from direct measurement) for both the cummulative mass of water with increasing radii and the incremental increase in mass of water for a 10.1 cm (4") radial interval.

heat energy that must be removed to freeze a unit volume of soil. The volume of soil increases at a rate of πr^2 with increasing radii from the center. Since the mass of water increases at a corresponding rate, the time for phase change increases greatly with increasing radii.

In Figures 5.10 through 5.12, temperature profiles are shown at various elapsed times for each test. These plots show the movement of the phase change boundary with increasing time. The position of the phase change boundary can be accurately tracked by creating similar profiles for all times and determining the radial location of the phase change temperature. The results of this analysis are shown in Figure 5.13 for each test. The phase change rates were also established by using the finite difference program and these are compared to the freezing rates determined from the temperature profiles in Figures 5.10 through 5.12.

The times given by the finite difference method increase expontentially with increasing radial distance. The times determined from the finite difference program for tests #2 and #3 are nearly identical. Suprisingly, the measured freezing rate for test #1 was approximately constant for the last two-thirds of the radial distance. This rate was calculated to be 0.276 cm./hour. The measured freezing rates of test #2 and #3 are similar to each other in trend and rate. There is a significant change in the measure freezing rates in tests #2 and #3 from the first 30
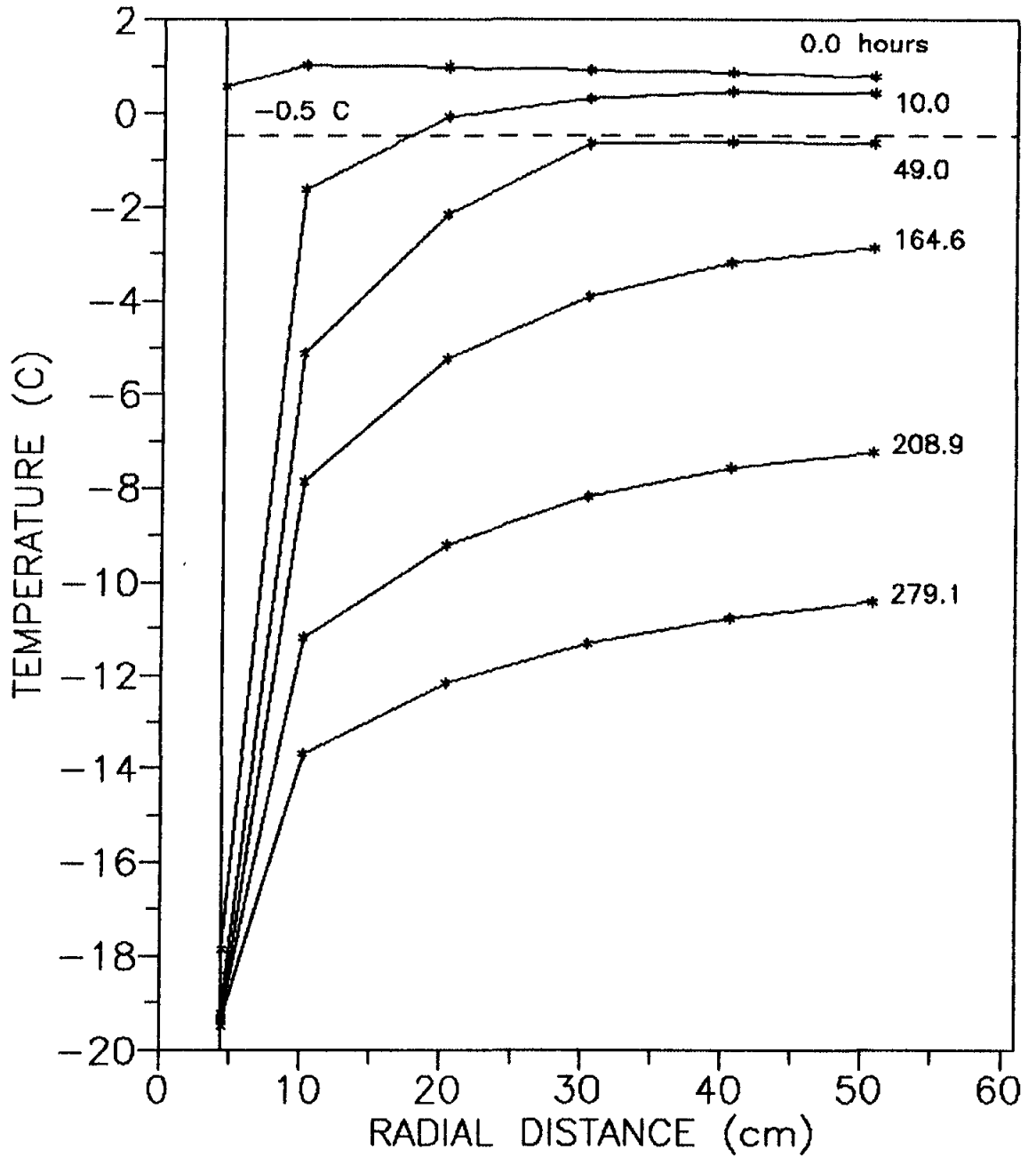
Figure 5.10   Temperature distributions in test #1 at specified times.
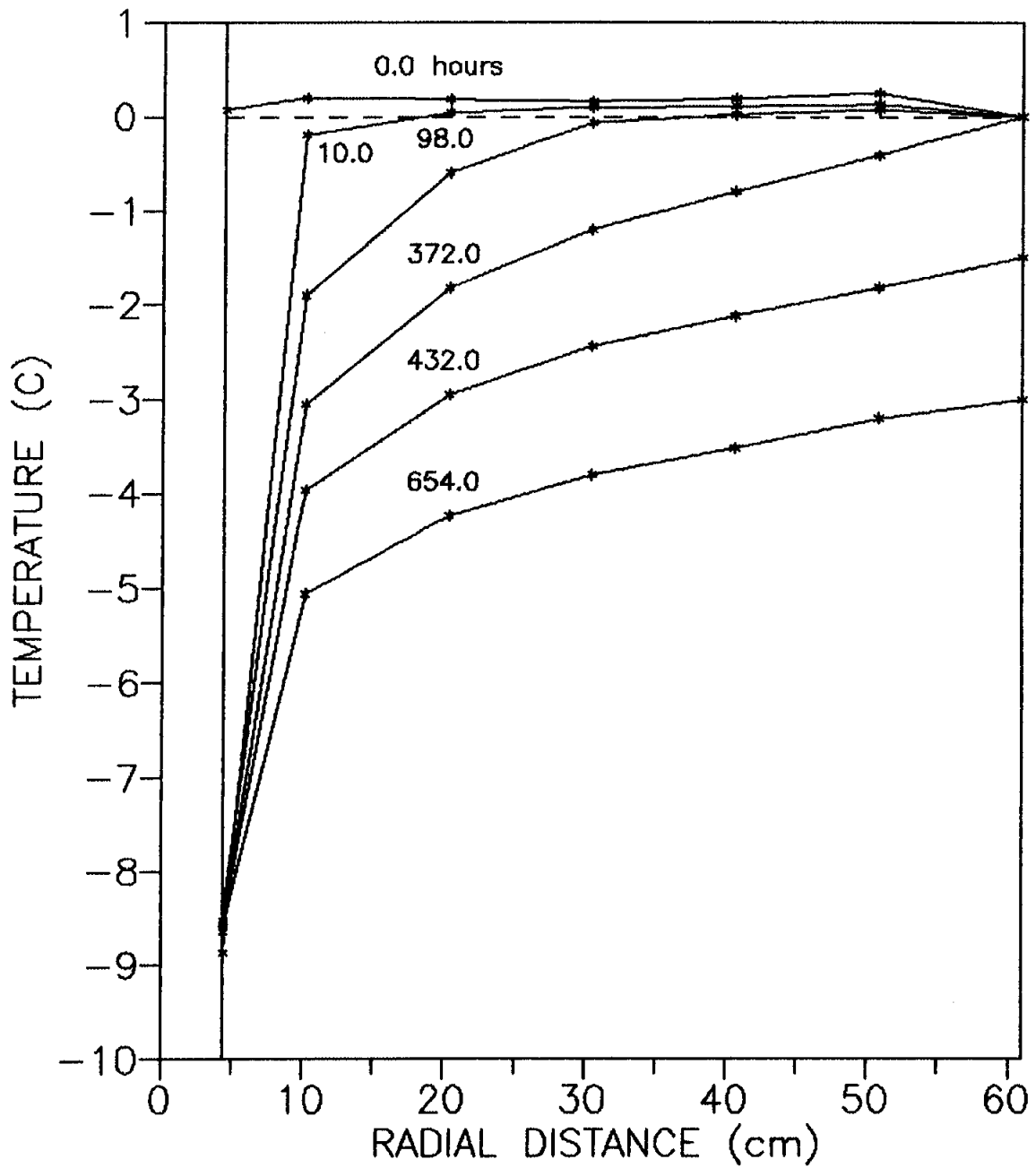
Figure 5.11   Temperature distributions in test #2 at
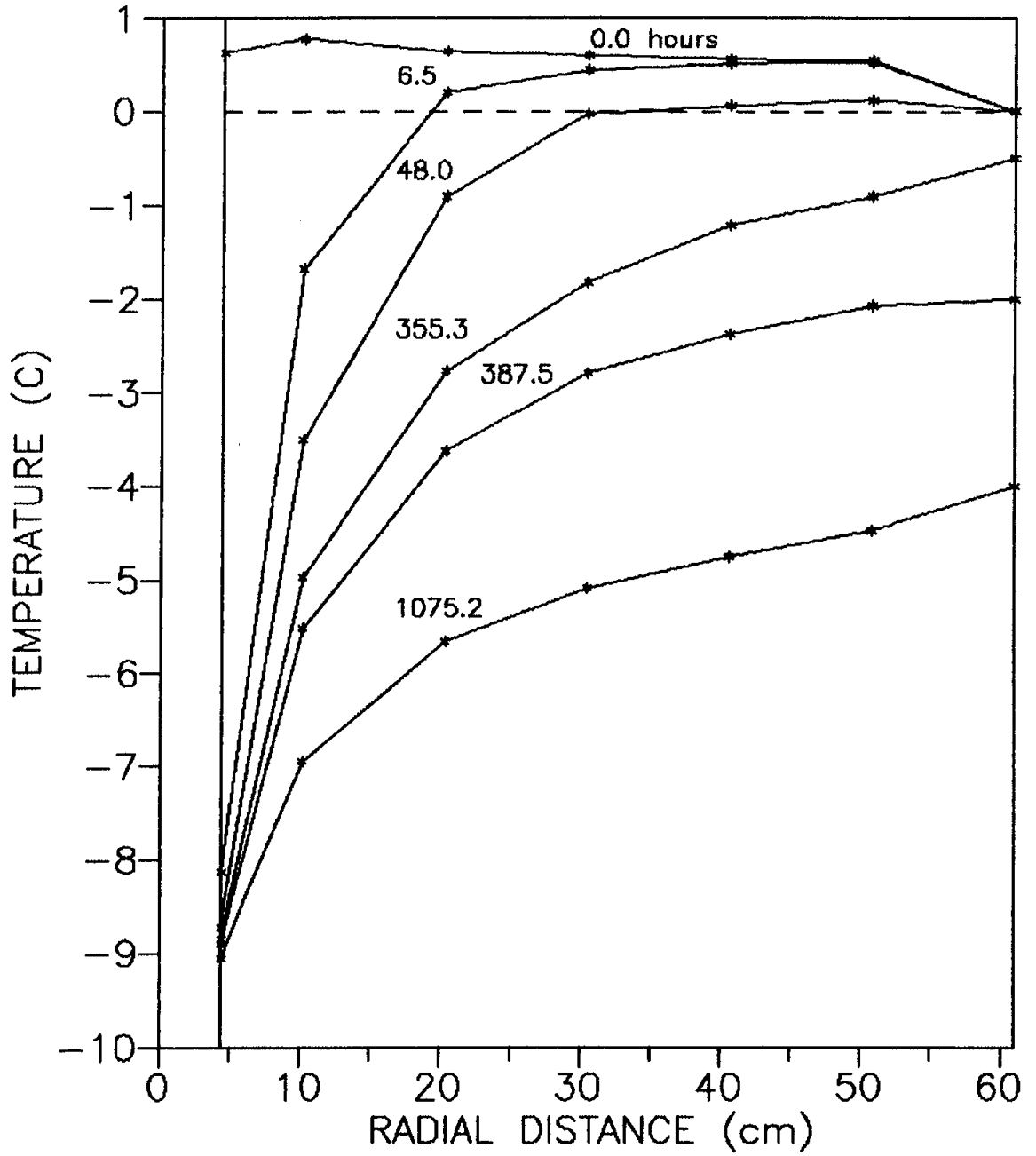   specified times.

Figure 5.12   Temperature distributions in test #3 at
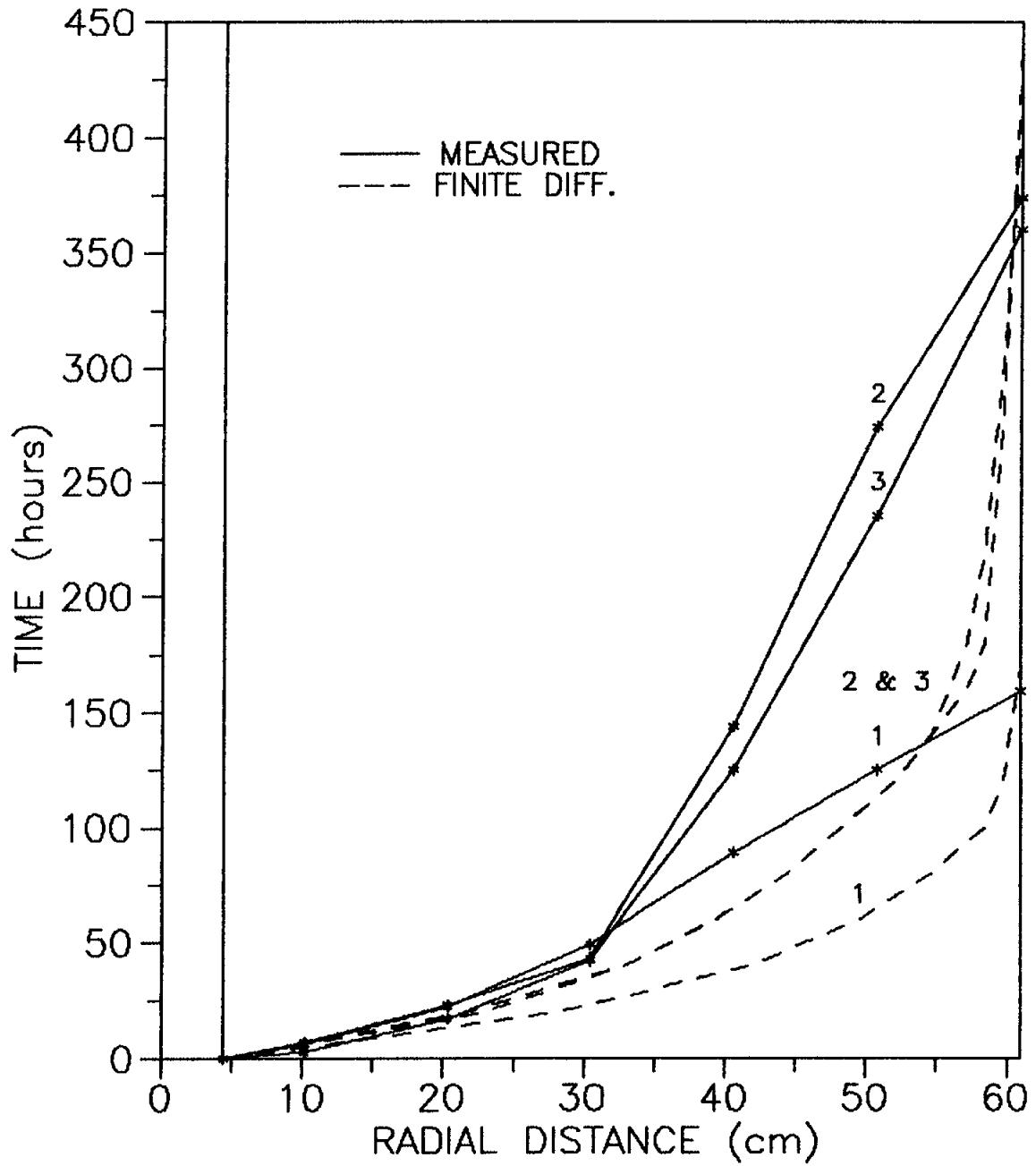specified times.

Figure 5.13   Measured and predicted phase change
boundary locations for each test.

centimeters to the last 30 centimeters. Both tests had a measured freezing rate of approximately 0.613 cm./hour up to a radius of 30 cm. The freezing rate then slowed abruptly to 0.092 cm./hour and 0.096 cm./hour for the last 30 cm. in test #2 and test #3 respectively.

5.3 Soil Suction Measurements

Little is known about the use of tensiometers in freezing soil experiments. This has resulted in a lack of information regarding the performance and reliabilty of this type of equipment under these conditions. The effects of cold temperatures and ethylene glycol on the tensiometer gauge and ceramic tip are not known (Ingersoll, 1982b). The tensiometers were initially planned to be used to determine moisture distribution before freezing and to monitor soil suctions and corresponding moisture contents during soil freezing. However, due to several undesirable observations and conclusions, the data obtained from the tensiometers was considered not to be reliable and therefore was not used in the analysis.

The soil surrounding the ceramic tip was found to be unfrozen during dissection of the frozen soil mass. The extent of thawed soil was about 3 cm. and the presence of

ethylene glycol was evident in the thawed soil. It is apparent that solution melting occurred as the glycol solution was pulled from the tensiometer tip at high soil suctions. This undoubtly, would effect the tensiometer readings.

The average moisture content calculated from the tensiometer readings for each test prior to freezing is given in Table 5.4. These values are based upon the soil-moisture characteristic curve and the nine tensiometers. The final average moisture contents are also listed in Table 5.4. These final moisture contents were determined from 25 to 30 samples obtained during dissection of the frozen soil mass. The total mass of water containted in the soil was easily calculated by knowing the soil volume, the average soil dry density, and the average moisture content. The change in total water mass was determined and is given in the following table.

The results of the initial and final moisture contents for test #1 indicate that a loss of water occurred during the freezing process. For tests #2 and #3, the tensiometer data suggest that there was substanial gains in the total mass of water during freezing. No external source of water was available to produce this effect.

Table 5.4

Initial and Final Moisture Contents Based
on Tensiometer Readings and Direct Measurements

| | Tensiometer Readings | | Direct Measurement | | |
| | Average Initial Moisture Content | Average Initial Mass of Moisture | Average Final Moisture Content | Average Final Mass of Moisture | Net Vol. of Moisture |
Test	(%)	(kg)	(%)	(kg)	(liters)
1	13.7	179.1	9.0	116.9	-62.2
2	4.0	49.3	6.9	85.6	+36.3
3	5.7	70.4	6.6	82.3	+11.9

Figures 5.14 through 5.16 show tensiometer readings and
corresponding tempertures for the mid-plane of the soil mass
in each test. Soil suctions increased dramatically as the
pore water froze however, the observed tensiometer readings
"lagged" behind the time of phase change indicated by the
thermistors. The tensiometer in test #1 (Figure 5.14) at a
radial distance of 30.5 cm developed a leak between the
flexible connecting tube and the ceramic tip. This was
repaired for the remaining tests. The tensiometers in test
#2 (Figure 5.15) behaved in a relatively nonresponsive
manner not consistent with either test #1 or test #3. These
tensiometer readings increased slowly resulting in the
greatest lag times and the lowest peak readings. In Figure
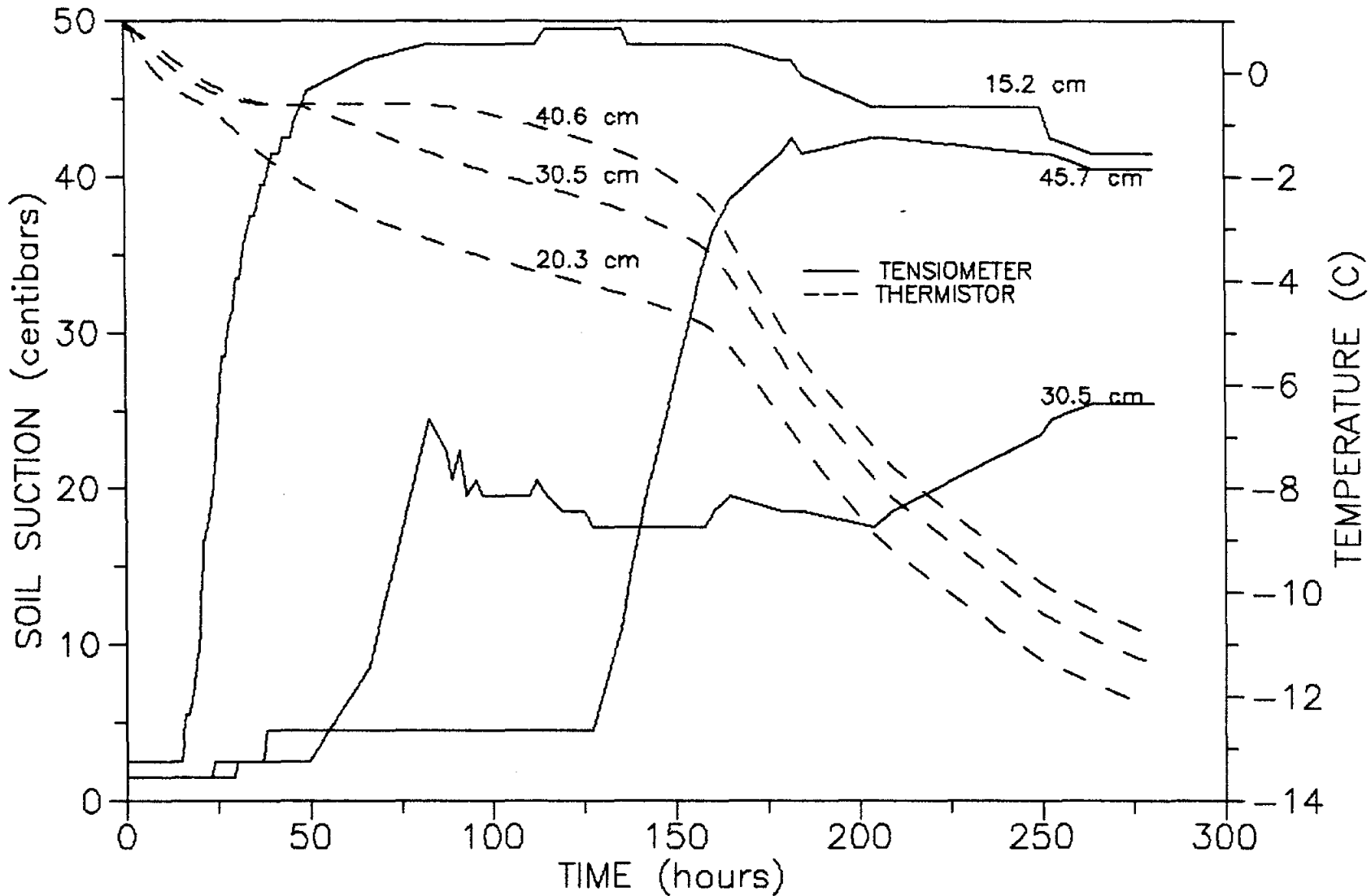5.16, the effect of temperature changes on the tensiometers

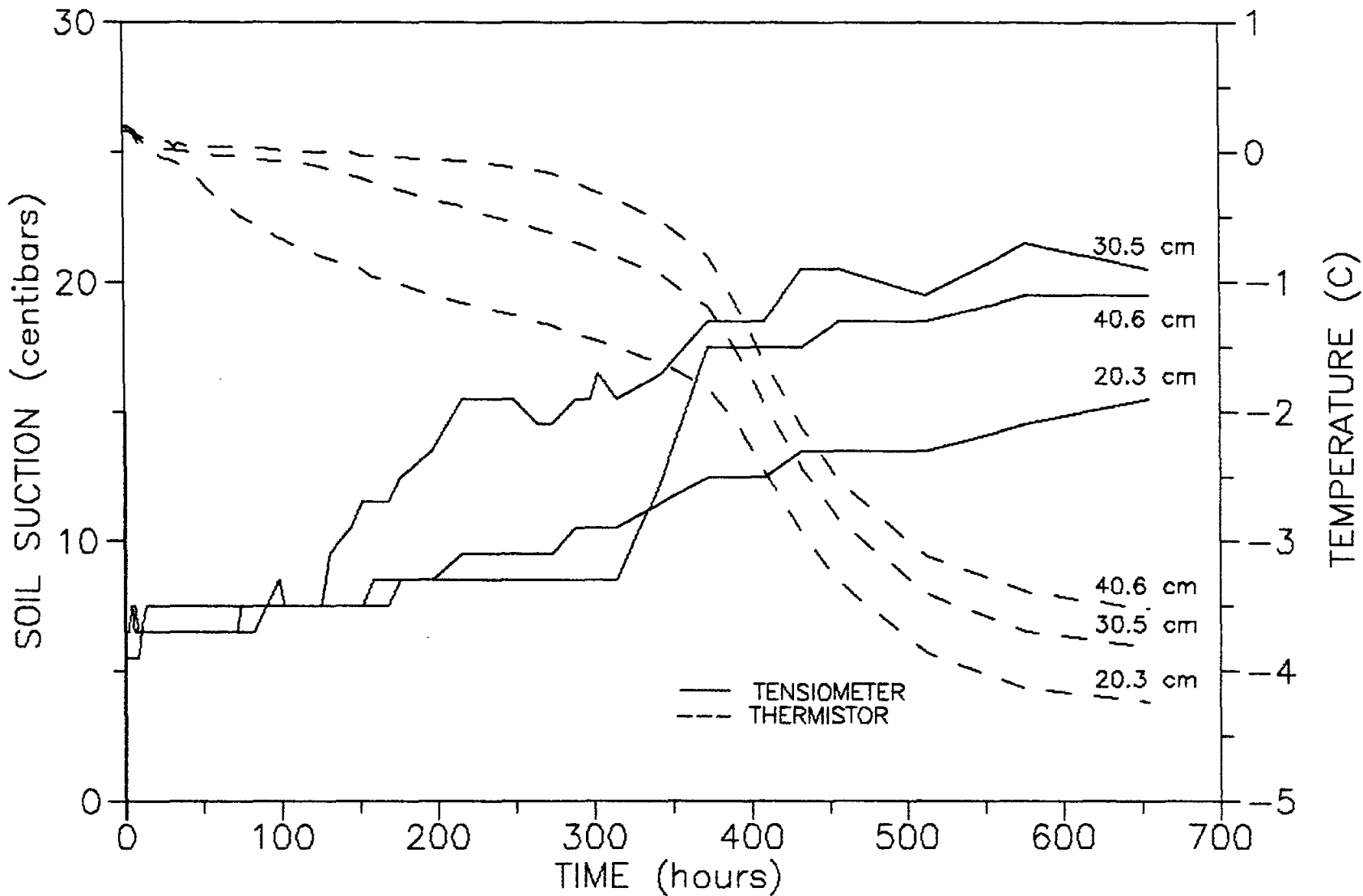Figure 5.14   Soil suctions and corresponding temperatures at mid-level of soil mass in test #1.

Figure 5.15   Soil suctions and corresponding temperatures at mid-level of soil
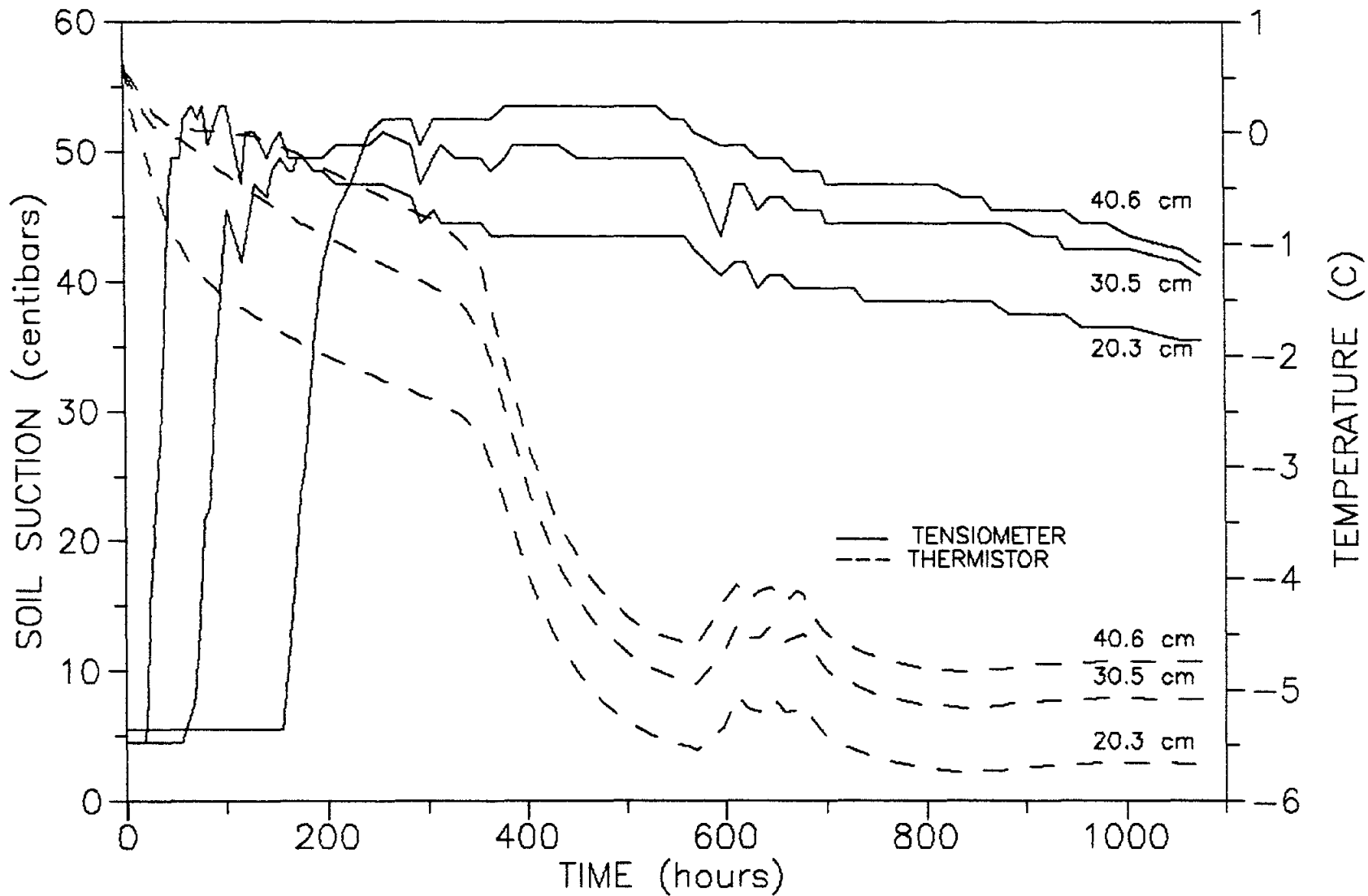mass in test #2.

Figure 5.16 Soil suctions and corresponding temperatures at mid-level of soil
mass in test #3.

can be seen. At approximately 600 hours into the test, the cold room failed and the ambient room temperature warmed up to nearly 15°C (Figure 5.4). The soil temperatures also changed but only about 0.5°C. The tensiometer readings dropped 5 centibars during this same time and continued dropping until the test was terminated.

As a result of these observations, the tensiometer data was only used in a qualitative manner. However, it is hoped that these observations will be helpful to future researchers considering the use of ethylene gylcol-filled tensiometers in their studies.

5.4 Moisture Redistribution

The effect of moisture distribution due to freezing can be determined by knowing the difference between the initial and the final moisture contents. The initial distributions of moisture contents for each test were assumed to be a function of the soil-moisture characteristic curve. This was necessary due to the problems encounterd with the tensiometers. The initial average moisture content was assumed to be equal to the average moisture content calculated from several samples collected during soil preparation and soil placement. The moisture contents determined in this manner varied only with respect to height above the tank base by the same amount given by the

moisture characteristic curve. The final distribution of moisture contents within each test was based on between 25 and 30 soil samples taken during the dissection of the frozen soil mass.

Figures 5.17 through 5.19, give contour plots of the final distribution of moisture contents for test #1 through #3 respectively. These plots show the moisture distribution with respect to the height above the freeze tank base and the radial distance from the tank center. Figure 5.17 shows no major trend in the distribution for test #1 except in height above the base. A minor trend however exists where the moisture contents rise slowly with increasing radius and drop slightly at the outer radius. In test #2 (Figure 5.18), the distribution of final moisture contents illustrates a trend of moisture redistribution towards the heat pipe. Likewise, test #3 (Figure 5.19) also shows a significant redistribution trend similiar to test #2.

Subtracting the initial moisture content from the final moisture content at a specific location, yields the net change in moisture content for that location. The net change in moisture content can be converted to a net change in mass of water per unit volume. This change in moisture per unit volume of soil is calculated by dividing the net moisture content change by 100 and multiplying by the soil dry density.
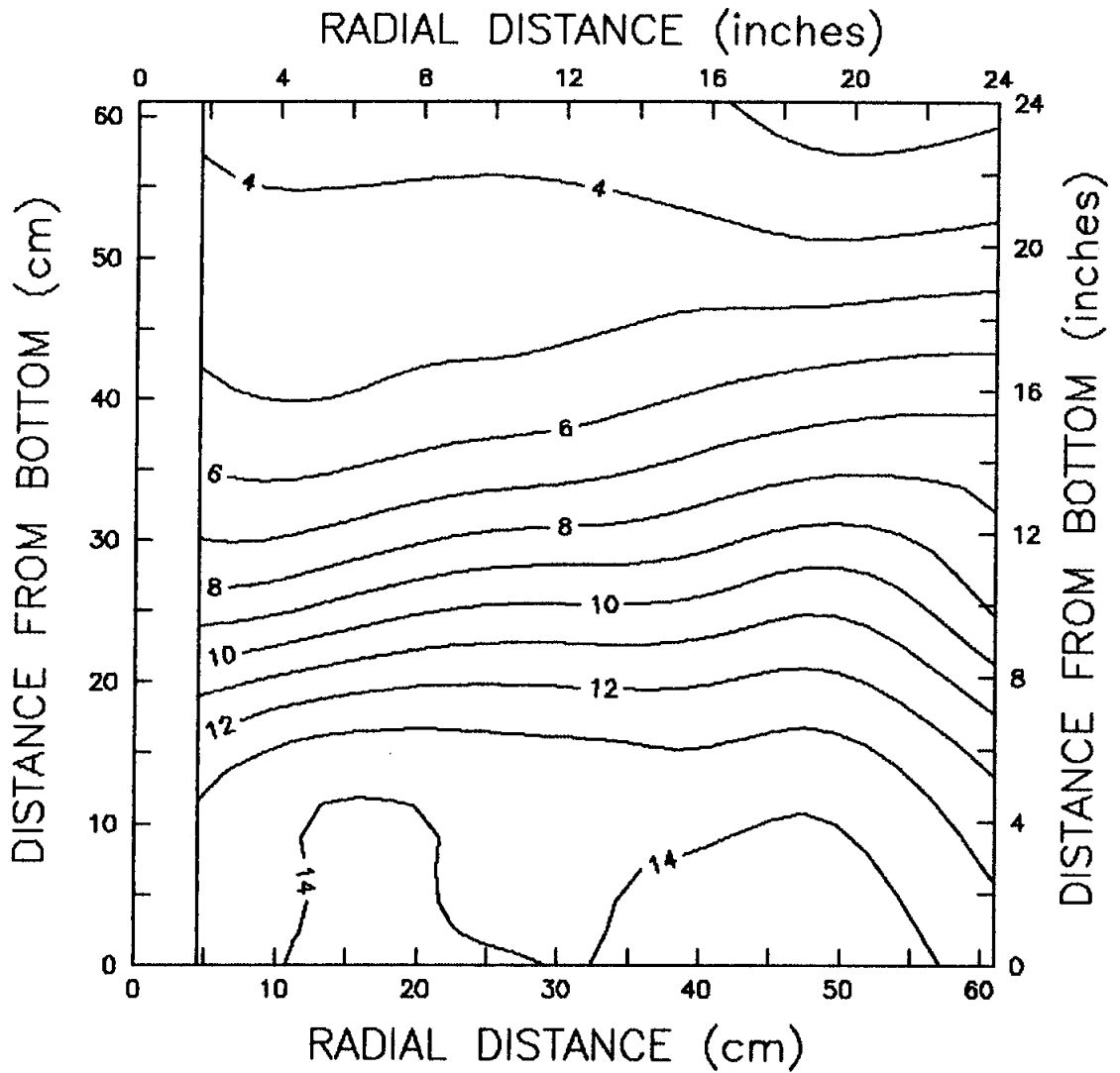
Figure 5.17   Contour plot of final moisture contents for
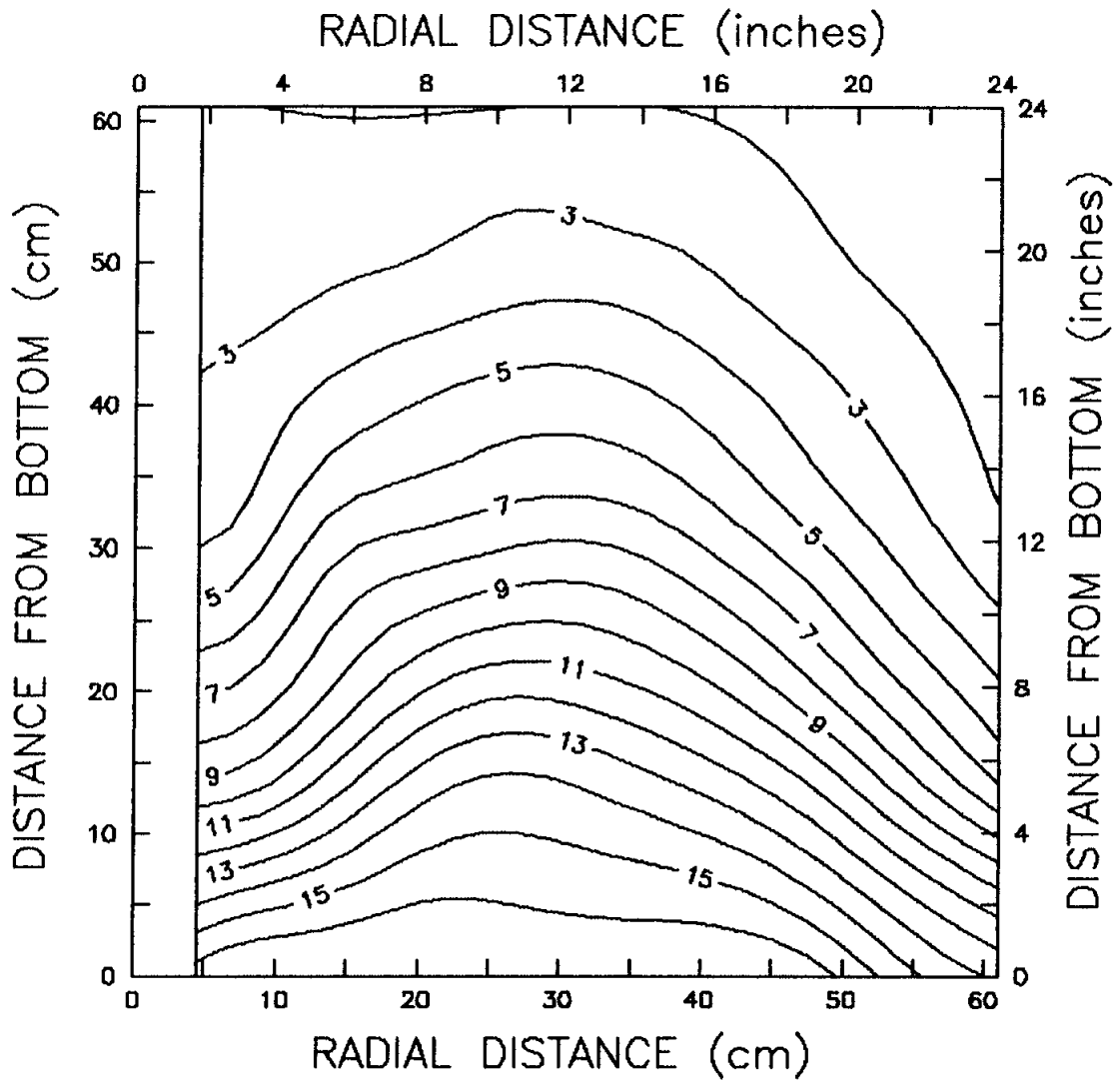test #1. Contour interval = 1%

Figure 5.18   Contour plot of final moisture contents for
test #2. Contour interval = 1%
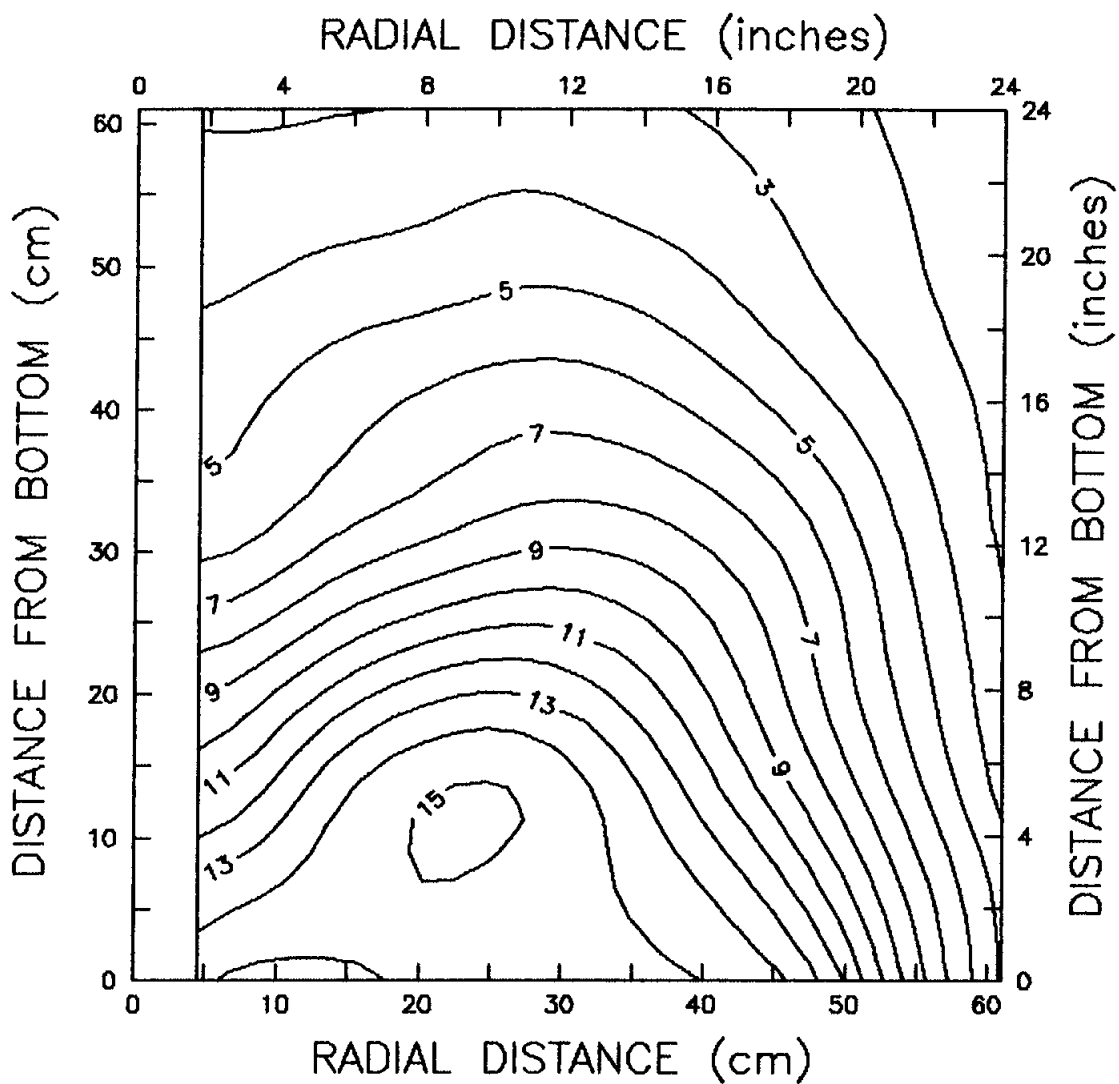
Figure 5.19   Contour plot of final moisture contents for
test #3. Contour interval = 1%

Figures 5.20 through 5.22 give contour plots of the changes in moisture resulting from freezing in test #1 through test #3 respectively. The change in moisture contour interval is 0.02 gm/cm^3 which is approximately equal to a 1.1 moisture content percent change.

Figure 5.20 (test #1) shows that an overall loss of water (negative values) had occurred due to freezing. No discernible trend is apparent except that the loss of water per unit volume increases with depth. This is due to pore water expulsion that occurred after freezing had been initiated. The loss of moisture increased with depth as the degree of saturation of the soil increased with depth.

The contour plot for test #2 (Figure 5.21) shows a distinct pattern of moisture redistribution. The soil in test #2 exhibited dessication near the center pipe and at the freeze tank wall with a resulting accumulation of moisture in the interior region. Figure 5.22 (test #3) gives a moisture redistribution pattern similar to test #2 except that no dessication occurred adjacent to the center pipe in test #3. Also, test #3 had a greater magnitude of accumulation and dessication than test #2. In both tests #2 and #3, the region of greatest accumulation is centered at a radius of 27 cm. and a height of 20 cm. above the tank base.
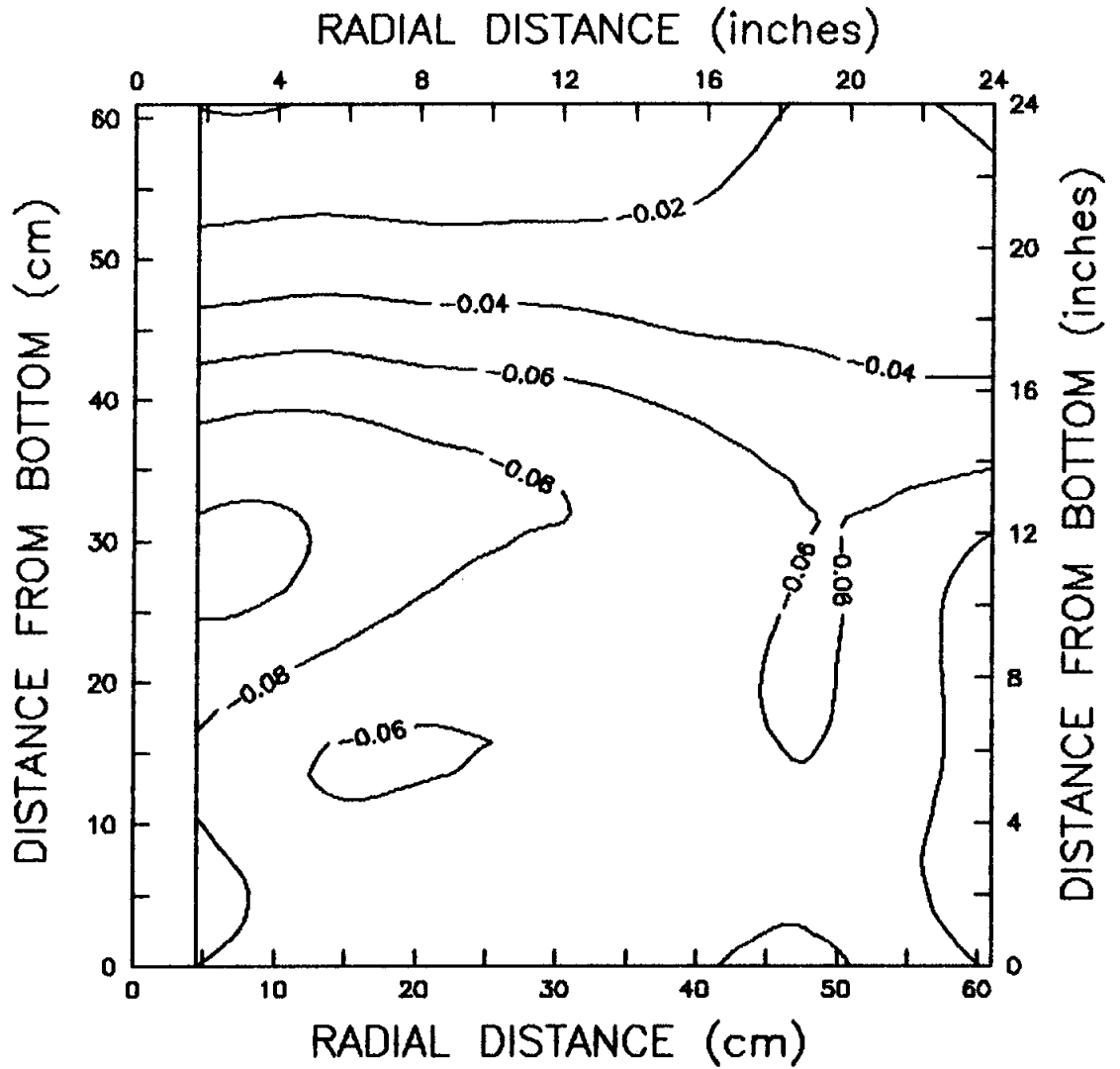
Figure 5.20   Contour plot of the net change in moisture
              for test #1. Contour interval = 0.02 gm /cm3.
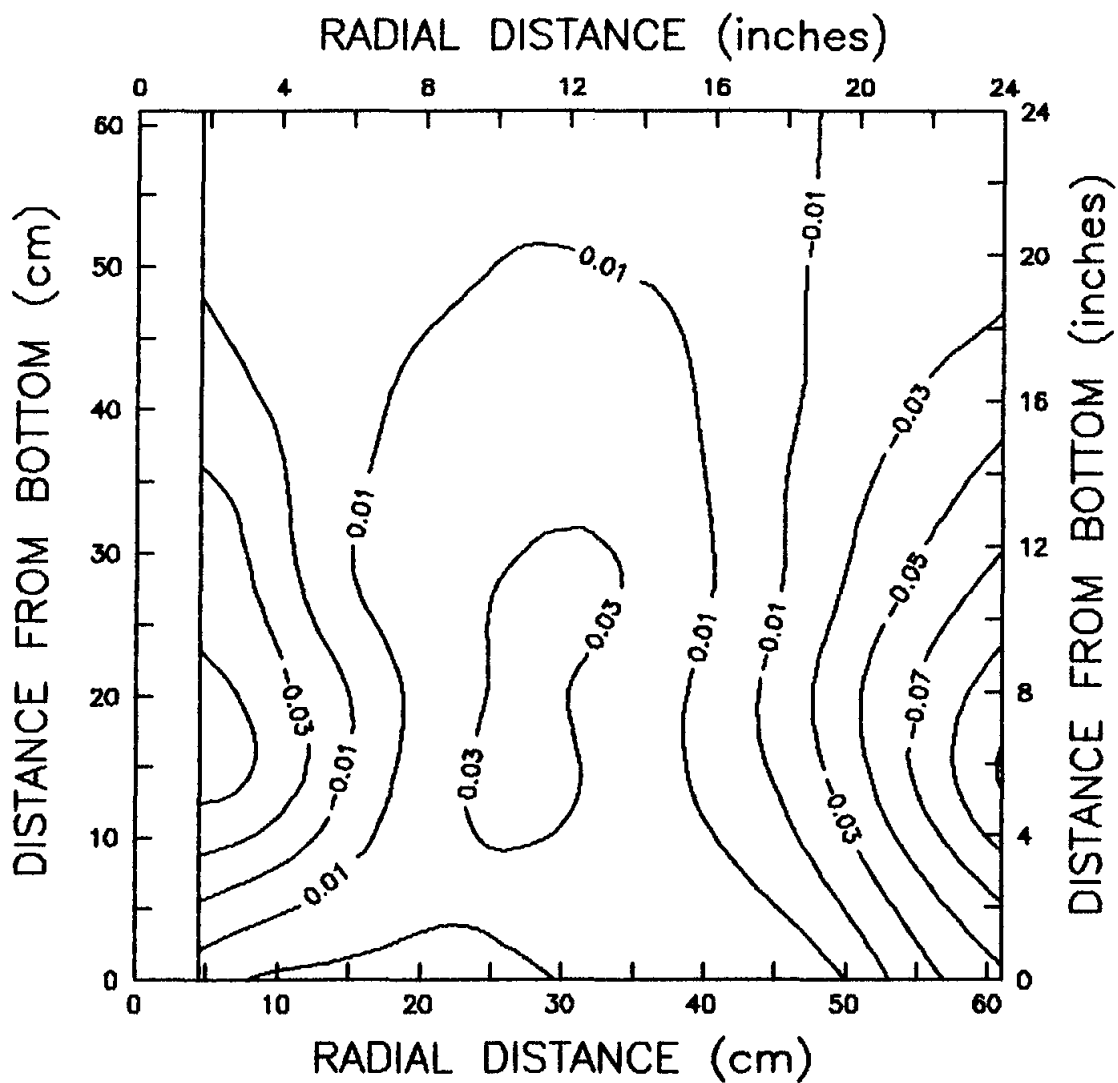
Figure 5.21   Contour plot of the net change in moisture
             for test #2. Contour interval = 0.02 gm /cm3.
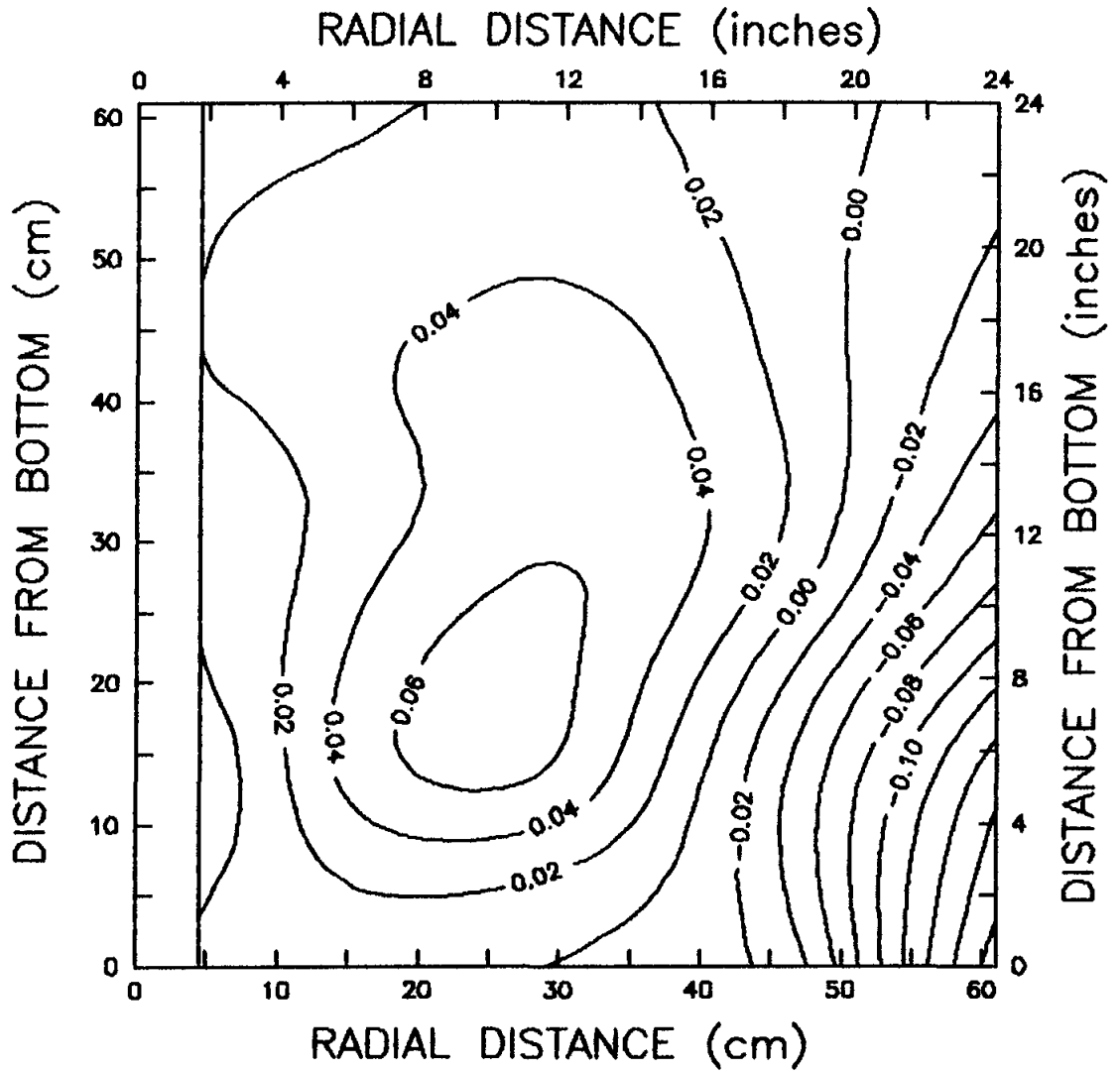
Figure 5.22 Contour plot of the net change in moisture
for test #3. Contour interval = 0.02 gm /cm3.

CHAPTER 6

SUMMARY

6.1 Discussion

Moisture migration and redistribution in the sand due to outward, radial freezing has been shown to have occurred in two of the three tests. No segregated ice features were observed in the frozen soil masses during cross-sectioning upon completion of the freezing tests. The soil-water system within each freezing test in this study is modelled as a closed system such that no additional moisture was introduced to the soil mass during freezing. The individual contributions of migration due to vapor phase transport and transport by the continuous liquid phase could not be determined.

In test #1, the average degree of saturation was 69% and the overall soil system experienced a loss of moisture. Since this type of soil ("clean" sand) is considered to be non-frost susceptible, the freezing of the pore water created an overall positive pore water pressure due to the volume changes associated with phase change. This positive pore water pressure caused an expulsion of the pore water.

149

This was observed when water drained from the freeze tank during freezing test #1. The continuity of air voids is lower at higher degrees of saturation. Therefore, vapor phase transport should be minimal in test #1. It is apparent that the positive pressures, associated with volume changes of the pore water, were greater than negative pressures associated with thermodynamic imbalances and capillary forces which resulted in a pressure gradient to develop decreasing outward away from the advancing freeze front.

Significant moisture redistribution occurred in tests #2 and #3 due to freezing. The degree of saturation was 37.0% and 34.6% for test #2 and #3 respectively. A lower degree of saturation would result in more interconnected, air voids necessary for vapor phase transport. Also, the expulsion of pore fluid upon freezing is easily accommodated to due a larger percentage of air voids. Therefore, no positive pore pressure was generated to cause pore water expulsion. In fact, negative pressures were generated due to freezing which resulted in a pressure gradient decreaseing inward towards the advancing freezing front and moisture migration occurred.

In tests #2 and #3, the centroid of greatest moisture flux occured at a radial distance of 27 cm. This correlates well to the abrupt reduction in freezing rate shown in Figure 5.13. The rate of phase change was reduced as

moisture migrated towards the freeze front. This is caused by an increase in the volumetric latent heat of fusion and therefore more heat energy per unit volume of soil must be removed before the phase change boundary can advance.

Once frozen, a soil with a net gain in moisture content will have a higher thermal conductivity thereby enhancing the phase change rate. In addition, the region of desiccated soil (loss of moisture) will have a lower volumetric latent heat of fusion further accelerating the phase change rate. This effect is slightly reduced by lower thermal conductivities in the desiccated region. This was illustrated in the analysis of the steady-state temperatures for test #3. It was shown that the thermal conductivity increased with increasing radius to a maximum at a radius of 35 cm. The thermal conductivity then dropped with increasing radius. The steady-state analysis performed on test #3 also showed a resulting distribution of moisture content similar to that given in Figure 5.19.

The time for complete phase change determined from Figure 5.1 for test #1 compared well to the time given by the finite difference program. However, times for tests #2 and #3 contrasted significantly with times predicted by the finite difference program. The finite difference program gave slower times for complete phase change than was observed in the two tests. This is due to an increase in

thermal conductivity of the interior region and a decrease in the volumetric latent heat of fusion in the outer soil mass.

6.2 Reccomendations

Further studies may help delineate the upper and lower saturation levels at which moisture migration occures in the test sand due to a thermal gradient. The upper limit is expected to be between 37% and 69% saturation for the soil used in the tests. The test sand was poorly-graded and exhibits less capillary potential than a well-graded sand of similar grain size. The effect of a well-graded sand is expected to inhance the redistribution potential due to freezing and may warrant attention in futher studies.

This study was limited to a vertical pipe in a closed system. Although no additional moisture was introduced to the soil mass during freezing, moisture redistribution did occur due to gravitational forces corresponding to the soil-moisture characteristic curve. An open system is expected to increase the amount of moisture in the soil mass when the degree of saturation is below 67% but would have little influence with higher initial soil mass saturations. It may be pertinent to examine the effects of radial freezing from a horizontal heat pipe in both an open and closed system.

Valuable information would be obtained if soil matrix

suctions could be monitored. This would involve more research on the use of tensiometers in freezing soil studies or the use of other types of equipment which can accurately measure negative pore pressures developed during soil freezing.

With additional freezing tests and more reliable pore pressure monitoring equipment, it is hoped that a better understanding between soil temperatures and moisture migration potential can be established. Future freezing studies would involve the following: testing additional varying degrees of soil saturation, using both an open and closed soil-water system, and comparing moisture migration potentials for both vertical and horizontal pipe orientations. With this understanding, a finite element model may be developed to analyze the thermal influences of moisture migration towards the evaporator section of thermosyphons. This model would include various boundary conditions to account for both vertical and horizontal positioning of the evaporator section. Also, the finite element model could analyze both open and closed soil-moisture systems.

6.3 Conclusions

The application of these results to field conditions

involving radial freezing in similar material will aid in the design of refrigerated foundations. No moisture migration or redistribution is expected to occur in situations where the evaporator sections are placed below a phreatic surface. This is due to the nonfrost susceptible nature of the sand and the inability to form segregated ice features. However, moisture migration will occur when the evaporator sections are situated in a sand with low to moderate degrees of saturation. The effect of moisture migration will decrease the thermal resistance in the region of moisture accumlulation. This effect, and the effect of decreasing the volumetric latent heat in the desiccated region will cause an increase in the maximum radius of freezing. Upon thawing, however, the dessicated regions will experience an accelerated rate of thawing. This may lead to degradation of the underlying thaw unstable soils for which the refrigerated foundation was intended to protect. Therefore, the thermal effects of moisture migration in soils surrounding evaporator sections must be considered when designing refrigerated foundations.

REFERENCES

Andersland, O. B. and D. M. Anderson, 1978, Geotechnical Engineering for Cold Regions, McGraw-Hill, New York, 566 p.

Anderson, D. M. and N. R. Morgenstern, 1973, Physics, Chemistry, and Mechanics of Frozen Ground, in the North American Contribution of the Second International Conference on Permafrost at Yakutsk, U.S.S.R., National Academy Press, pp. 257-288.

Bell, G. E., 1979, Solidification of a Liquid About a Cylindrical Pipe, International Journal of Heat Mass Transfer, Vol. 22, pp. 1681-1686.

Benkelman, A. C., and F. R. Olmstead, 1931, A New Theory of Frost Heaving, Highway Research Board, Vol. 11, pp. 152-165.

Beskow, G., 1938, Prevention of Detrimental Frost Heave in Sweeden, Highway Research Board Proceedings, Vol. 18, Pt. 11, pp. 366-370.

Callinan, J. P., 1983, An Analysis of the Thermal Fixation of Pilings, Journal of Energy Resources Technology, Vol. 105, June 1983, pp. 236-24.

Callinan, J. P., and M. J. Kaiseman, 1976, Heat Transfer in Soils with Freezing and Melting of Moisture, ASME No. 76-WA/HT-22, December 1976.

Carslaw, H. S., and J. C. Jaeger, 1959, Conduction of Heat in Solids, 2nd edition, Oxford University Press, London, pp. 282-296.

Casagrande, A., 1931, Discussion on Frost Heaving (Abstract), Highway Research Board, Vol. 11, pp. 168-172.

Chamberlain, E. J., 1981, Frost Susceptibility of Soil- Review of Index Tests, Cold Regions Research and Engineering Laboratory, Monograph 81-2, 121 p.

Churchill, S. W., and Gupta, J. P., 1977, Approximations For Conducting With Freezing or Melting, International Journal of Heat Mass Transfer, Vol. 20, pp. 1251-1253.

155

Dillon, H.B. and O. B. Andersland, 1966, Predicting Unfrozen Water Contents in Frozen Soils, Canadian Geotechnical Journal, Vol. 3, No. 2, pp. 53-60.

Farouki, O. T., 1981, Thermal Properties of Soils, Cold Regions Research and Engineering Laboratory, Monograph 81-1, 151 p.

Gold, L. W., 1957, A Possible Force Mechanism Associated With the Freezing of Water in Porous Materials, Highway Research Board Bulletins, No. 168, pp. 65-73.

Havens, J. A., and R. E. Babcock, 1975, Heat and Moisture Conduction in Unsaturated Soils, University of Arkansas Water Resources Research Center, Publication No. 25, 108 p.

Haynes, F. D., and J. P. Zarling, 1982, A Comparative Study of Thermosyphons Used for Freezing Soil, ASME Paper No. 82-WA/HT-40, 1982.

Hillel, D., 1971, Soil and Water-Physical Principles and Processes, Academic Press, New York, New York, 288 p.

Hillel, D., 1980, Fundamentals of Soil Physics, Academic Press, New York, New York, 413 p.

Hillel, D., 1982, Introduction to Soil Physics, Academic Press, New York, New York, 288 p.

Heuer, C. E., 1979, The Application of Heat Pipes on the Trans-Alaskan Pipeline, Cold Regions Research and Engineering Laboratory, Special Report 79-26, 33 p.

Heuer, C. E., E. L. Long, and J. P. Zarling, 1985, Ground Temperature Control, in Thermal Design Considerations in Frozen Ground Engineering, T. G. Krzewinski and R. G. Tart, eds., ASCE Nomograph, New York, pp. 72-154.

Holden, J. T., R. H. Jones, and S. J. M. Dudek, 1981, Heat and Mass Flow Associated With a Freezing Front, Engineering Geology, Vol. 18, No. 1-4, Special Issue-Ground Freezing 1980, pp. 153-164.

Horiguchi, K., and R. D. Miller, 1983, Hydraulic Conductivity Functions of Frozen Materials, Proceedings of the 4th International Conference on Permafrost: Fairbanks, Alaska, National Academy Press, Washington D. C., pp. 660-665.

Ingersoll, J. E., 1982a, Method For Coincidentally Determining Soil Hydraulic Conductivity and Moisture Retention Characteristics, Cold Regions Research and Engineering Laboratory, Special Report 81-2, 13 p.

Ingersoll, J. E., 1982b, Laboratory and Field Use of Soil Tensiometers Above and Below 0 C, Cold Regions Research and Engineering Laboratory, Special Report 81-7, 22 p.

Ingersoll, J. E. and R. L. Berg, 1985, Hydraulic Properties of Selected Soils, in Freezing and Thawing of Soil-Water Systems, pp. 26-35, Cold Regions Engineering Monograph, American Society of Civil Engineers.

Johnston, G. H., 1981, Permafrost, Engineering Design and Construction, Wiley, Toronto, 540 p.

Jones, R. H., and K. J. Lomas, 1983, The Frost Susceptibility of Granular Materials, Proceedings of the 4th International Conference on Permafrost: Fairbanks, Alaska, National Academy Press, Washington D. C., pp. 660-665.

Jumikis, A. R., 1957a, Soil Moisture Transfer in the Vapor Phase Upon Freezing, Highway Research Board Bulletin, No. 168, pp. 96-115.

Jumikis, A. R., 1957b, The Effect of Freezing on a Capillary Meniscus, Highway Research Board Bulletin, No. 168, pp. 116-122.

Jumikis, A. R., 1977, Thermal Geotechnics, Rutgers University Press, New Jersey, 375 p.

Kaplar, L. W., 1969, Phenomenon and Mechanism of Frost Heaving, Highway Research Record, No. 304, pp. 1-13.

Kersten, M. S., 1949, Thermal Properties of Soils, Univ. of Minnesota Experiment Station, Bulletin No. 28, 227 p.

Kinosita, S., 1979, Effects of Initial Soil-Water Conditions on Frost Heaving Characteristics, Engineering Geology, Vol. 13, No. 1-4, Special Issue-Ground Freezing 1979, pp. 41-52.

Konrad, J. M., and N. R. Morgenstern, 1980, A Mechanistic Theory of Ice Lens Formation in Fine-grained Soils, Canadian Geotechnical Journal, Vol. 17, No. 4, pp. 473-486.

Konrad, J. M., and N. R. Morgenstern, 1981, The Segregation
Potential of a Freezing Soil, Canadian Geotechnical
Journal, Vol. 18, No. 4, pp. 482-491.

Konrad, J.M., and N.R. Morgenstern, 1982, Effects of Applied
Pressure on Freezing Soils, Canadian Geotechnical
Journal, Vol. 19, No. 4, pp. 494-505.

Konrad, J. M., and N. R. Morgenstern, 1983, Frost Suscepti-
bility of Soils in Terms of Their Segregation
Potential, Proceedings of the 4th International
Conference on Permafrost: Fairbanks, Alaska, National
Academy Press, Washington D. C., pp. 660-665.

Lambe, T. W. and R. V. Whitman, 1969, Soil Mechanics, Wiley,
New York, 553 p.

Linell, K. A., and C. W. Kaplar, 1959, The Factor of Soil
and Material Type in Frost Action, Highway Research
Board Bulletin, No. 225, pp. 81-126.

Loch, J. P. G., 1979, Influence of the Heat Extraction Rate
on the Ice Segregation Rate of Soils, Frost i Jord, NR
20, pp. 19-30.

Long, E. L., and E. Yarmak, 1982, Permafrost Foundations
Maintained by Passive Refrigeration, Energy-Sources
Technology Conference and Exhibition.

Lovell, C. W., 1983, Frost Susceptibility of Soils,
Proceedings of the 4th International Conference on
Permafrost: Fairbanks, Alaska, National Academy Press,
Washington D. C., pp. 735-739.

Low, P. F. and C. W. Lovell, 1959, The Factor of Moisture in
Frost Action, Highway Research Board Bulletin, Vol.
225, pp. 23-39.

Lunardini, V. J., 1980, Phase Change Around a Circular Pipe,
Cold Regions Research and Engineering Laboratory,
Report 80-27, December, 1980, 26 p.

Lunardini, V. J., 1981a, Heat Transfer in Cold Climates, Van
Nostrand Reinhold, New York, 731 p.

Lunardini, V. J., 1981b, Phase Change Around a Circular
Cylinder, Journal of Heat Transfer, ASME, Vol. 103,
August, 1981b, pp. 598-600.

Lunardini, V. J., 1983, Approximate Phase Change Solutions For Insulated Buried Cylinders, Journal of Heat Transfer, ASME, Vol. 105, February, 1983, pp. 25-32.

Lunardini, V. J., 1987, Freezing of Soil with Phase Change Occurring Over a Finite Temperature Zone, Proceedings of the 4th International Offshore Mechanics and Arctic Engineering Symposium, Vol. II, ASME, pp. 38-45.

Lunardini, V. J., 1988, Heat Conduction With Freezing and Thawing, Cold Regions Research Engineering Laboratory, Monograph 88-1, 334 p.

Mageau, D. W., and N. R. Morgenstern, 1980, Observations on Moisture Migration in Frozen Soils, Canadian Geotechnical Journal, Vol. 17, No. 1, pp. 54-60.

McFadden, T., 1985, Performance of the Thermotube Permafrost Stabilization System in the Airport Runway at Bethel, Alaska, Report No. AK-RD-86-20, Dept. of Trans. and Public Facilities, State of Alaska, December 1985.

McKim, H. L., J. E. Walsh, and D. N. Arion, 1980, Review of Techniques For Measuring Soil Moisture In Situ, Cold Regions Research and Engineering Laboratory, Special Report 80-31, 30 p.

McGaw, R. W., R. L. Berg, and J. W. Ingersoll, 1983, An Investigation of Transient Processes in an Advancing Zone of Freezing, Proceedings of the 4th International Conference on Permafrost: Fairbanks, Alaska, National Academy Press, Washington D. C., pp. 660-665.

Miller, R. D., 1972, Freezing and Heaving of Saturated and Unsaturated Soils, Highway Research Record, No. 393, pp. 1-11.

Miller, R. D., 1978, Frost Heaving in Non-Colloidal Soils, Proceedings of the 3rd International Conference on Permafrost: Edmonton, Alberta, Vol. 1, pp. 708-713.

Nakano, Y., A. R. Tice, J. L. Oliphant, and T. F. Jenkins, 1983, Cold Regions Research and Engineering Laboratory, CRREL Report 83-22, 13 p.

Nixon, J. F., 1978, Geothermal Aspects of Ventilated Pad Design, Proceedings of the Third International Conference on Permafrost, National Research Council of Canada, pp. 841-846.

Nixon, J. F., 1983, Geothermal Design of Insulated Foundations For Thaw Prevention, Proceedings of the Fourth International Conference on Permafrost, Vol I, National Academy Press, pp. 924-927.

Nixon, J. F., 1987, Ground Freezing and Frost Heave-A Review, The Northern Engineer, Vol. 19, No.3 & 4, pp. 8-18.

Nixon, J. F., and E. C. McRoberts, 1973, A Study of Some Factors Affecting the Thawing of Frozen Soils, Can. Geotech. Journal, Vol No. 10, pp. 439.

Oliphant, J. L., A. R. Tice, and Y. Nakano, 1983, Water Migration Due to a Temperature Gradient in Frozen Soil, Proceedings of the 4th International Conference on Permafrost: Fairbanks, Alaska, National Academy Press, Washington D. C., pp. 660-665.

Ozisik, M. N., and Uzzell, J. C., 1979, Exact Solution for Freezing in Cylinderical Symmetry With Extended Freezing Temperature Range, Journal of Heat Transfer, Vol. 101, May 1979, pp. 331-334.

Penner, E., 1956, Soil Moisture Tension and Ice Segregation, Highway Research Board Bulletin, No. 168, pp. 50-64.

Penner, E., 1957, Soil Moisture Tension and Ice Segregation, Highway Research Board Bulletin, No.225, pp. 1-13.

Penner, E., 1959, The Mechanism of Frost Heaving in Soils, Highway Research Board Bulletin, No.225, pp. 1-13.

Penner, E., 1970, Thermal Conductivity of Frozen Soils, Canadian Journal of Earth Sciences, Vol. 7, No. 3, pp. 982-987.

Penner, E., 1972, Influence of Freezing Rate on Frost Heaving, Highway Research Record, No. 393, pp. 56-64.

Penner, E., 1979, Effects of Temperature and Pressure on Frost Heaving, Engineering Geology, Vol. 13, No. 1-4, Special Issue-Ground Freezing 1979, pp. 29-39.

Phukan, A., 1985, Frozen Ground Engineering, Prentice-Hall, New Jersey, 336 p.

Rieke, R. D., Vinson, T. S., and D. W. Mageau, 1983, The Role
of Specific Surface Area and Related Index Properties
in The Frost Heave Susceptibility of Soils, Proceedings
of the 4th International Conference on Permafrost:
Fairbanks, Alaska, National Academy Press, Washington
D. C., pp. 660-665.

Riseborough, D. W., M. W. Smith, and D. H. Halliwell, 1983,
Determination of the Thermal Properties of Frozen
Soils, Proceedings of the 4th International Conference
on Permafrost: Fairbanks, Alaska, National Academy
Press, Washington D. C., pp. 660-665.

Romkens, M. J. M., and R. D. Miller, 1973, Migration of
Mineral Particles in Ice With a Temperature Gradient,
Journal of Colliod and Interface Science, Vol. 24, No.
1, pp. 103-111.

Taber, S., 1929, Frost Heaving, Journal of Geology, Vol. 37,
pp. 428-461.

Taber, S., 1931, Discussion on Frost Heaving (Abstract),
Highway Research Board, Vol. 11, pp. 173-177.

Takagi, S., 1978, Segregation Freezing as the Cause of
Suction Force For Ice Lens Formation, Colds Regions
Research and Engineering Laboratory, CRREL Report 78-6,
17 p.

Takagi, S., 1979, Segregation Freezing as the Cause of
Suction Force For Ice Lens Formation, Engineering
Geology, Vol. 13, No. 1-4, Special Issue-Ground
Freezing, pp. 93-100.

Thornton, D. E., 1976, Steady-state and Quasi-static Thermal
Results For Bare and Insulated Pipes in Permafrost,
Canadian Geotechnical Journal, Vol. 13, No. 2, May,
1976, pp. 161-171.

Touloukian, Y. S., J. D. Bottorf, and T. Harsen, 1951, Heat
Transfer and Temperature Distribution in Solids For
Transient Heat Flow Due to Cylinderical Sources and
Sinks, Highway Research Board, Special Report #2,
pp. 147-160.

Van Wylen, G.J., and R. E. Sonntag, 1985, Fundamentals of
Classical Thermodynamics, 3rd Edition, SI Version,
Wiley & Sons, New York, 722 p.

Voller, V. and M. Cross, 1980, Accurate Solutions of Moving Boundary Problems Using the Enthalpy Method, Internat. Journal of Heat and Mass Transfer, Vol. 24, pp 545-556.

Watkins, W. I., 1931, Discussion on Frost Heaving (Abstract), Highway Research Board, Vol. 11, pp. 165-168.

Williams, P. J., 1964, Unfrozen Water Content of Frozen Soils and Soil Moisture Suction, Geotechnique, Vol. 14, No. 3, pp. 231-246.

Williams, P. J., 1972, Use of the Ice-Water Surface Tension Concept in Engineering Practice, Highway Research Record, No. 393, pp. 19-29.

Winterkorn, H. F., 1955, Discussion of "Suction Forces in Soils Upon Freezing" by A. J. Jumikis, Proceedings of American Society of Civil Engineers, Vol. 81, No. 656, pp. 6-9.

Zarling, J. P., 1987, Approximate Solutions to Neumann Problem, Proceedings of the 1987 International Symposium on Cold Regions Heat Transfer, K. C. Cheng, V. J. Lunardini, and N. Seki, eds., pp. 47-54.

Zarling, J. P. and F. D. Haynes, 1985, Thermosyphon Devices and Slab-On-Grade Foundation Design, Report No. AK-RD-86-16, Dept. of Trans. and Public Facilities, State of Alaska, June 1985.